

**Evaluations Of Severe Acute Respiratory Syndrome Coronavirus Therapeutics
And A Viral Capacity For Plasticity And Escape.**

Meagan Elise Bolles

A dissertation submitted to the faculty of the University of North Carolina at Chapel Hill
in partial fulfillment of the requirements for the degree of Doctor of Philosophy
in the Department of Microbiology and Immunology.

Chapel Hill
2013

Approved by:

Ralph S. Baric, Ph.D.

Mark T. Heise, Ph.D.

Aravinda deSilva, Ph.D.

Eric Donaldson, Ph.D.

William Funkhouser, M.D.

Raymond Pickles, Ph.D.

© 2013
Meagan Elise Bolles
ALL RIGHTS RESERVED

ABSTRACT

MEAGAN ELISE BOLLES: Evaluations Of Severe Acute Respiratory Syndrome Coronavirus Therapeutics And A Viral Capacity For Plasticity And Escape.
(Under the direction of Ralph S. Baric, Ph.D.)

The Severe Acute Respiratory Syndrome Coronavirus (SARS-CoV) emerged in 2002/2003, causing the deaths of almost a tenth of the 8000 individuals infected worldwide before it was controlled by public health measures. While the 2003 epidemic strain is likely extinct, the importance of coronaviruses as emergent zoonotic viruses was again realized with the emergence of a novel human coronavirus in Saudi Arabia in 2012. Despite a decade of research on SARS-CoV no approved vaccine or therapeutic yet exists, and development of broadly neutralizing and effective therapeutics for coronaviruses remains a priority. Neutralizing antibodies targeting the Spike glycoprotein (S) are both necessary and sufficient for protection against SARS-CoV, but the high genetic diversity and mutability of SARS-CoV in natural infections presents a challenge to both vaccine- and antibody-based therapeutics. Thus, an effective SARS-CoV therapeutic should provide S-specific immunity that is nonetheless broad enough to counter heterologous and derivative S variants. This work was designed to assess immunization strategies towards SARS-CoV, to explore the plasticity and neutralization networks of the Spike glycoprotein, and to assess the utility of molecular models to predict host range and antibody neutralization.

In the first study we explored the limitations of a doubly inactivated SARS-CoV vaccine, identifying a vaccine-induced immunopathology and emphasizing the importance of rigorous challenge viruses and animal models that accurately recapitulate age-associated lung pathology. Second, in two collaborative studies we assessed multi-generational monoclonal antibodies designed to be broadly neutralizing or escape resistant, and extended our characterization of the Spike receptor binding domain (RBD) as a highly plastic antiviral target. Finally, we characterized ten recombinant Combinatorial Escape Viruses (CEVs) engineered from a database of antibody escape substitutions in the RBD. These CEVs were designed to assess the plasticity of the S-RBD, the utility of predictive modeling, and the neutralization

networks across the RBD. The tools developed this study will assist in the development of predictive models and standardized platforms for combination monoclonal antibody immunotherapies for emergent viruses. These studies of SARS-CoV have extended our understanding of a key neutralizing target and have provided a valuable foundation for the rapid characterization of novel coronaviruses and potential therapeutics.

TABLE OF CONTENTS

| | |
|--|-------------|
| LIST OF TABLES | vii |
| LIST OF FIGURES | viii |
| LIST OF ABBREVIATIONS | x |
| CHAPTER 1: SARS-CoV and Emergent Coronaviruses: Viral Determinants of Interspecies Transmission | 11 |
| 1.1. Overview | 11 |
| 1.2. Introduction | 11 |
| 1.3. Coronavirus Phylogeny and Mechanisms of Genome Diversity | 12 |
| 1.4. Multiple incidents of cross-species transmission | 15 |
| 1.5. SARS-related CoVs in Bats | 15 |
| 1.6. Genesis of an Epidemic..... | 18 |
| 1.7. Coronavirus Cross-Species Transmission: Role of Spike-Receptor Interactions in Viral Entry..... | 19 |
| 1.8. Plasticity of the Spike glycoprotein | 22 |
| 1.9. Conclusions | 24 |
| 1.10. Contributions..... | 26 |
| CHAPTER 2: A Double-Inactivated SARS-CoV Vaccine Provides Incomplete Protection In Mice And Induces Increased Eosinophilic Pro-Inflammatory Pulmonary Response Upon Challenge | 27 |
| 2.1. Overview | 27 |
| 2.2. Introduction:..... | 28 |
| 2.3. Methods and Materials | 30 |
| 2.4. Results | 35 |
| 2.5. Discussion | 52 |
| 2.6. Contributions..... | 59 |
| CHAPTER 3: Iterative Development of Potent and Broadly Neutralizing Antibodies Targeting the Spike Receptor Binding Domain. | 60 |
| 3.1. Overview | 60 |
| 3.2. Introduction | 61 |
| 3.3. Increased Antibody Affinity Confers Broad In Vitro Protection against Escape Mutants of Severe Acute Respiratory Syndrome Coronavirus | 65 |
| 3.3.1. Overview | 65 |

| | |
|---|------------|
| 3.3.2. Introduction | 65 |
| 3.3.3. Materials and Methods: | 66 |
| 3.3.4. Results | 68 |
| 3.3.5. Discussion | 72 |
| 3.4. Effects of Targeting Spike Protein Receptor Binding Domain on Neutralization Escape and Fitness of SARS-Coronavirus | 74 |
| 3.4.1. Overview | 74 |
| 3.4.2. Introduction | 75 |
| 3.4.3. Materials and Methods | 77 |
| 3.4.4. Results | 80 |
| 3.4.5. Discussion | 87 |
| 3.4.6. Contributions | 90 |
| CHAPTER 4: Structural Plasticity and Antibody Escape in the SARS-CoV Spike Receptor Binding Domain. | 91 |
| 4.1. Overview | 91 |
| 4.2. Introduction | 92 |
| 4.3. Methods | 94 |
| 4.4. Results | 97 |
| 4.5. Discussion | 110 |
| CHAPTER 5: Discussion and Future Directions..... | 115 |
| 5.1. Summary | 115 |
| 5.2. SARS-Coronavirus whole inactivated vaccine studies | 116 |
| 5.2.1. Ongoing studies | 117 |
| 5.3. Live attenuated vaccine studies | 119 |
| 5.4. Iterative development and characterization of anti-spike antibodies | 120 |
| 5.5. Combinatorial Escape Viruses | 121 |
| 5.5.1. Future directions and ongoing studies | 122 |
| 5.6. SARS-Coronavirus | 124 |
| REFERENCES | 126 |

LIST OF TABLES

Table

| | |
|---|----|
| 3.3.2: Amino acid changes in the RBD of spike protein found in the neutralization escape mutants. | 69 |
| 3.3.3 Amino acid differences in the RBD of the spike protein | 71 |

LIST OF FIGURES

Figure

| | |
|--|-----|
| 1.1: Spike Phylogeny of Representative CoVs and Models of SARS-CoV Emergence..... | 14 |
| 1.2: Sequence changes over the SARS-CoV epidemic..... | 18 |
| 1.3: Crystal structures of coronavirus receptor binding domains (RBD) complexed with their receptors..... | 22 |
| 1.4: Experimental Evolution at the SARS S Glycoprotein RBD-Ligand Interface..... | 26 |
| 2.1: DIV vaccination and nonlethal heterologous challenge in aged animals..... | 37 |
| 2.2: Neutralizing antibody titers of vaccinated mice..... | 39 |
| 2.3: Morbidity and Mortality of lethal MA and zoonotic challenges following DIV immunization..... | 41 |
| 2.4: Pathology in young mice challenged with icMA15 or icHC/SZ/61/03-S..... | 43 |
| 2.5: Pathology following immunization and subsequent lethal challenge in aged Harlan mice..... | 44 |
| 2.6: Cytokine and chemokine mRNA expression profiles in aged mice..... | 46 |
| 2.7: Visual identification of eosinophils following lethal challenge..... | 47 |
| 2.8: Flow cytometry gating strategy for cell populations..... | 49 |
| 2.9: Flow cytometric analysis of additional lung immune cell populations in young and aged mice following immunization and subsequent lethal challenge..... | 50 |
| 2.10: Eosinophilia influx is conserved across Group 2b N-proteins..... | 52 |
| 3.3.3: Neutralization activity of the SK4 and RSK scAbs in comparison to 80R..... | 69 |
| 3.3.4: Cross neutralization studies of high-affinity scAbs with escape mutants with the D480A and D480Y mutations..... | 70 |
| 3.3.5: SK4 neutralization of escape variants..... | 72 |
| 3.4.2: Prophylactic treatment of SARS-CoV infections in 12-month-old aged BALB/c mice by 80R and Fm6 nAbs..... | 81 |
| 3.4.4: Broadly neutralization activity of nAbs, fm6 and Y112A..... | 82 |
| 3.4.5: Locations of neutralization escape variant mutations on the structure of the SARS-CoV RBD and effects on the binding to human ACE and viral growth..... | 84 |
| 3.4.6: Effect of neutralization escape on in vivo replication..... | 86 |
| 4.1: Combinatorial Escape Viruses..... | 98 |
| 4.2: Panel of antibody-escape profiles..... | 99 |
| 4.3: Predicted localized destabilization in CEV-9..... | 100 |
| 4.4: Predicting CEV viability..... | 102 |
| 4.5: Growth curves to assess replication and virus production..... | 104 |
| 4.6: CEV neutralization results..... | 105 |

| | |
|---|-----|
| 4.7: Expanded binding tract for mAb s230.15. | 106 |
| 4.8: Mechanisms of escape from m396..... | 109 |
| 4.9: Co-neutralization with s227.14 and s230.15..... | 110 |
| 4.10: Summary of prediction methodologies..... | 114 |
| 5.1 IL-4 signaling phenotypes following lethal MA15 SARS-CoV infection..... | 118 |
| 5.2: MA-ExoN vaccination protects from lethal challenge..... | 119 |
| 5.3 Morbidity of 4 CEVs in young mice..... | 123 |

LIST OF ABBREVIATIONS

| | |
|------|-----------------------------------|
| Ab | antibody |
| CEV | Combinatorial Escape Virus |
| CoV | coronavirus |
| ExoN | exonuclease |
| nAb | neutralizing antibody |
| MA | mouse-adapted |
| mAb | monoclonal antibody |
| RBD | receptor binding domain |
| S | spike glycoprotein |
| SARS | Severe Acute Respiratory Syndrome |
| scFv | single chain variable fragment |
| WT | wild type |

CHAPTER 1: SARS-CoV and Emergent Coronaviruses: Viral Determinants of Interspecies Transmission¹

1.1. Overview

Most new emerging viruses are derived from strains circulating in zoonotic reservoirs. Coronaviruses, which had an established potential for cross-species transmission within domesticated animals, suddenly became relevant with the unexpected emergence of the highly pathogenic human SARS-CoV strain from zoonotic reservoirs in 2002. SARS-CoV infected approximately 8000 people worldwide before public health measures halted the epidemic. Supported by robust time-ordered sequence variation, structural biology, well-characterized patient pools, and biological data, the emergence of SARS-CoV represents one of the best studied natural models of viral disease emergence from zoonotic sources. This review article summarizes previous and more recent advances into the molecular and structural characteristics, with particular emphasis on host-receptor interactions, that drove this remarkable virus disease outbreak in human populations.

1.2. Introduction

Coronaviruses have an established potential for cross-species transmission that became broadly recognized with the emergence of a novel human coronavirus in 2002. Severe Acute Respiratory Syndrome (SARS) was first identified as an atypical pneumonia in isolated patients in Guangdong Province, China. The disease, caused by SARS-coronavirus (SARS-CoV), spread into epidemic disease proportions following key super spreader events that were associated with a novel respiratory virus introduction into a globalized community. SARS-CoV rapidly spread around the world, causing about 8,000 infections and 800 deaths worldwide, before aggressive public health intervention strategies contained the epidemic by July 2003. The epidemic went through three distinct phases: early, middle, and late, as determined by

¹ Meagan Bolles^a, Eric Donaldson^b, Ralph Baric^{a,b}. Department of Microbiology and Immunology^a and Department of Epidemiology^b, University of North Carolina at Chapel Hill, Chapel Hill, North Carolina. First published in *Current Opinion in Virology*, December 2011, 1(6): 624-34. DOI:10.1016/j.coviro.2011.10.012. Reproduced with permission from Elsevier.

molecular analysis. The decimating lethality of SARS-CoV emergence was borne largely by the elderly, in whom mortality rates approached 50% or more. Aggressive public health measures limited and eventually ended the epidemic in July 2003, absent any effective therapeutics [1]. A subsequent explosion of coronavirus research identified SARS-CoV in several small carnivores (palm civets and raccoon dogs) of the Chinese wet markets and SARS-like CoV in the predicted reservoir host, horseshoe bats (genus *Rhinolophus*). The vastly expanded CoV phylogeny includes two novel human coronaviruses (NL63 and HKU1) and ultimately tripled the number of full length genome sequences available in GenBank. SARS-CoV was shown to use a novel host receptor, Angiotensin Converting Enzyme 2 (ACE2), for docking and entry and the viral attachment protein, Spike, was extensively characterized both as a determinant of host specificity and as a therapeutic target. The more recent studies of coronaviruses have progressed to increased surveillance and characterization of numerous new coronaviruses circulating in bats, birds, and other species, integrated bioinformatics and microbiological studies, and extensive evaluations of potential therapeutics [2].

1.3. Coronavirus Phylogeny and Mechanisms of Genome Diversity

Following the SARS-CoV outbreak a surge in global coronavirus genome sequencing efforts vastly expanded our insight into the CoV phylogeny and resulted in the definition of several sub-classifications (Fig 1). The greatest contribution of new strains was derived from the newly discovered bat coronavirus (BtCoV), which may be the source of most, if not all, mammalian CoVs [3-9]. The high diversity of coronaviruses is attributable to three viral traits [10]. The first characteristic is the potentially high mutation rates associated with RNA replication, generally estimated as 10^{-3} to 10^{-5} . Surprisingly, the estimated mutation rate for SARS-CoV and other coronaviruses approached 2×10^{-6} [11-13]. In contrast to other RNA viruses, recent data suggests that coronaviruses encode an RNA proof-reading activity associated with the 3' to 5' exonuclease activity encoded within nsp14 [14]. It is not clear whether RNA proof-reading fidelity is altered in changing environmental settings or during virus replication under stress related conditions, but such possibilities may allow for rapid virus evolution in changing ecologic conditions [14]. Second, recombination frequencies within the coronavirus family have been calculated to be as high as 25% during mixed infection, likely the result of discontinuous RNA transcription and the presence of full length and subgenomic negative strand RNAs that allow for frequent strand switching and

recombination between viral genomes and subgenomic replication complexes [15,16]. The role of discontinuous transcription in recombination is supported by the higher rate of recombination at the 3' ends of viral genomes and by targeted RNA recombination techniques designed to genetically manipulate the 3' end of the genome [17]. Although poorly studied, conservation of transcription regulatory sequence (TRS) sites across viral species may implicate these sequences as foci or hot spots of recombination [17]. Thirdly, as the largest of the RNA viruses at ~27-31kb, coronaviruses have both increased opportunity for change and room for modification, clearly evidenced by the presence of numerous unique open reading frames and protein functions encoded at the 3' end of the genome [10]. These genomic characteristics allow for rapid adaptation to novel hosts, ecological niches, tissue tropism, and even generation of novel coronavirus species, as seen in the generation of FIPV type II strains from double recombination events between FIPV type I and CCoV [10].

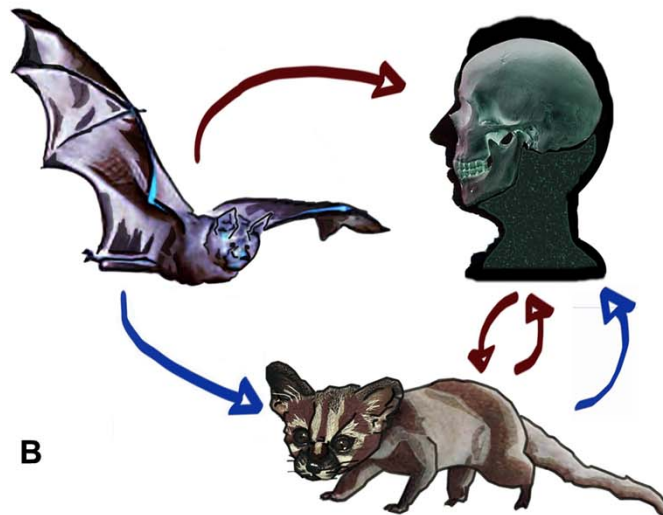
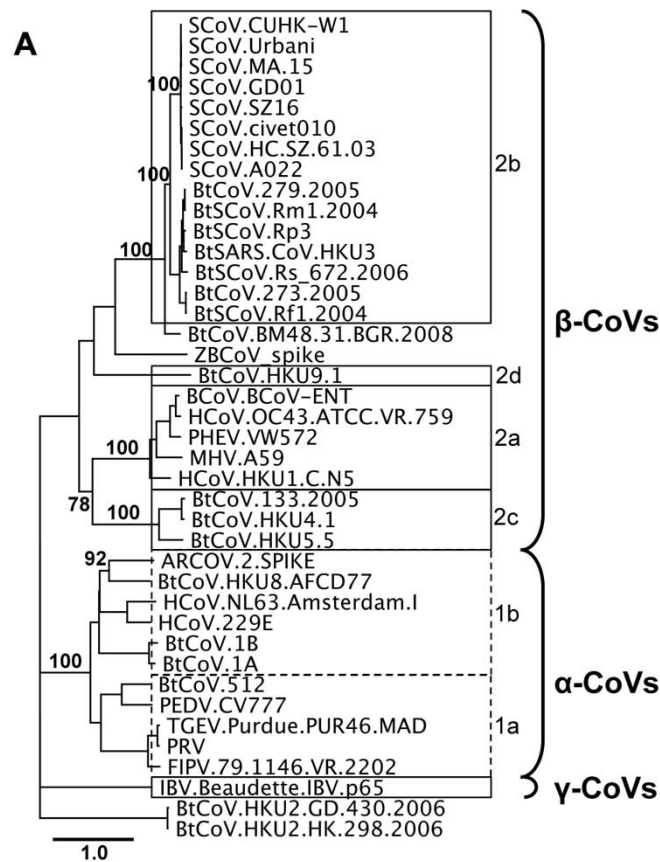


Figure 1.1: Spike Phylogeny of Representative CoVs and Models of SARS-CoV Emergence.

A) The Spike peptide sequence of 40 representative CoVs demonstrates that CoVs make up three distinct groups named alpha, beta, and gamma. These names replaced the former group 1, 2 and 3 designations, respectively. Classical subgroup clusters are marked as 2a-2d for the beta CoVs and 1a and 1b for the alpha CoVs. The tree was generated via Maximum Likelihood using the PhyML package. Major branch labels represent bootstraps that were greater than 70. SCoV, SARS CoV; BtSCoV, bat SARS-like CoV; BtCoV, ZBCoV, and ARCoV, bat CoVs; HCoV, human; FCoV and FIPV, feline CoVs; BCoV, bovine; IBV, avian; PHEV, TGEV, PRV, PEDV, porcine CoVs; and MHV, murine hepatitis virus. B) Competing models of SARS-CoV emergence. Early data suggested that SARS-CoV initially jumped from the zoonotic reservoir, bats, to palm civets, followed by a second jump from civets to humans (blue arrow). More recent

phylogenetic and receptor analysis studies suggest a direct emergence from bats to humans, with subsequent cross transmission between humans and civets (red arrow).

1.4. Multiple incidents of cross-species transmission.

Coronaviruses have a strong history of host shifting as evidenced by phylogenetic incongruences in the family tree [18]. In addition to SARS-CoV, two human coronaviruses, HCoV-OC43 and HCoV-229E, are now also recognized as having likely emerged from animal reservoirs. HCoV-OC43 and bovine coronavirus (BCoV), betacoronaviruses, have very high sequence similarity, suggesting a recent and common origin (Fig 1). Molecular clock analysis of the Spike glycoprotein of both species estimates that HCoV-OC43 originated from a BCoV ancestor around 1890 [19]. Similarly, HCoV-229E likely emerged from a bat alphacoronavirus approximately 200 years ago [20]. In an example of reverse zoonosis, porcine epidemic diarrhea virus emerged suddenly in the early 1980's, most likely originating from HCoV-229E [20]. Additionally, a coronavirus isolated in 1988 from a child with acute diarrhea, HECV-4408, was shown to be more closely related to bovine coronavirus (BCoV), indicating the continued introduction of zoonotic coronaviruses into human populations [21]. The origins of HCoV-NL63 and HCoV-HKU1, the most recently discovered human coronaviruses, remain under study. The most recent example of zoonotic emergence of a human coronavirus is the example of SARS-CoV, which had at least two independent emergence events from zoonotic reservoirs, recognized in 2002 and 2003 [22]. The most recent phylogenetic data estimate the emergence of SARS-CoV some seven years earlier, consistent with the identification of low sero-positive cases from archived serum samples in 2001 in China [23].

1.5. SARS-related CoVs in Bats

Following its emergence in 2003, SARS was quickly identified as a zoonotic virus, and the identification of the wet markets as a potential source may have assisted epidemiological control of the disease [24]. While palm civets, raccoon dogs, and horseshoe bats (*Rhinolophus* genus) have all been identified as hosts of SARS-like CoVs, it is suggested that only the horseshoe bats are likely reservoir hosts. Bats are widely distributed, highly diverse, and extremely mobile mammals with an established role as hosts of emergent RNA viruses. Coronaviruses occupy an exceptionally wide distribution in bats; recent surveillance studies have extended our recognition of this range to Africa, Europe, South America, and North America [4,9,25-27]. The genetic variation encoded within many recently discovered coronaviruses

hosted by bats is far greater than the diversity noted between many human coronaviruses, despite a proportionally small sampling of the ~1200 bat species, leading some researchers to speculate that all mammalian coronaviruses are derived from bat reservoir strains [4,28]. The extensive sequence diversity provides considerable opportunity for the emergence of new animal and human coronaviruses, which would be sufficiently antigenically distinct as not to be influenced by preexisting exposure and memory immune responses to established human CoVs. For example, little antigenic cross reactivity exists between the S glycoproteins of more distantly related group 2b bat coronaviruses and the SARS-CoV [29]. From a historic context, the next emergent event is likely dependent only on ecological and epidemiological situations and time, as the viral potential is well-established [30,31].

Repeated efforts have been made in recent years to identify the zoonotic reservoir and path of emergence for SARS-CoV, both by sampling zoonotic populations and by attempting to clarify SARS-CoV receptor usage in alternate hosts. A recent study attempting to address the paucity of bat SARS-related coronavirus sequences gathered and analyzed SARS-related coronaviruses in *Rhinolophus* bats (SARSr-Rh-BatCoV) (Rp3) genomes from horseshoe bats in China [32]. Interestingly, several bats sampled were coinfecting with HKU2, an alphacoronavirus, providing direct evidence that individual bats can host divergent coronaviruses, even across groups. Further, tagging and clinical assessment of infected bats over a four year period showed only minor weight loss associated with Rp3 infection, and viral clearance occurring between two weeks and four months. Analysis of the ten novel genomes gathered in this study combined with previously published sequences demonstrated evidence of frequent recombination between the strains. They also note a 26-bp deletion in ORF8 near, but not identical to, the 29-bp deletion seen in human SARS-CoV epidemic strains, suggesting ORF8 may undergo frequent deletions [32]. Whether the epidemic 29-bp deletion was neutral to or critical for human adaption remains undetermined.

Angiotensin Converting Enzyme 2 (ACE2) is the receptor for SARS-CoV, but following the identification of several SARS-like CoVs (SL-CoVs) in several horseshoe bats (genus *Rhinophus*), the ACE2 molecule of *R. pearsonii* proved incapable of serving a receptor for SARS-CoV [3,33]. These and other initial studies suggested that the ancestral SARS-CoV strain in bats used an alternate receptor and that the emergence of SARS-CoV was dependent upon either acquisition of an ACE2 binding region or initial utilization of an alternative human receptor [33]. However, while human ACE2 is genetically conserved,

the bat ACE2 sequences are highly heterogeneous, with 78-84% amino acid identity between families [34,35]. Despite this, the residues that interface with the SARS S RBD are more conserved [36]. A recent study determined that a minimum three substitutions in the ACE2 of *R. pearsonii* (RpACE2) allowed this protein to serve as a receptor for SARS [37]. Looking more broadly at the ACE2 molecules from seven bat species, the ACE2 proteins from *Myotis daubentoni* and *Rhinolophus sinicus* are capable of supporting Spike-mediated pseudovirus and SARS-CoV infection, though less efficiently than human ACE2 [34]. Assessment of receptor usage by early phase and civet isolate Spike proteins might better inform our understanding of emergence pathways, determining if SL-CoV jumped directly from bat to human hosts or whether civet or other intermediate hosts were required as early intermediates prior to human adaptation.

Although original data suggested a bat to civet to human origin, evidence supporting direct bat to human transmission of SL-CoV emerged from recent phylogenetic studies, in addition to the receptor studies mentioned above (Fig 1b). Initially, a reanalysis of published genome sequences developed phylogenies using outgroups that were non-SARS-CoV sequences, designed to test the monophyly of the SARS-CoV sequences [38]. Under this assessment, bat isolates are ancestral host to all SARS-CoVs, while civet and raccoon dog sequences (small carnivores), as well as pig isolates cluster within the human SARS-CoV sequences. The small carnivore CoVs are consistently shown to be terminal branches with human CoVs intermediate, with subsequent bidirectional transmission of CoV between carnivores and humans responsible for isolated cases such as GD03 [38]. A more recent study analyzed CoV sequences gathered from 24 *Rhinolophus sinicus* bats in geographically distant regions of China, characterizing two distinct genotypes, Rs672 and Rs806 [39]. Interestingly, one sequence (Rs672) and the previously published Rp3 are shown in a monophyly more closely related to human-SCoV than to bat SARS-like CoV strains, based on the strong similarity of Rs672 ORF1a/b region to human SARS sequences. This study also provided further evidence of recombination between Bat-SLCoV, with a recombination breakpoint identified immediately after the start codon of Spike, identical to the recombination position in the Rp3 genome [39]. The combination of highly diverse BtCoV species and divergent ACE2 molecules among bat hosts suggests direct bat to human transmission may be feasible. Thus, the field is left with two potentially competing models for the origins of the SARS-CoV epidemic, however, in both models civets and raccoon dogs became key amplifying hosts for virus persistence and reintroduction into human populations.

1.6. Genesis of an Epidemic

The SARS-CoV outbreak is unique in that a chronological set of sequence changes are available that span the epidemic, providing an unparalleled opportunity to identify the genetic basis for zoonotic virus cross species transmission and human adaptation during an expanding epidemic. Molecular changes noted at with the end of the early phase and expansion into the middle phase of the epidemic include A3047V, A3072V in the replicase and D778Y and perhaps E1163K in the Spike gene. Transition from the middle to late phase of the epidemic included an A2552V in ORF1a, E1389D in ORF1b, D77G and T244I in the S gene, respectively (Fig 2) [40]. It has been hypothesized that these alterations were key to an expanding epidemic, yet empirical data to support these claims and functional significance of these alterations remains unavailable. For example, it is not clear whether the ORF8 29 bp deletion is central for human adaptation as suggested, or a genetic hitchhiker amplified and maintained following a selective sweep mediated by other beneficial mutations located elsewhere in the genome [3,40]. In addition to these changes, the SARS-CoV Spike glycoprotein was under strong positive selection, with 23 substitutions evolving during the expanding phases of the epidemic [41]. Experimental evidence suggests both adaptation to ACE2 and antibody selection contributed to Spike changes [40,42].

| Phase | Gene | ORF 1A | | | | | | | | | | 1B | Spike | | | | | | | | | | | | | M | X1 | | | | | | | | | | |
|-----------------|----------|--------|------|------|------|------|------|------|------|------|------|------|-------|------|------|----|-----|-----|-----|-----|-----|-----|-----|-----|-----|-----|-----|-----|-----|-----|-----|------|----|------|-------|-------|--------|
| | | 549 | 1021 | 1121 | 1136 | 1663 | 2116 | 2222 | 2269 | 2746 | 2971 | 3047 | 3072 | 1389 | 2532 | 77 | 227 | 239 | 244 | 261 | 344 | 360 | 479 | 487 | 607 | 665 | 701 | 743 | 754 | 778 | 849 | 1163 | M4 | X1-7 | X1-81 | X1-93 | X1-121 |
| Animal strains | SZ16 | S | A | T | L | I | F | Y | S | W | A | A | A | E | R | D | K | L | T | K | R | S | R | S | S | S | L | A | A | D | A | E | S | I | S | Y | G |
| | HC/SZ/63 | A | V | T | P | I | L | C | L | C | A | A | A | E | R | D | K | S | T | T | R | S | R | S | S | S | S | T | V | D | T | E | S | I | S | H | G |
| Early isolates | ZS-A | A | A | T | P | I | L | Y | L | W | A | A | A | E | K | D | N | L | T | T | R | F | N | T | S | L | S | T | V | D | T | K | G | F | C | H | C |
| | ZS-B | A | V | T | P | I | L | Y | L | W | A | A | A | E | K | D | N | L | T | T | R | F | N | T | S | L | S | T | V | D | T | K | G | F | C | H | C |
| | GZ02 | A | V | T | P | I | F | Y | L | W | A | A | A | E | K | D | N | L | T | T | R | F | N | T | S | L | S | T | V | D | T | E | G | F | C | H | C |
| | GD01 | A | V | T | P | L | F | Y | L | C | A | A | A | E | R | D | N | L | T | T | R | F | N | T | S | L | S | T | V | D | T | K | G | F | C | H | C |
| | HSZ | A | V | I | P | L | L | C | L | C | V | A | A | E | R | D | N | S | T | T | K | F | N | T | S | L | S | T | V | D | T | E | G | F | C | H | C |
| Middle isolates | CUHK-W1 | A | V | I | P | L | L | C | L | C | V | A | A | E | R | D | N | S | T | T | K | F | N | T | S | L | S | T | V | Y | T | K | G | F | C | H | C |
| | BJ01 | A | V | I | P | L | L | C | L | C | V | A | V | E | R | D | N | S | T | T | K | F | N | T | S | L | S | T | V | Y | T | K | G | F | C | H | C |
| | HZS2-A | A | V | I | P | L | L | C | L | C | V | V | V | E | R | D | N | S | T | T | K | F | N | T | S | L | S | T | V | Y | T | K | G | F | C | H | C |
| | HZSZ-F | A | V | I | P | L | L | C | L | C | V | V | V | E | R | G | N | S | T | T | K | F | N | T | S | L | S | T | V | Y | T | K | G | F | C | H | C |
| GZ-C | A | V | I | P | L | L | C | L | C | V | A | V | D | R | G | N | S | I | T | K | F | N | T | S | L | S | T | V | Y | T | K | G | F | C | H | C | |
| Epidemic | Urbani | A | V | I | P | L | L | C | L | C | V | V | D | R | G | N | S | I | T | K | F | N | T | S | L | S | T | V | Y | T | K | G | F | C | H | C | |

| |
|------------------|
| Original residue |
| Civet to Human |
| Early to middle |
| Middle to late |

Figure 1.2: Sequence changes over the SARS-CoV epidemic.

Shown here are the most significant changes important for transition of SARS from Civet to early, middle and late phases of epidemic strains. Mutations indicative of lineages that were not likely to have contributed to the expansion to other phases have been removed. All other positions in the genome are identical.

1.7. Coronavirus Cross-Species Transmission: Role of Spike-Receptor Interactions in Viral Entry.

Coronavirus receptor interactions are key determinants regulating host range, cross-species transmission, and tissue tropism. The various coronaviruses demonstrate broad receptor and co-receptor usage, from proteases such as aminopeptidase N for transmissible gastroenteritis virus (TGEV), canine-CoV, feline infectious peritonitis virus (FIPV), and HCoV-229E, to cell adhesion molecules such as CEACAM1a for MHV, to sugars as co-receptors for some alpha, beta, and gammacoronaviruses [36,43,44]. This diverse receptor usage directly impacts host range and tissue tropism as demonstrated by the closely related PRCoV and TGEV. PRCoV lacks the sugar-binding region of TGEV, and consequently is limited to a respiratory rather than enteric tropism [45]. The recently crystallized structure of the Group2a coronavirus MHV complexed with its receptor, murine CEACAM1a, emphasizes again the broad diversity and flexibility of CoV Spike glycoproteins, as the core structure is hypothesized to have been derived from a host sugar-binding protein (galectin) and subsequently modified to allow mCEACAM1a binding, thus enhancing MHV affinity for host cells [43]. Other coronaviruses encode a second putative viral attachment protein, the hemagglutinin esterase (HE), which was likely derived from influenza C strains by recombinatory mechanisms [46]. Coronaviruses selected *in vitro* to broaden host range oftentimes mutate to bind heparin sulfate for docking and entry [47]. It is notable that OC43 and BCoV have carbohydrate (sialic acid) binding capacities, as well as broader host ranges [44]. The capacity to bind carbohydrates for docking and entry may provide an additional pathway for coronavirus host range expansion, cross-species transmission, and disease emergence, and requires further study.

The key determinant of SARS coronavirus host specificity is the Spike glycoprotein, an envelope-anchored trimeric protein responsible for binding human Angiotensin Converting Enzyme 2 (ACE2) as the principle receptor for virus docking and entry. SARS-CoV S glycoprotein also binds C-type lectins like DC- and/or L-Sign as a co-receptor, an interaction which is blocked by mannose binding lectin [48,49]. Importantly, SARS-CoV docking and entry is also highly dependent upon transmembrane protease/serine subfamily member 2 (TMPRSS2) S and ACE2 cleavage, especially in airway and alveolar sites, and cathepsin L cleavage and subsequent S2 fusion activation [50-52]. Several studies in the past two years have worked to clarify the plasticity of this protein, with particular emphasis on the receptor binding domain (RBD). The Spike glycoprotein underwent rapid evolution during the human epidemic [40], was

the most significantly variable protein across civet and human isolates [22], and shows evidence of positive selection during both inter- and intraspecies transmission events [10,22,40,53]. The SARS Spike can recognize and use bat, civet, mouse, and raccoon dog ACE2 receptor molecules for docking and entry, indicating that SARS trafficked along receptor orthologue networks to move between species [34,54,55]. As several alphacoronaviridae also use APN from different species, these data suggest a common theme in coronavirus host range switching: recognizing receptor orthologues from different species [36]. Additionally, the role of different orthologue proteases for facilitating coronavirus S glycoprotein cleavage and entry processes remains undefined, and could significantly contribute to the efficiency of virus cross species transmission processes.

SARS-CoV replicates but does not produce clinical disease in mice. Two experimental adaptations of SARS-CoV to murine hosts by serial passage independently identified a substitution in the Spike gene at residue 436 which alone has been shown to enhance infectivity and pathogenesis in mice, and is predicted to allow stronger binding to the murine ACE2 receptor [29,56]. However, substitutions outside of Spike are necessary for the full lethal disease phenotype in MA15, and presumably also in v2163 [57]. For example, two other proteins, nsp9 and nsp13, contained mutations in both mouse-adapted strains, MA15 and v2163. Additionally, single substitutions in the M gene are common to MA15 and adaptation to persistent infection of human tubular kidney cells, suggesting the M protein influences tropism or pathogenesis by facilitating the efficiency of particle egress [58]. The substitutions common to both mouse-adapted strains suggest potential SARS-CoV virulence factors in the later stages of adaption to a novel host, and indicate potential mutation driven emergence pathways. The mouse-adapted viruses may not represent true cross-species transmission events, as SARS could already replicate in the mouse lung, but it is notable that the most conserved change in both mouse-adapted strains enhances receptor binding at the same Spike residue. Further, serological studies indicate multiple cross-species transmissions into humans in the years before the epidemic, suggesting that the virulence factors contributing to the later stages of adaptation to novel hosts, in Spike or elsewhere, are critically important [23].

The receptor binding domain (RBD, aa318-510) is the strongest determinant of host range for SARS-CoV and other coronaviruses [29]. Single substitutions within the receptor binding domain can significantly affect the binding affinity of Spike to its receptor [59]. Indeed, a minimum of 1-2 substitutions

in the RBD are sufficient to allow the virus to alter host receptor specificity [60]. Experimental adaptation of civet-Spiked SARS virus to human ACE2 receptor by Sheahan et al. demonstrated the minimal requirements for host range expansion. In these studies, a civet-Spiked SARS-CoV was incapable of propagating in Vero cells until a human-tropic substitution was introduced at residue 479. When the Civet-Spiked virus included the K479T substitution it was capable of propagating on Vero cells and further capable of replicating on human airway epithelial cells (HAE) and hACE2-expressing DBT cells, demonstrating that single substitutions are capable of expanding the virus host range. Interestingly, when the K479T-civet-SARS was experimentally selected for enhanced replication on human airway epithelial cells, the substitutions that improved replication did not exactly replicate the substitutions seen in the epidemic strains. Rather, an initial substitution at 479 was necessary for the civet-SARS to use primate ACE2 and propagate in Vero cells, but the adaptive mutations following passage on human airway epithelial cells (HAE) selected for substitutions at two different contact interface sites at residues 442 and 472, rather than the 487 site identified in the epidemic strain [60,61]. This suggests that multiple genetic pathways exist which can improve S RBD-human ACE2 receptor interactions, providing the virus with multiple strategies to adapt to new host species [55]. It is interesting to note that this alternative pathway for recognizing hACE2 ablated interactions with the cACE2 receptor, supporting the hypothesis that epidemic SARS-CoV strains were co-selected to efficiently recognize both civet and human ACE2 receptors.

Antibodies that neutralize SARS-CoV predominantly bind to the RBD of Spike. Rockx et al selected and sequenced a number of different escape mutants to a panel of 23 human monoclonal antibodies, the majority of which contained single substitutions along the RBD interface with ACE2 [62]. All but one escape site mapped within 4 angstroms of contact interface residues, and yet all viruses grew to comparable peak titers in Vero and hACE2-restricted DBT cells. However, growth on civet-ACE2-restricted DBT cells was restricted for all escape viruses, suggesting that escape from antibody neutralization can alter Spike-receptor binding and, consequently, host range [62]. That antibody escape variants can stably adopt substitutions in the Spike-ACE2 receptor interface suggests that the host response to an infection may select for host range variants by a mutation-driven mechanism.

Extensive structural modeling tools are available to predict receptor binding, antibody neutralization, or the stability of substitutions within the receptor binding domain of the SCoV Spike. Three

coronavirus Spike receptor binding domains have been complexed with receptors to date, allowing for prediction and validation of the structural determinants of binding to host and orthologous receptors (Fig 3). Application of mathematical modeling to Spike-receptor and Spike-antibody structural models allowed for the prediction of escape substitutions with a high probability of fixation in a viral population [63]. These predictions are partially in accordance with published data, predicting selection with antibody 80R would select for a substitution at D480 of Spike, as seen in vitro following SARS-CoV escape from 80R neutralization [63,64].

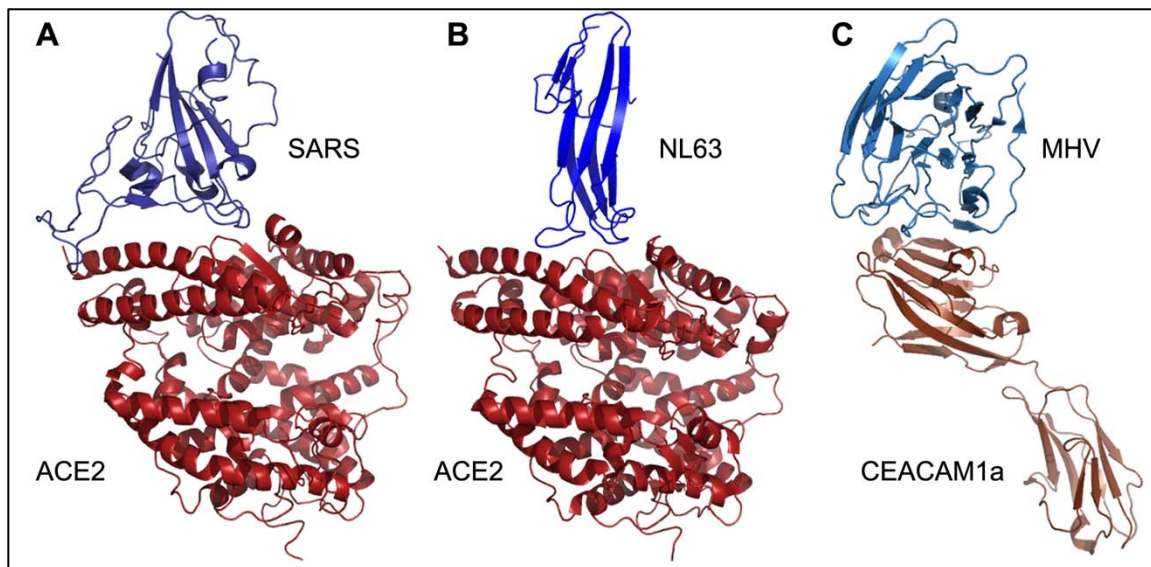


Figure 1.3: Crystal structures of coronavirus receptor binding domains (RBD) complexed with their receptors.

To date, the crystal structures of three coronavirus Spike RBD-receptor complexes have been solved: A) the RBDs of SARS complexed with human ACE2 (pdb 2AJF) [61], B) NL63 complexed with human ACE2 (3KBH) [65], and C) MHV complexed with murine CEACAM1a (3R4D) [43].

1.8. Plasticity of the Spike glycoprotein

The coronavirus Spike glycoprotein is remarkably plastic, capable of accommodating mutations and deletions up to 479 (MHV) or 681 nucleotides (PRCoV) while retaining receptor binding and entry functions [66-68]. To date, large deletions in the SARS-CoV S glycoprotein have not been reported. The S protein is divided into discrete domains: an N-terminal domain, receptor binding domain (RBD), two heptad repeats, a transmembrane anchor, and an intracellular tail [43]. Discrete regions can be exchanged between strains while preserving both protein function and antibody binding [29,36]. Multiple coincident

substitutions as well as contact interface site substitutions can be tolerated to allow escape from antibody neutralization while maintaining receptor specificity [42,59,69,70]. This flexibility allows for multiple genetic pathways from the use of zoonotic receptors to the human ACE2 receptor [55].

Diversity and flexibility of the Spike glycoprotein is characteristic of coronaviruses beyond SARS-CoV. The lack of a clear ACE2 receptor binding motif (RBM) in the horseshoe Bat-SLCoV Spike, and the inability to use hACE2 as a receptor, led to an early hypothesis that the human SCoV emerged from Bat-SLCoV following a recombination event, perhaps with a NL63-like CoV, as NL63 also uses ACE2 as a receptor. Such a recombination event would have allowed direct acquisition of an ACE2 binding motif and the resulting cross-species transmission [35]. Alternatively, SARS-CoV used batACE2 for docking and entry and introduction into human/civet populations selected for mutations that enhanced interaction with the civet or humanACE2 receptor. The recently published crystal structure of NL63-CoV complexed with the ACE2 receptor shows no structural homology with the SARS-CoV RBM or the core RBD (Fig 3) [65,71]. This suggests that convergent evolution, rather than recombination-mediated transfer, lead to the common use of ACE2 by NL63 and SARS-CoV [71].

Early data suggested that the RBD of SARS-CoV and perhaps HCoV-NL63 were derived by recombination processes, rather than mutation driven evolution. While these ideas remain highly speculative, these data suggested that the S glycoprotein RBDs and/or fusion cores of CoVs may be interchangeable between distant strains. In support of this hypothesis, the consensus bat SARS-like genome HKU3 was replication competent, but was not sufficient for sequential rounds of infection, presumably because of the lack of appropriate receptors for docking and entry. The insertion of the SARS RBD into the HKU3 Spike allowed for the production of progeny virus that grew to high titer in ACE2-expressing DBT cells, and was capable of replicating in human airway epithelial cells and mouse lungs, although it grew with reduced efficiency in the latter [29]. Thus, under certain conditions, recombination processes can result in bat CoV host shifting. Further, the bat-SARS-like coronavirus with the SARS RBD was capable of replicating in mouse lungs, although with greatly reduced efficiency. It is notable that attempts to isolate CoV from bats have repeatedly failed, limiting our ability to study adaptive mechanisms or pathogenesis of CoV in host species, but that synthetic biology provides alternative sources of these viruses. The construction of a synthetic bat SARS-like coronavirus provided strong evidence that the interspecies

movement of coronaviruses, specifically SARS-like coronaviruses, resides strongly in the RBD [29]. While previous studies had indicated that small changes in the Spike glycoprotein could alter host specificity of coronaviruses, the sufficiency of a discrete RBD change in the context of a divergent 30kb genome demonstrates the RBD is a minimum determinant of species tropism. Further, it suggests a potential mechanism of host range expansion, suggesting recombination or single substitution events may allow for infection of novel hosts. Determining receptor specificities for these novel bat coronaviruses offer considerable opportunity to enrich our understanding of coronavirus receptor interactions, identify new receptors that coronaviruses use for docking and entry, and provide novel models for studying the ease and mechanism of cross species transmission.

1.9. Conclusions

Fundamental insights into the molecular mechanisms and pathways that govern virus cross species transmission is central to protecting global health. Coronaviruses readily traffic between host species and the Spike glycoprotein is the most extensively characterized viral determinant of host range expansion. Binding of the coronavirus spike to the host receptor is the minimum determinant of infectivity and species specificity, and many recent studies have demonstrated the ability of S RBD to mutate and engage ortholog receptors or escape antibody neutralization [60,62]. We need to know more about the breath of novel coronavirus receptors that are used in nature and the mechanisms governing ortholog receptor recognition. Importantly, the coronavirus RBD interface is a robust iterative model for predicting structure-function relationships between mutation-driven host range expansion, virus-receptor interactions, and antibody binding and neutralization. The SARS S-RBD model captures highly-regulated variables that recapitulate real-life biological processes critical for coronavirus cross-species transmission and host immune response (Fig 4). The SARS RBD, receptor, neutralizing antibody interface provides considerable opportunity for predicting and studying the role of mutations in cross species transmission and immunity. In addition, recent work has also expanded our appreciation of how intragenic recombination may influence coronavirus host range, as evidenced by targeted recombination, recombination between different bat coronaviruses, and identifying the RBD as a minimum determinant of host-range expansion [29,39]. While the precise ancestor and route of emergence for SARS-CoV remains unidentified, extensive sampling and phylogenetic studies of bat CoVs has raised the possibility that the epidemic strain may have jumped

directly to humans before jumping to civets. Thus, future coronavirus epidemics may be more frequent than appreciated as compared with a two step emergence model that required an intermediate host. Additionally, while it remains unclear whether recombination or mutation of Spike mediated the emergence of SARS, both mechanisms can readily impact coronavirus host range. Future studies are needed to clarify the potential roles of host proteases or antibody mediated selection in cross-species transmission, and whether modulation of RNA proof-reading activity could impact viral adaptation to a novel host. Further, structural and mathematical modeling tools offer novel predictive capabilities that, when integrated with experimental studies, will assist in predicting the ease of cross species transmission and emergence and improved therapeutic design.

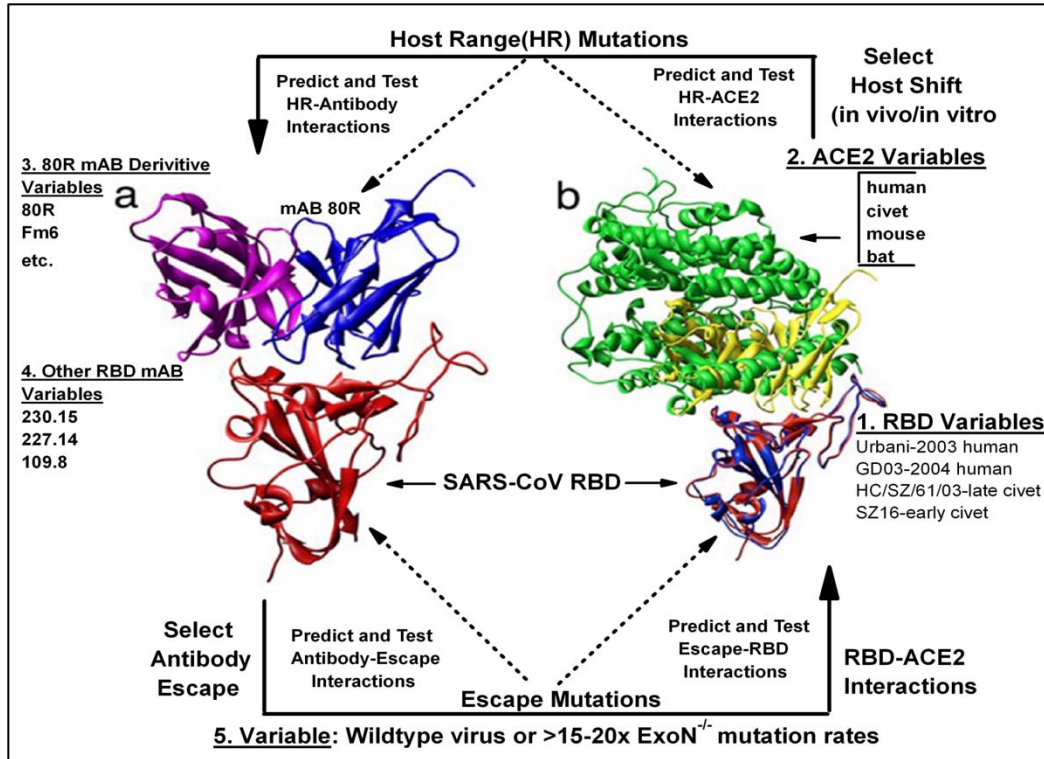


Figure 1.4: Experimental Evolution at the SARS S Glycoprotein RBD-Ligand Interface.

The SARS RBD is heterogeneous and includes defined sequence variation at specific residues that engage the ACE2 receptor from different species (Part 1 and 2). Bioinformatics can be used to predict and then test the impact of targeted mutations on variant virus-receptor interactions. Iterative rounds of mutation driven selection are also possible using recombinant viruses encoding targeted mutations and variant ACE2 receptors for docking and entry. The model allows a deep structural understanding of the potential pathways and molecular mechanisms that govern cross species transmission and pathogenesis. The biological impact of host shifting on antigenicity can be predicted using structural models of antibody-RBD interfaces, and then studied using a panel of well characterized human and mouse monoclonal antibodies targeting the different SARS-CoV RBD domains (Part 3). In parallel, neutralizing monoclonal antibodies can be used to select for escape mutations (Part 4), allowing for iterative rounds of prediction and testing on how these mutations impact host range and ACE2 recognition.

1.10. Contributions.

This work was supported by grants from the National Institutes of Health (U54 AI057157-08 and RO1 RO1AI085524) and the UNC-CH Medical Science Training Program (T32GM008719 (MEB)).

CHAPTER 2: A Double-Inactivated SARS-CoV Vaccine Provides Incomplete Protection In Mice And Induces Increased Eosinophilic Pro-Inflammatory Pulmonary Response Upon Challenge¹

2.1. Overview

SARS-CoV is an important emerging virus that is highly pathogenic in aged populations and is maintained with great diversity in zoonotic reservoirs. While a variety of vaccine platforms have shown efficacy in young animal models and against homologous viral strains, vaccine efficacy has not been thoroughly evaluated using highly pathogenic variants that replicate the acute end stage lung disease phenotypes seen during the human epidemic. Using an adjuvanted and unadjuvanted doubly-inactivated SARS-CoV vaccine (DIV), we demonstrate an eosinophilic immunopathology in aged mice comparable to that seen in mice immunized with the SARS-nucleocapsid protein, and poor protection against a nonlethal heterologous challenge. In young and one year aged animals, we demonstrate that adjuvanted DIV provides protection against lethal disease in young animals following homologous and heterologous challenge, although enhanced immune pathology and eosinophilia is evident following heterologous challenge. In the absence of alum, DIV performed poorly in young animals challenged with lethal homologous or heterologous strains. In contrast, DIV vaccines (both adjuvanted and unadjuvanted) performed poorly in aged animal models. Importantly, aged animals displayed increased eosinophilic immune pathology in the lungs, and were not protected against significant virus replication. These data raise significant concerns regarding DIV vaccine safety and highlight the need for additional studies into the molecular mechanisms governing DIV induced eosinophilia and vaccine failure, especially in the more vulnerable aged animal models of human disease.

¹ Meagan Bolles^a, Damon Deming^a, Kristin Long^b, Sudhakar Agnihothram³, Alan Whitmore^b, Martin Ferris^b, William Funkhouser^d, Lisa Gralinski^c, Allison Totura^a, Mark Heise^{a,b,c}, and Ralph S. Baric^{a,c}. Department of Microbiology and Immunology^a, Carolina Vaccine Institute^b, Department of Epidemiology^c, Department of Pathology^d, and Department of Genetics^c, University of North Carolina at Chapel Hill, Chapel Hill, North Carolina.
Copyright © American Society for Microbiology [Journal of Virology, December 2011, 85(23): 12201–12215. doi:10.1128/JVI.06048-11.]

2.2. Introduction:

Emerging in 2002 from the Guangdong province of China, Severe Acute Respiratory Syndrome (SARS) presented as an atypical pneumonia with an overall mortality rate of 10-12% that exceeded 50% in aged (>60) populations [72-74]. The etiological agent was the novel coronavirus SARS-CoV, a zoonotic virus that likely emerged from bats and spread into civets and raccoon dogs either concurrent with or prior to the human epidemic [3,40,75]. While the epidemic strain was controlled by aggressive public health intervention strategies, the possibility of a re-emergence is fueled by the presence of SARS-like CoV strains circulating in animal reservoirs [3,7,76]. Indeed, phylogenetic analysis of outbreak strains isolated during the late 2003/early 2004 epidemic suggest multiple independent emergences into the human population [22,75].

SARS-CoV is a cytoplasmically replicating, positive polarity ssRNA virus with three major membrane-bound structural proteins, Spike (S), envelope (E), and membrane (M), several unique glycoproteins, and one structural protein within the virus core, the nucleocapsid protein (N). Multiple candidate antiviral and immunomodulatory therapeutics have been developed in response to the epidemic, and vaccines would likely be a major tool in controlling any new SARS-CoV outbreak [77]. Key to the development of effective SARS vaccines appears to be the generation of neutralizing antibodies, targeting the S glycoprotein, which provide complete protection upon passive transfer and are consistently associated with protection in multiple vaccine formulations [42,78-80]. SARS vaccine strategies consist of varied formulations of inactivated [81,82], live attenuated [83], recombinant subunit [84], DNA [85,86], or subunit-vectored vaccines [87-89]. Live attenuated vaccines with deletions in nonessential proteins show some efficacy in young mice, but low antibody titers preclude sterilizing immunity and they remain untested in more vulnerable aged animals [83]. Vectored vaccines incorporating the Spike glycoprotein alone show significant protection, but are limited by strain specificity and immunosenescence [90]. Inactivated whole virus vaccines have the advantages of relative ease of production in large quantities, stable expression of conformation-dependent antigenic epitopes, and the contribution of multiple viral immunogens. However, disadvantages to inactivated formulations include the risk of vaccine preparations containing infectious virus, as well as the inclusion of antigenic determinants not associated with protection that may unpredictably skew the immune response [91]. With few exceptions, SARS vaccine formulations

have not been tested against heterologous challenges in immunosenescent models of severe end stage lung disease [90].

Effective SARS vaccines must achieve several criteria, including a) the ability to protect against heterologous viral variants that arise during independent emergence events, since many S-targeted antibodies have significantly reduced neutralization titers against heterologous spike glycoproteins [42,88,92]; b) the ability to elicit robust immune responses in elderly populations that are difficult to immunize and at increased risk for SARS-CoV-induced morbidity and mortality [93,94], and c) avoidance of adverse vaccine outcomes, such as the vaccine-induced immune pathology that has been demonstrated following vaccination with the SARS-N protein [88,95]. Whole inactivated SARS-CoV vaccines have demonstrated efficacy in young animal models, generating high titers of neutralizing antibodies, yet most challenge studies have used a virus replication model devoid of clinical disease [96-98]. In humans, inactivated SARS-CoV vaccines have been shown to induce neutralizing antibodies in healthy, young subjects in Phase 1 clinical trials [81,84,85]. However, in neither humans nor animal models have inactivated vaccines been assessed for their ability to provide protection in aged populations or to protect against heterologous challenges. Given the severity of disease in aged populations and the possibility that emergent SARS viruses will be antigenically distinct from the 2002 epidemic strain, animal models that capture severe age-related disease and allow assessment of heterologous SARS challenges are essential for the preclinical validation of any vaccine or therapeutic candidate. The aged BALB/c model reproduces the age-related susceptibility to SARS-CoV disease similar to that noted in human infections, including increased levels of SARS-CoV viral replication, more severe clinical disease, and enhanced pulmonary histopathology [41,99,100]. When challenged with zoonotic and human chimeric SARS-CoV incorporating variant Spike glycoproteins, the aged BALB/c model reproduces severe lung damage associated with human disease including diffuse alveolar damage, hyaline membrane formation, and death, thereby also providing a model for assessing vaccine-mediated protection against heterologous viruses [41].

To test these hypotheses, we characterize the efficacy of an inactivated whole SARS-CoV vaccine in a highly lethal homologous and heterologous challenge model that recapitulates the age-related susceptibility and pathologic findings seen in lethal human cases. The vaccine used was the CDC strain (AY714217) of SARS-CoV, doubly inactivated by formalin and UV irradiation, hereafter referred to as

doubly inactivated virus (DIV) [98]. The vaccine had initially been characterized in tissue culture and young mice, where it was shown to induce neutralizing antibodies and provide protection from viral replication. Adjuvanting with alum had minimal effect on the serum neutralizing titers or protection in these young mouse protection studies [98]. In this study, we chose to advance the protection and safety studies of DIV by assessing homologous and heterologous challenges in mice. We initially assess the vaccine's efficacy and potential for enhancement in a nonlethal animal model using icGD03-S. This synthetically derived virus incorporates the Spike of a human strain isolated in 2004, providing a human virus challenge that is nonetheless divergent from the vaccine strain [41]. Extending this protection study to the more stringent test of a lethal challenge, we utilize a mouse-adapted virus, icMA15, which is lethal in both young and old BALB/C mice, and is minimally different from the vaccine strain [57]. A chimeric virus incorporating the Spike of a civet strain (HC/SZ/61/03) onto the Urbani backbone provides a lethal heterologous and zoonotic challenge model [41]. These three viral challenge regimens, varied adjuvants, and an aged mouse model, help to accurately model potential challenges of vaccinating a human population against future emergences of a SARS-CoV-like zoonotic virus. Our results demonstrate a vaccine-induced enhancement of eosinophilia and inflammatory response following challenge, as well as a failure to protect against heterologous challenge and in an aged animal model. This work highlights the challenge of vaccine design for zoonotic viruses, the need for developing broadly neutralizing therapeutics, the particular difficulty of immunizing aged populations, and offers new routes for understanding SARS-CoV pathogenesis.

2.3. Methods and Materials

The generation and characterization of each of the recombinant infectious clones (icUrbani, icGD03-S, and icHC/SZ/61/03-S) have been described previously [41,101]. Briefly, all recombinant icSARS-CoV strains were propagated on Vero E6 cells in Eagle's minimal essential medium (Invitrogen, Carlsbad, CA) supplemented with 10% fetal calf serum (HyClone, Logan, UT), kanamycin (0.25 µg/ml), and gentamicin (0.05 µg/ml) at 37°C in a humidified CO₂ incubator. All work was performed in a biological safety cabinet in a biosafety level 3 laboratory containing redundant exhaust fans. Personnel were equipped with powered air-purifying respirators with high-efficiency particulate air and organic vapor

filters (3 M, St. Paul, MN), wore Tyvek suits (DuPont, Research Triangle Park, NC), and were double gloved.

VIRUSES AND CELLS.

The icGD03-S (AY525636) [102], icMA15 (FJ882957) and icHC/SZ/61/03-S [41] strains of SARS-CoV were propagated on Vero E6 cells in Eagle's MEM supplemented with 10% fetal calf serum, kanamycin (0.25 µg/ml) and gentamycin (0.05 µg/ml) at 37°C in a humidified CO₂ incubator. For virus growth, cultures of Vero E6 cells were infected at an approximate MOI of 1 for 1 hr, the monolayer washed twice with 2mls of PBS, then overlaid with complete media. At thirty hours post infection, supernatant was clarified by centrifugation at 1600 rpm for 10 minutes, aliquoted, and frozen at -70°C. Virus stocks were titrated by plaque assay.

MICE:

Vaccination and challenge. Due to the poor availability of aged mice, two slightly divergent mouse strains were utilized during the course of this research. BALB/c mice (Harlan Labs, Indianapolis, IN) were challenged with lethal viruses (icMA15 and icHC/SZ/61/03-S), while the National Institute of Aging provided BALB/cBy mice for nonlethal/epidemic strain challenges. Prior studies in our lab have shown conserved susceptibility phenotypes in these mouse strains following SARS-CoV challenge, with slightly increased morbidity and mortality in the NIA (BALB/cBy) strain. Therefore, in the nonlethal icGD03-S challenge we expected slightly more morbidity than normally would have been predicted in Harlan mice.

Female BALB/cAnNHsd mice (young [6-8 weeks old] and aged [12-14 months old]; Harlan Labs, Indianapolis, IN) were separated into 4 groups of 12 young and 12 aged mice. Mice within each group were vaccinated by footpad injection with 20 µL volumes consisting of: 0.2 µg of double-inactivated SARS-CoV vaccine; 0.2 µg of double-inactivated SARS-CoV vaccine with alum; 0.2 µg of inactivated influenza; or 0.2 µg of inactivated influenza with alum. The mice were boosted with the same regimen 22-28 days later. Aged female BALB/cBy mice (12-14 months old; NIA) were vaccinated with PBS-, alum-, or VAP- adjuvated iFlu (n=8,10,9 respectively) or DIV (n=10,9,10) immunogens, respectively. Vaccine formulations consisted of 0.2µg of DIV or iFlu, plus either PBS, 0.69mg/mL alum, or 10⁵ infectious units of VAP (VEE replicon adjuvanting particle), a dose which had previously been demonstrated to provide

protective immunity in young mice [103,104]. These mice were then boosted with the same regimen 22-28 days later.

We collected blood from tail veins prior to challenge with icMA15, icHC/SZ/61/03, or icGD03-S on day 36 post vaccination. Mice were anesthetized with a ketamine (1.3 mg/mouse)-xylazine (0.38 mg/mouse) mixture administered intraperitoneally in a 50- μ L volume. Mice were intranasally inoculated with 10^5 PFU of icMA15, icHC/SZ/61/03, or icGD03-S in 50 μ L volumes and weighed daily. At two or four days postinfection, mice were euthanized by isoflurane, and lung and serum samples were collected for analysis. For studies involving VRP vaccinations, female BALB/C mice that were 5 weeks old were immunized with 10^5 IU of VRPs expressing SARS N, Bt.CoV 279N or HA in 10 μ L volume by footpad injections. Three weeks later, blood was collected by tail nick method for ELISA, and the mice were boosted with 10^5 IU of respective VRPs. Three weeks post boost, blood was collected by tail nick for assessing antibody responses. Mice were moved to satellite facility under BSL3 conditions, acclimatized and were challenged with 10^5 pfu of rMA15 icGDO3 virus [90] by intranasal inoculation as described above.

All mice were housed under sterile conditions in individually ventilated Sealsafe cages using the SlimLine system (Tecniplast, Exton, PA). Experimental protocols were reviewed and approved by the Institutional Animal Care and Use Committee at the University of North Carolina, Chapel Hill.

PLAQUE ASSAY TITRATION OF VIRUS FROM LUNGS.

One quarter of each lung was taken for viral titer. Samples were weighed and homogenized for 60sec at 6000rpm in four equivalent volumes of PBS to generate a 20% solution. The solution was centrifuged at 13,000 rpm under aerosol containment in a table top centrifuge for 5 min, the clarified supernatant was serially diluted in PBS, and 200- μ L volumes of the dilutions were placed onto monolayers of Vero E6 cells in six-well plates. Following 1 hour of incubation at 37°C, the cells were overlaid with 0.8% agarose-containing medium. Two days later, the plates were stained with neutral red and the plaques were counted.

PLAQUE REDUCTION NEUTRALIZATION TITER ASSAYS.

We heat-inactivated mouse sera at 55°C for 30 minutes then serially diluted it to 1:200, 1:400, 1:800, and 1:3200 in PBS to a volume of 125 μ L. Next, we added 125 μ L of PBS containing 125 pfu of

icSARS-CoV to each sera dilution, incubated the virus/serum mixtures at 37°C for 30 minutes, added 200 µL of each mixture to confluent cultures of Vero E6 monolayers, and allowed them to incubate at 37°C for hour. Following the one-hour infection, we covered each monolayer with 4 mL of 0.8% agarose melted in standard Vero E6 cell medium and resolved plaques with neutral red staining two days later. Finally, we calculated the PRNT50 values—the sera-dilution at which 50% of plaques formed relative to virus not treated with sera.

LUNG HISTOPATHOLOGY.

One half of each lung was fixed in 4% PFA in PBS (pH 7.4) for at least seven days, imbedded in paraffin, sectioned to 5µm, and stained with H&E. Sections were blindly evaluated by Dr. Funkhouser for extent of tissue damage and characterization of inflammation.

VISUAL ENUMERATION OF EOSINOPHILS.

Lung tissues were prepared as above and stained with H&E or Congo Red (+hematoxylin) [105]. For each slide, an initial assessment of gross lung pathology was followed by selection of a lung section and enumeration of eosinophils within the viewing field at 400x magnification. Representative images were minimally and identically processed to enhance contrast in Adobe Photoshop CS4. For both H&E and Congo-red stained slides, multiple 160µm² sections proximate to airways were assessed and eosinophils counted were averaged per lung.

QUANTITATIVE REAL-TIME PCR.

One quarter of a lung from each mouse was placed into RNAlater® (Ambion) for 4 days at 4°C then frozen at -70°C. Lung samples were transferred from RNAlater® to Trizol®, homogenized for 60sec at 6000rpm, and RNA was extracted by chloroform/isopropanol precipitation. cDNA was prepared using random hexamers and SuperScriptII Reverse Transcriptase (Invitrogen) by standard protocols. Quantitative PCR was conducted on a Lightcycler 480II (Roche) using ABI Taqman Gene Expression Assays specific for mouse GAPD or mouse IL-4, IL-5, IFN-γ, IL-13, CCL11 (eotaxin), Cxcl1(KC). Relative quantification was calculated as log₁₀ fold-change (2^{ΔΔcT}) relative to mock-vaccinated, mock-challenged controls.

FLOW CYTOMETRY.

Mice vaccinated with PBS, DIV, or DIV + alum were challenged with 10⁵ pfu of icHC/SZ/61/03, weighed and monitored daily for morbidity, and euthanized four days postinfection by isofluorane

inhalation. Lungs were perfused with 10mLs PBS by cardiac puncture, dissected, manually minced, and vigorously agitated for two hours in digestion media [RPMI, 10%FBS, 15mM HEPES, 1.7mg/mL DNase1, (Sigma), 2.5mg/mL Collagenase A (Roche), 1x streptomycin, 1x gentamycin]. Lungs were then passed through a 75 micron cell strainer, resuspended in RPMI media [RPMI, 10%FBS, 15mM HEPES], and overlaid onto a density gradient of iodixanol diluted to a density of 1.079 gm/cm³ with RPMI 1640 containing 10% FBS (Optiprep, Sigma-Aldrich Co., St. Louis, MO). Following centrifugation cells were collected from the interface, washed, and viable cells counted by Countess® automated cell counter (Invitrogen). Cells were then incubated with the following panel of antibodies: APC anti-leukocyte common antigen (LCA, CD45PE-Cy7 anti-CD11b; and PE-Cy5 anti-MHC classII antigens, all from eBioscience (San Diego, CA); FITC anti-Gr-1 and PE anti-SiglecF, from BD-Pharmingen (San Diego, CA) and PE-Texas Red anti-CD11c (Molecular Probes (Invitrogen, Carlsbad, CA). Following staining cells were washed with FACS wash buffer [1x HBSS, 1%FBS], fixed with 2% formalin, and flow cytometry conducted on a CyAn ADP (Beckman-Coulter) with 300,000 live cell events gathered per lung sample. Analysis was performed on the Summit software (version 5.2; Beckman-Coulter). First, we gated on LCA+ and CD11c+ cells by plotting those parameters against forward scatter and gating on positive cells. Then, Gr-1 was plotted against SigLecF as shown in figure 8A. SigLecF high, Gr-1 intermediate cells were selected and CD11b versus CD11c signal was plotted for cells in that region. CD11b +, CD11c - cells are classified as eosinophils while alveolar macrophages are CD11c +, as shown in figure 8b. As seen in figure 8a, after gating on LCA+ and CD11c+ cells, Gr-1 positive cells are classified as neutrophils. Of the cells that remain after gating out SiglecF+ and neutrophils, we classify MHC class II negative, CD11b+ and B220 negative cells as monocyte-derived DCs, or mDCs. Cell counts per lung was calculated as the product of the total viable lung cell population by the percentage of gated cells in live cell events. We used a two-factor ANOVA to assess the statistical significance of age and vaccine on the overall number of eosinophils. If the ANOVA determined a factor was significant, post-hoc analyses using Tukey's Honestly Significant Differences (HSD) were used to further determine effects of treatment on eosinophil levels.

ENZYME-LINKED IMMUNOSORBANT ASSAY.

Antigen-specific IgG and IgG sub-isotype titers were determined by ELISA. Briefly, purified recombinant SARS nucleocapsid (N) protein or spike protein (S) were coupled to high-binding 96-well

ELISA plates (Greiner) in basic carbonate buffer (pH = 9.6). After washing with ELISA wash buffer (EWB – PBS with .016% Tween 20), diluted serum was added to the wells in EWB with 10% Blocking Buffer (Sigma-Aldrich). After 2 hours at 4°C, the plates were washed again and horseradish peroxidase conjugated goat anti-mouse IgG, IgG1 or IgG2a was added to the appropriate wells diluted in EWB + blocking buffer. After another 2 hours, chromogenic substrate (o-phenylene diamine in citrate buffer with added hydrogen peroxide) was added to each well. After 30 minutes, the reaction is stopped with the addition of 0.1M sodium flouride and read at 450 nm. A sigmoidal curve is fit to each set of optical density versus log₁₀ of serum dilution values using the curve-fitting software of the SigmaPlot graphics package (Systat Software, Inc.) and the inflection point (where the OD is one half of the maximum value recorded for that isotype/antigen combination) is calculated and reported as ‘half-max titer’.

2.4. Results

DIV PROVIDES PARTIAL PROTECTION AGAINST NONLETHAL HETEROLOGOUS CHALLENGE IN AGED ANIMALS

The efficacy of doubly inactivated SARS-CoV vaccines has not been evaluated in aged animals, which show immunosenescence, increased susceptibility to clinical disease, and increased pathology, reflecting conditions in the more vulnerable SARS-CoV-infected aged populations [98]. One year old National Institute of Aging mice were vaccinated with doubly inactivated SARS vaccine (DIV) or nonspecific immunogen (iFlu) in unadjuvanted form, adjuvanted with alum, or adjuvanted with VEE adjuvanting particles (VAP). SARS-specific total IgG responses, as measured by ELISA, show a significant increase in the alum adjuvanted group as compared to PBS adjuvanted group for both N-specific (3.580 vs 2.625 log₁₀ half-max titer) and S-specific (3.743 vs 2.781 log₁₀ half-max titer) antibody (Fig 1A). Unexpectedly, the VAP adjuvant nearly ablated total IgG antibody compared to PBS, reducing total S- and N-specific antibodies to titers of 0.7432 and 1.182 log₁₀ half-max, respectively (Fig 1A). The alum-adjuvanted DIV induced a strong skew in the N- and S-specific antibodies towards IgG1, a subtype associated with Th2 immune responses, while the non-adjuvanted DIV resulted in a more balanced or IgG2a-skewed antibody populations (Fig 1B).

To assess protection from heterologous SARS infection, the aged DIV-vaccinated mice were challenged with 10⁵ pfu of icGD03-S, a recombinant heterologous human strain that closely resembles circulating zoonotic strains in 2004. Both DIV and DIV +alum –vaccinated groups showed significant,

though incomplete, reductions in morbidity (as measured by weight loss) by day four postinfection, while none of the nonspecific vaccination groups showed any reduction in morbidity or lung viral titer by four days postinfection (Fig 1E,F). The VAP-adjuvanted DIV group predictably showed no reduction in morbidity or titer, consistent with the failure of DIV +VAP to induce SARS-specific antibody responses in the aged animals (data not shown). When the viral titers in the lungs were assessed, only the DIV+alum group showed significant reductions in day four lung titers, while all other groups, including DIV unadjuvanted, showed high levels of viral replication (Fig 1F). These results demonstrate that while DIV does provide some heterologous protection in highly susceptible aged populations, this vaccine is unable to provide complete protection from either viral replication or virus-induced morbidity.

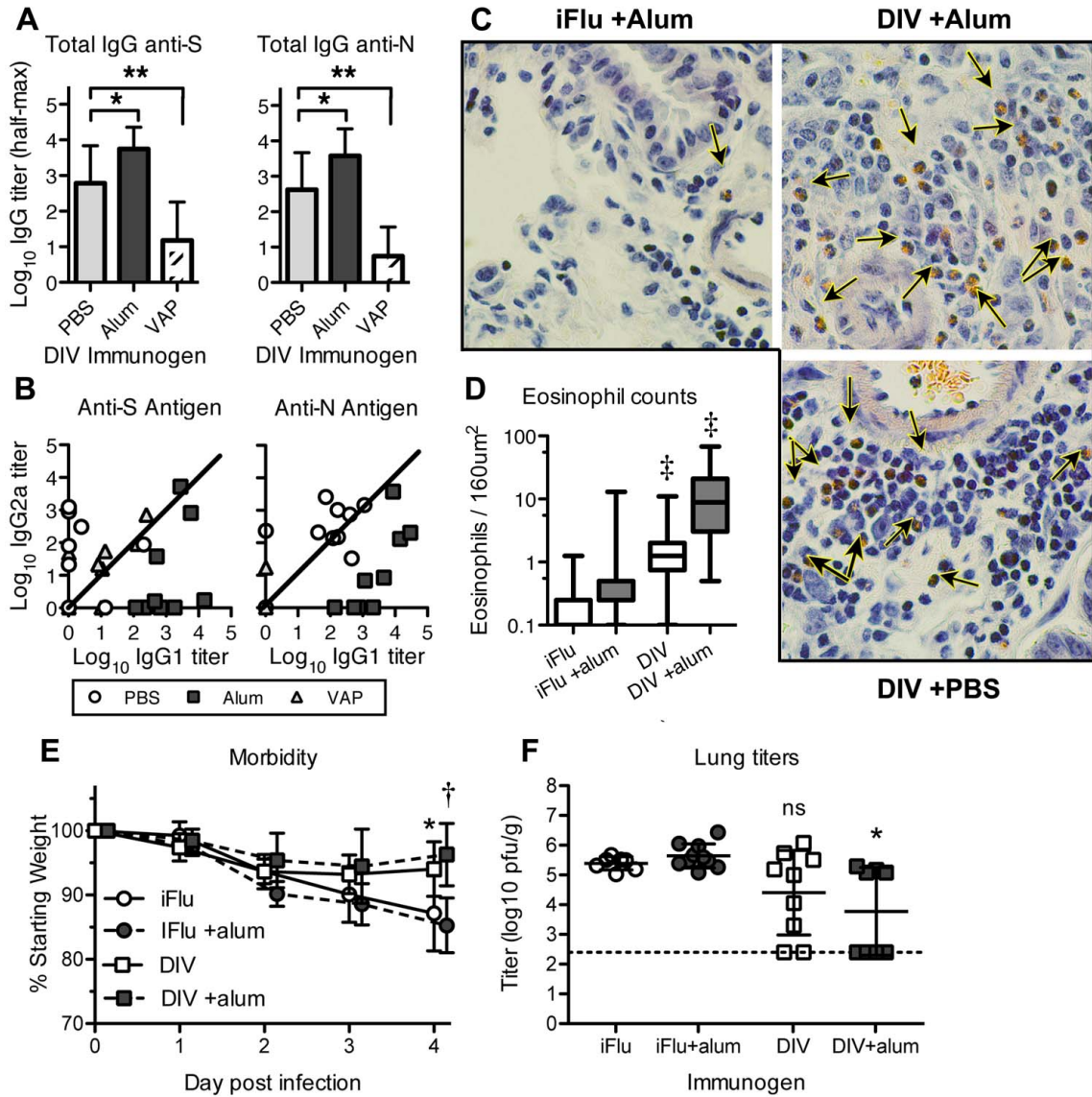


Figure 2.1: DIV vaccination and nonlethal heterologous challenge in aged animals.

A) Log₁₀ half-maximum ELISA titers for anti-N and anti-S total IgG antibodies following DIV immunization. One year aged NIA mice were immunized with DIV (n=10), DIV +alum (n=9), or DIV +VAP (n=9). Values were statistically compared by Mann-Whitney test. B) Log₁₀ half-maximum ELISA titers of IgG1 vs IgG2a subtypes. Each point represents log₁₀ IgG1 and IgG2a half-max titers for a single mouse. C) Representative images (400x magnification) of eosinophil infiltration in icGD03-S-challenged mice following DIV or iFlu vaccination regimens. Lungs taken 4 days postinfection were sectioned and stained with congo red, a reliable and specific stain for eosinophils (arrow). D) Box and whisker counts of eosinophils proximal to airways in icGD03-S-challenged aged mice, with range in whiskers. Eosinophils were counted in 4x160µm² regions proximal to airways, 5 airways per mouse. Counts were statistically compared to adjuvanted controls by t-test with Welch's correction. E) Mice challenged with the icGD03-S virus were weighed daily and visually assessed for morbidity. DIV and DIV +alum immunogens significantly reduced the morbidity associated with icGD03-S challenge by day four post-challenge. F) Mice were harvested on day 4, and one quarter of the lung homogenized and titered by plaque assay. Lung

titers were sporadically reduced for both DIV and DIV+alum groups, with only DIV +alum reaching statistical significance by Mann-Whitney. (* $p < 0.05$; ** < 0.01 ; † < 0.001 ; ‡ < 0.0001)

Previous work from our group and others has demonstrated that vaccination with SARS N protein fails to protect from SARS replication while driving a vaccine-induced eosinophilic pathology. Therefore, given that none of the DIV vaccine strategies resulted in complete protection from viral replication in the aged animals, we assessed whether any of the vaccine groups exhibited signs of eosinophilic immune pathology. Importantly, both the DIV and DIV +alum groups showed increased numbers of eosinophils in the lungs following challenge (Fig 1C). Mice vaccinated with iFlu and iFlu +alum showed a low number of eosinophils in regions proximate to airways by congo red staining: both iFlu and iFlu+alum groups had a median count of 1.0 eosinophils per region (Fig 1D). Both DIV and DIV+Alum vaccinated groups showed significant increases in eosinophil counts over the comparable nonspecific immune groups, at 5.0 and 35.0 eosinophils per region, respectively. Further, adjuvanting with alum significantly increased the eosinophil influx compared to DIV alone.

IMMUNIZATION OF YOUNG AND AGED ANIMALS

Few candidate vaccines have been tested in aged animals following homologous and heterologous lethal challenge, and no whole virus vaccines have been thus tested. Therefore, we assessed whether the DIV formulations would protect against heterologous and homologous lethal challenges in young and aged animal models. As a control, vaccination with inactivated influenza virus with or without alum did not induce detectable levels of anti-SARS (Urbani) antibody in either 12-week young or 59-week aged mice (data not shown). When young mice were vaccinated with 0.2 μ g of the SARS-CoV DIV, 8/16 generated detectable levels of SARS-neutralizing antibody titers. Vaccination with DIV +Alum induced detectable levels of neutralizing antibody in 15/15 mice and at significantly increased PRNT levels compared to DIV alone (Fig 2). Specifically, the mean (\pm SD) PRNT50 value for DIV alone was 221 \pm 220, which significantly differed from the DIV+Alum group's neutralizing titer of 2710 \pm 992 (Fig 2). Importantly, DIV alone did not induce detectable levels of anti-SARS antibodies in aged mice, while the addition of alum increased the response in aged animals, with 8/14 aged animals generating detectable levels of neutralizing antibodies. The PRNT50 value had a mean of 425 \pm 806, significantly reduced by about 6-fold as compared with DIV +alum vaccinated young animals. Thus in young and aged animals, the presence of alum in the

DIV vaccine formula significantly improved the induction of SARS-CoV neutralizing antibody: from moderate to high levels in young, and from immeasurable to moderate levels in aged animals.

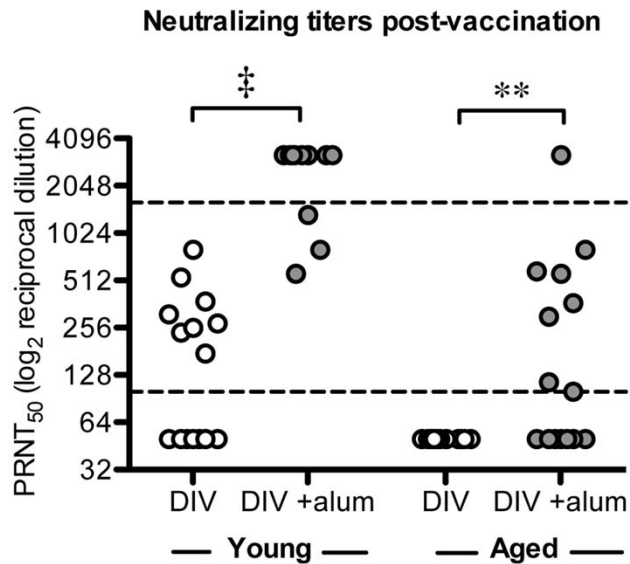


Figure 2.2: Neutralizing antibody titers of vaccinated mice.

PRNT₅₀ values of sera collected from young and aged mice vaccinated with DIV or DIV +alum. Neutralizing titers were significantly reduced in both aged vaccination groups compared to young groups (DIV $p < 0.01$, DIV+alum $p < 0.0001$; Fisher exact test). Alum adjuvant significantly increased neutralization titers for both young and aged animals (** $p < 0.01$, ‡ $p < 0.0001$; 2-tailed Mann-Whitney test). No neutralizing antibody was detectable for young or aged mice vaccinated with iFlu ($n=15$, $n=16$ respectively) or iFlu+alum ($n=14$, $n=15$ respectively); data not shown. PRNT₅₀ values below the limit of detection were assigned a value of 50 and those above the upper limit of quantification a value of 3200. (LLOQ = 100 and ULOQ = 1600).

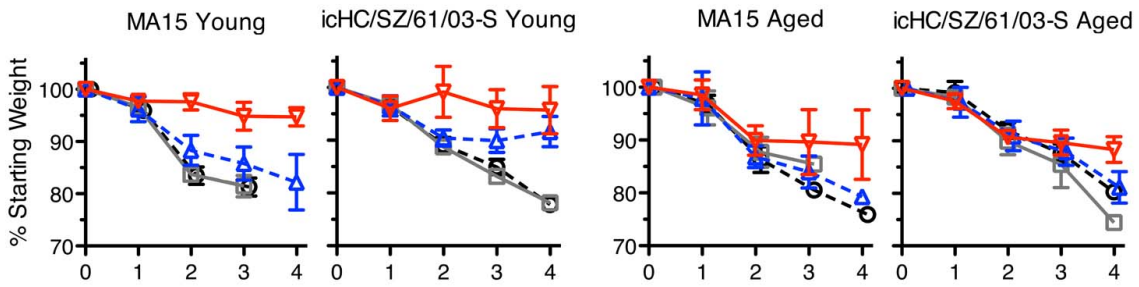
LETHAL MOUSE-ADAPTED AND ZOONOTIC CHALLENGES IN YOUNG MICE

To directly assess vaccine mediated protection from lethal disease in young and old animals, mice were challenged either with the homologous mouse adapted icMA15 virus or the heterologous zoonotic virus icHC/SZ/61/03-S. In young animals, DIV provided partial protection, increasing survival following challenge with icMA15 from 0% to 83.3%, and significantly reducing morbidity by day 3 ($p < 0.01$, 2-tailed Mann-Whitney test). In contrast, DIV +alum provided complete protection from morbidity and mortality by 4 days post-infection in icMA15-challenged mice (Fig 3A,B). When young mice were challenged with icHC/SZ/61/03-S, both DIV alone and DIV +alum groups provided complete protection from mortality. The DIV +alum group showed complete protection from morbidity, while DIV-immunized groups showed mild weight loss. The nonspecifically vaccinated groups (iFlu and iFlu+alum) lost ~20% of their starting

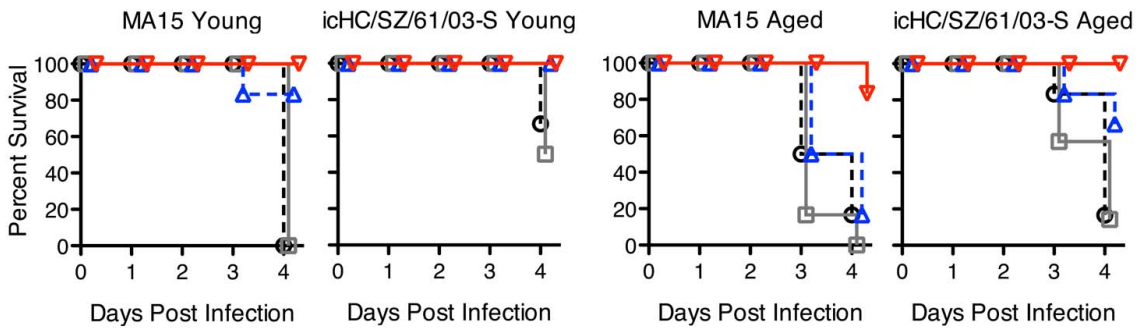
weight by day 3 (icMA15) or day 4 (icHC/SZ/61/03-S) post-infection, respectively. Furthermore, the iFlu and iFlu +alum vaccinated icMA15-infected animals showed 0% survival by day 4, while the same groups challenged with icHC/SZ/61/03-S showed 67% and 50% survival, respectively. In short, although DIV-mediated protection was not complete, there was partial protection from homologous and heterologous lethal challenges in young animals, and this protection from weight loss and death was enhanced by the inclusion of alum adjuvant.

When viral titers were assessed in the lungs at day 4 post infection, young mice vaccinated with DIV+alum showed no detectable viral titer following either viral challenge (Fig 3C). In contrast, for DIV alone, lung titers following icMA15 challenge were reduced to undetectable levels in only 1 of 5 surviving mice, and the remaining 4 had titers ranging from 5.65 to 6.41 log₁₀ pfu/g. Following icHC/SZ/61/03-S challenge, viral titers in DIV-vaccinated mice were reduced to undetectable levels for all but 1 mouse (3.74 log₁₀pfu/g). In comparison, the iFlu-immunized groups had titers ranging from 3.65 to 4.83 log₁₀ pfu/g (iFlu) and 4.72 to 5.14 log₁₀ pfu/g (iFlu +alum). Therefore, in agreement with morbidity data, DIV +alum was able to provide complete protection in young animals, while DIV alone reduced but did not eliminate viral replication following homologous or heterologous challenge.

A Morbidity



B Survival



C Lung viral titer

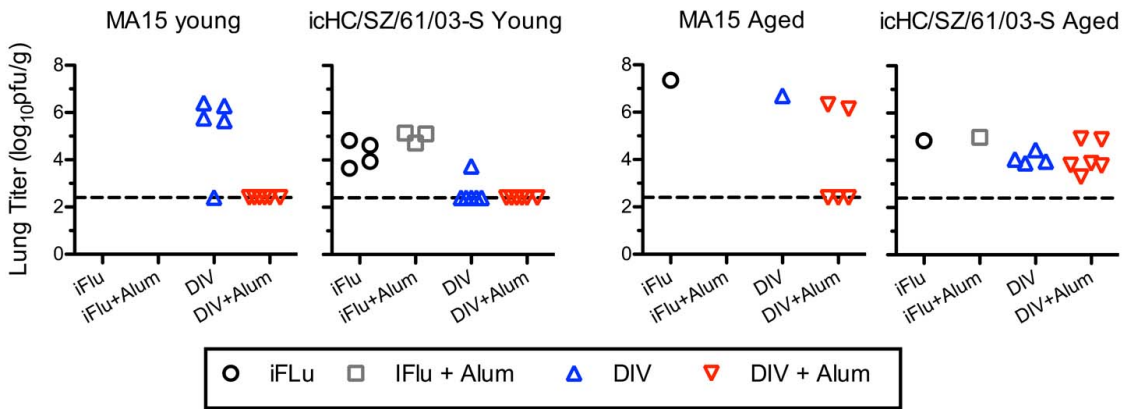


Figure 2.3: Morbidity and Mortality of lethal MA and zoonotic challenges following DIV immunization.

Young and aged mice were vaccinated with iFlu, iFlu +alum, DIV, or DIV +alum (n=6 per group) and subsequently mock infected (data not shown) or challenged with 10^5 pfu of icMA15 or icHC/SZ/61/03-S. Mice were weighed daily and monitored for morbidity (A) and mortality (B). Four days postinfection lungs were harvested and viral load assessed by plaque assay (C). Values were statistically compared by Mann-Whitney test.

LETHAL MOUSE-ADAPTED AND ZOONOTIC CHALLENGES IN AGED MICE

In stark contrast to the encouraging results seen in young animals, one year aged animals vaccinated with either DIV alone or DIV +alum did not show complete protection from mortality, and both groups demonstrated significant morbidity with weight loss and high levels of viral replication. As in young animals, iFlu vaccinated groups showed a ~20% weight loss by day 3 (icMA15) or 4 (icHC/SZ/61/03-S) post-infection. Survival following icMA15 challenge was 16.7 and 0% on day 4 for iFlu and iFlu+alum, respectively; following icHC/SZ/61/03-S challenge these rates were 16.7% and 0%, respectively. Unlike young animals, aged groups vaccinated with DIV alone did not show promising reductions in morbidity, mortality, or viral titer following these lethal challenges (Fig 3). icMA15 or icHC/SZ/61/03-S-challenged groups vaccinated with DIV alone had greater than 20% weight loss by day four, and the DIV immunization provided no significant increases in survival for either virus challenge (16.7% icMA15, 66.7% icHC/SZ/61/03-S). The one surviving mouse following icMA15 challenge had a lung viral titer of 6.70 log₁₀ pfu/g, and following icHC/SZ/61/03-S challenge the surviving mice had lung titers ranging from 3.89 to 4.44 log₁₀ pfu/g, which was slightly reduced compared to the peak titers seen in surviving iFlu vaccinated control mice (4.83 and 4.98 log₁₀ pfu/g). In contrast to DIV alone, DIV +alum did significantly increase survival rates for aged mice after both icMA15 and icHC/SZ/61/03-S challenges compared to the iFlu +alum immunized groups. Following icMA15 challenge, aged mice vaccinated with DIV+alum showed 83.3% survival by day four (vs 0% iFlu+alum; p<0.01, 2-tailed Fisher Exact Test), and the comparable group challenged with icHC/SZ/61/03-S showed 100% survival (vs 0% iFlu+alum; p<0.01, 2-tailed Fisher Exact Test). However, mice in both icMA15 and icHC/SZ/61/03-S-challenged groups had significant weight loss compared to mock-infected controls (p<0.05 for both) (Fig 3A). Additionally, DIV +alum reduced lung titers to undetectable levels by day four in only 3 of the 5 surviving icMA15-challenged animals, and did not eliminate virus from any of the surviving icHC/SZ/61/03-S-challenged animals despite 100% survival in these animals (Fig 3C).

PATHOLOGIC FINDINGS IN icMA15 OR icHC/SZ/61/03-S CHALLENGED ANIMALS.

DIV alone failed to provide complete protection from SARS replication and disease in both young and old animals, while DIV +alum failed to prevent weight loss in aged animals, suggesting that neither vaccine formulation would protect from SARS-induced respiratory pathology. We therefore evaluated the

lungs of animals from each of the vaccination groups for vaccine-induced pathology. Lethal challenges to naïve mice generally result in a denuding bronchiolitis and apoptotic debris in the airways of both young and old animals. Young mice challenged with icHC/SZ/61/03-S displayed diffuse parenchymal alveolitis, while challenge with icMA15, and both challenges to aged mice, demonstrate additional pathology including diffuse alveolar damage (DAD) and hyaline membrane formation, both hallmarks of acute respiratory distress syndrome (ARDS) in SARS cases (young: Fig 4; Aged: Fig 5).

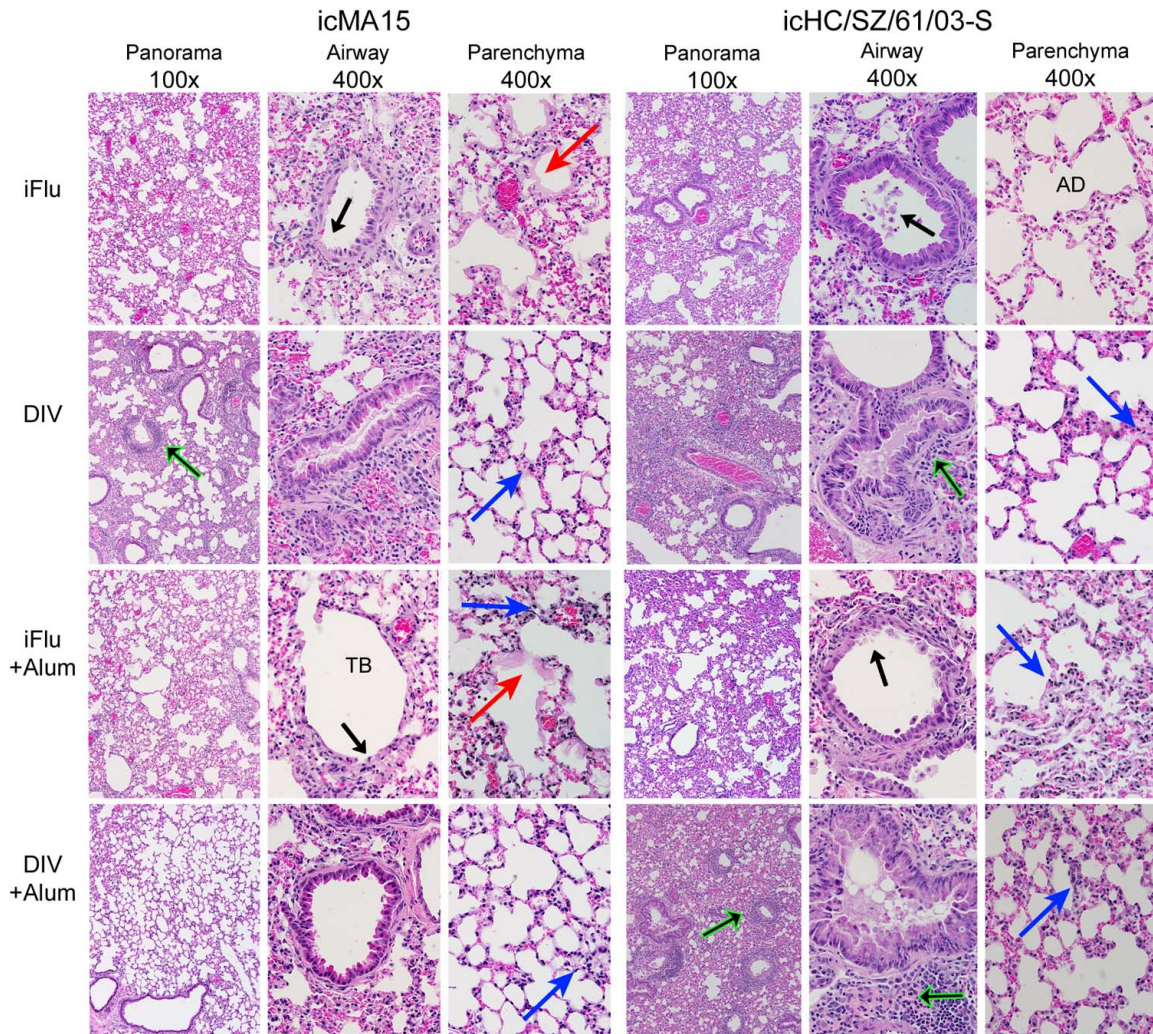


Figure 2.4: Pathology in young mice challenged with icMA15 or icHC/SZ/61/03-S.

Representative images of H&E stained lung panorama (100x), airway (400x), and parenchyma (400x) sections from young mice vaccinated with the indicated immunogen and challenged with icMA15 or icHC/SZ/61/03-S. TB = terminal bronchiole; AD = alveolar duct; black arrow = denuded airway; blue arrow = acute alveolitis and septal congestion; green arrow = peribronchovascular cuffing; red arrow = hyaline membrane.

Young animals vaccinated with DIV suffered significant pathologic changes that were generally worse in icMA15 than icHC/SZ/61/03-S challenged animals. Compared to mock-vaccinated groups, the DIV-vaccinated groups showed increased perivascular and peribronchial cuffing as well as scattered infiltrates in the parenchyma, including neutrophils, alveolar macrophages, and eosinophils (Fig 4). DIV-vaccinated aged animals showed greater pathology than young, particularly perivascular cuffing and interstitial thickening (Fig 5). These results indicate that not only did the DIV vaccine fail to protect from viral replication and morbidity/mortality, but the vaccine actually promoted the development of enhanced inflammatory damage within the lungs.

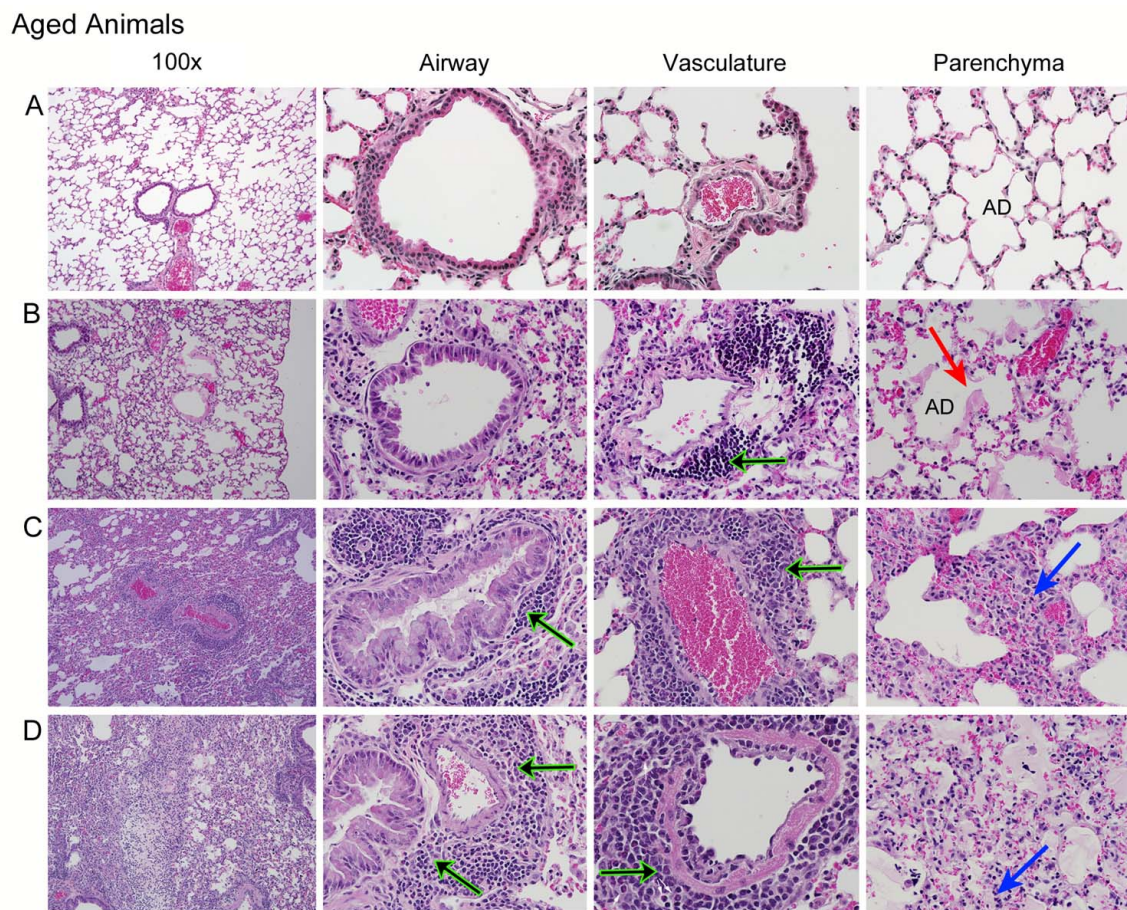


Figure 2.5: Pathology following immunization and subsequent lethal challenge in aged Harlan mice.

Representative H&E stained sections of panorama (100x), airway (400x), vasculature (400x), or parenchyma (400x) lung regions from aged mice. A) mock infected B) iFlu+alum vaccinated, icHC/SZ/61/03-S challenge C) DIV+ alum vaccinated, icHC/SZ/61/03-S challenge D) DIV+alum vaccinated, icMA15 challenge.

The adjuvanted vaccine, DIV+alum, well protected young mice from icMA15 challenge, showing minimal pathologic changes. Yet despite good protection from weight loss or lethality, DIV+Alum icHC/SZ/61/03-S-challenged mice showed histopathology more extensive than in unvaccinated mice, with increased peribronchiovascular cuffing consisting of mature lymphocytes, macrophages, and eosinophils (Fig 4). In aged animals, DIV+Alum provided little protection against either challenge, demonstrating pathology beyond the unvaccinated, with additional perivascular and peribronchial cuffing, as well as fibrinous exudates in the alveolar parenchyma (Fig 5C,D).

AGED ANIMALS HAVE INCREASED TH2 EFFECTOR AND EOSINOPHIL-ASSOCIATED CYTOKINE MRNA

Given the Th2-associated skew in antibody profiles (Fig 2), and the broad influx of inflammatory cells in vaccinated mice (Figs 4,5), we used quantitative RT-PCR to analyze in vivo cytokine mRNA expression following vaccination and challenge (Fig 6). Aged mice vaccinated with DIV+alum and challenged with icHC/SZ/61/03 have elevated mRNA levels of Th2 effector cytokines, including IL-13 and IL-5, at two and four days post-infection ($p < 0.01$ for each). The eosinophil chemoattractant CCL11 (eotaxin) is significantly increased in the lungs of vaccinated mice at both 2 and 4 days post-infection ($p < 0.01$). By contrast, IL-4 and IFN- γ shows no significant changes at these timepoints (the earliest of which is day 2), and the neutrophil associated chemokine, Cxcl1, is elevated in mock-vaccinated rather than DIV-vaccinated groups ($p < 0.05$).

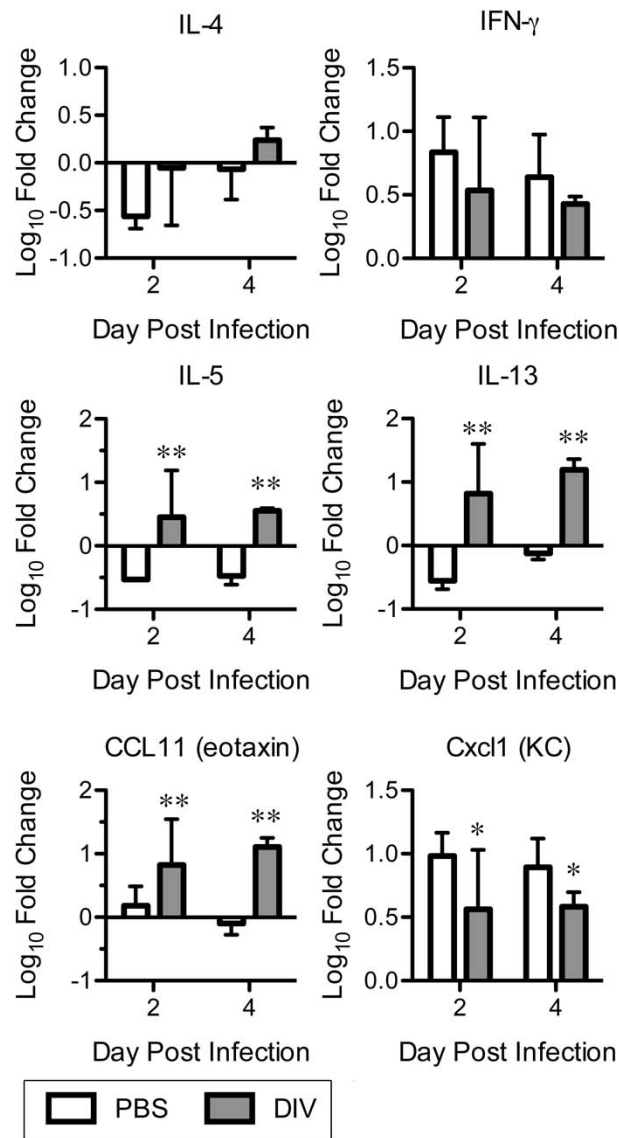


Figure 2.6: Cytokine and chemokine mRNA expression profiles in aged mice.

RNA was taken from the lungs of aged mice vaccinated with DIV+alum and challenged with icHC/SZ/61/03 at 2 and 4 days post-infection. Cytokine and chemokine mRNA was measured by quantitative rt-PCR. Values are shown as Log₁₀ fold-change over an unvaccinated, unchallenged control. (*p<0.05; **<0.01)

VACCINATION AND LETHAL CHALLENGE INDUCE AN EOSINOPHILIC PULMONARY INFILUX

The presence of high numbers of eosinophils among the inflammatory infiltrates following vaccination and subsequent challenge has been a consistent observation associated with RSV and measles vaccine-induced immunopathology, and was observed in vaccination experiments with the SARS-nucleocapsid immunogen peaking at four days post-infection [88,95]. To assess the eosinophilic influx

following whole virus immunization and lethal challenge, we blindly assessed H&E-stained lung sections of aged mice challenged with HC/SZ/61/03-S and enumerated eosinophils proximate to airways.

Representative images of 400x magnification regions proximate to airways are shown in Figure 7A, with counts of eosinophils per 160 μ M2 in Figure 7B. A median 9.0 eosinophils per 160 μ M2 were present around airways of DIV-vaccinated groups, comparable to the median 11.0 present in DIV+alum groups. These counts are significantly greater than in the iFlu (median 1.0) and iFlu +alum (median 0.0) groups, respectively (Fig 7B). These data suggested that increased eosinophilia occurs following DIV and DIV+alum vaccination in young and aged animals, especially following heterologous challenge.

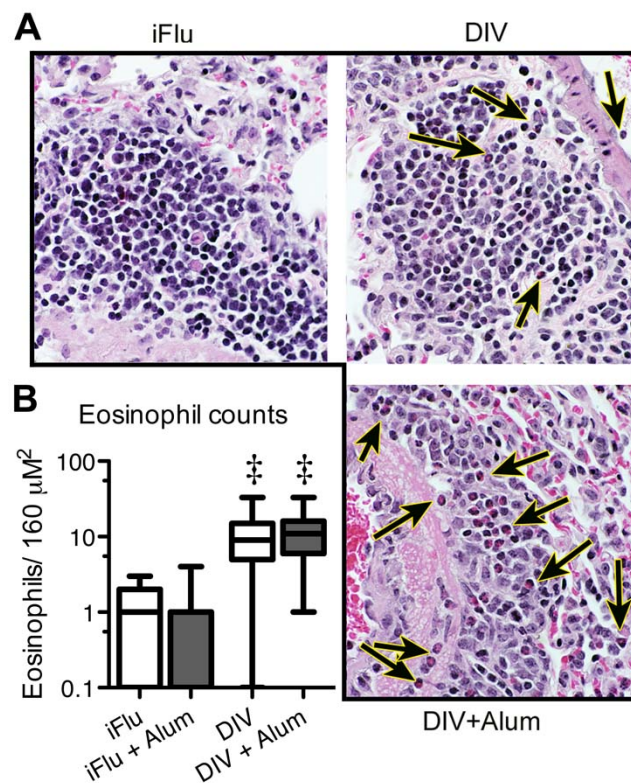


Figure 2.7: Visual identification of eosinophils following lethal challenge.

Eosinophils proximal to airways were counted in H&E stained sections of lung from aged icHC/SZ/61/03-S-infected mice. A) Representative images of regions counted, with eosinophils highlighted by black arrows. B) Box and whisker counts of eosinophils proximal to airways in icGD03-S-challenged aged mice, with range in whiskers. Eosinophils were counted in 4x160 μ m² regions proximal to airways, n=31 fields per group. Both DIV and DIV+alum immunized mice had visibly more eosinophils present following challenge compared to the nonspecific immunogen groups (\ddagger $p < 0.0001$, t-test with Welch's correction).

To precisely characterize the inflammatory infiltrate following DIV vaccination, we challenged PBS, DIV, or DIV+alum immunized young and aged mice with icHC/SZ/61/03-S and examined whole

lungs by flow cytometric analysis at four days post-infection. Eosinophils, defined as LCA+ SiglecF+ CD11b+ CD11c- populations (Fig 8), were significantly increased in all vaccinated populations compared to unvaccinated following lethal challenge (Fig 8A, $F_{2,32}=14.739$, $p<1\times 10^{-4}$) (Fig 9A). Post-hoc analysis using Tukey's HSD shows that both DIV ($p=0.0003433$) and DIV+alum ($p<1\times 10^{-4}$) groups had significantly increased numbers of eosinophils compared to PBS-immunized animals. Adjuvant had no measurable effect on eosinophilic influx, as DIV- and DIV+alum-immunized mice did not have statistically significant differences in their overall numbers of eosinophils in either age group. Importantly, the elevated eosinophil counts were comparable between young and aged populations despite divergent clinical presentations. Further analysis of the inflammatory cell infiltrates of vaccinated mice shows a strong influence of age on the neutrophil ($F_{1,32}=22.0339$, $p<1\times 10^{-4}$) and monocytic dendritic ($F_{1,32}=26.681$, $p<1\times 10^{-4}$) cell influx, with both cell populations significantly increased in aged relative to young animals (Fig 9B,D). Alveolar macrophage counts showed no significant differences compared to mock vaccinated in either young or aged animals (Fig 9C). Finally, the vaccinated animals showed significantly fewer monocytic DC counts by day 4 post-challenge, independent of age ($F_{2,32}=11.18$, $p=0.0002079$), and post-hoc analysis shows differences were enhanced by the alum adjuvant ($p=0.04402$) (Fig 9D). Vaccination with DIV clearly induces a strong eosinophilic infiltrate independent of age and regardless of whether it protects from morbidity, and raises the possibility that DIV will elicit immune pathology in the face of heterologous SARS challenge.

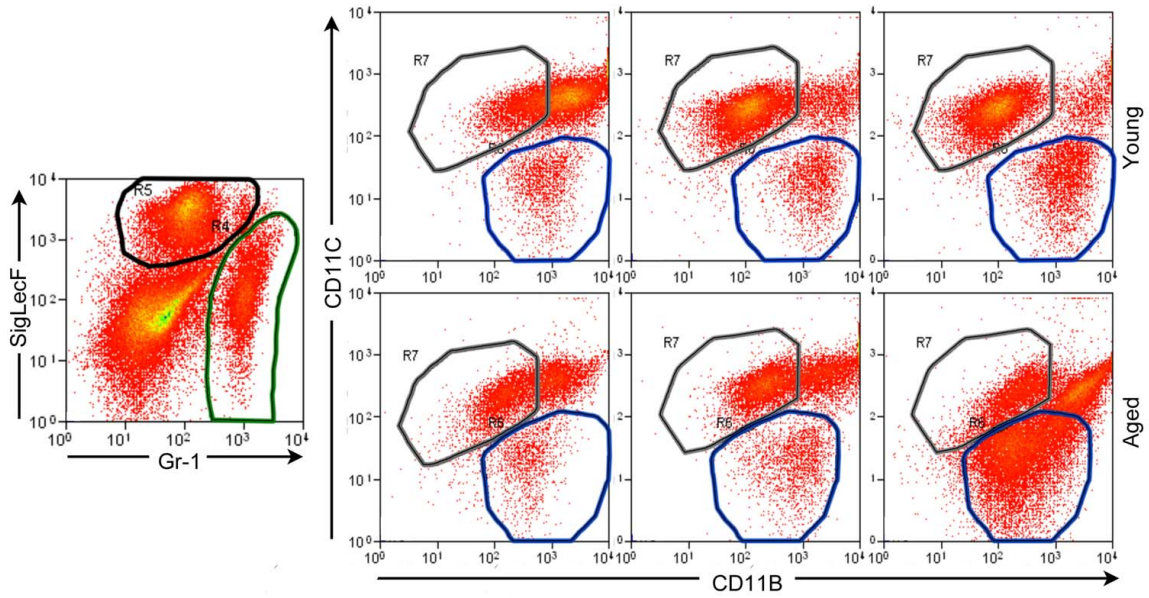


Figure 2.8: Flow cytometry gating strategy for cell populations.

A) Representative (PBS vaccinated) plot of LCA+ lung cell populations. Neutrophils were defined as live cells, LCA+, Siglec-, GR-1+ (green gate). SiglecF+ populations (black gate) from young and old mice were further analyzed, as shown in B. B) Representative images of eosinophil (CD11b+, CD11c-; blue gate) and alveolar macrophage gates (CD11c+; grey gate) for young and aged mice vaccinated with PBS, DIV, or DIV+alum.

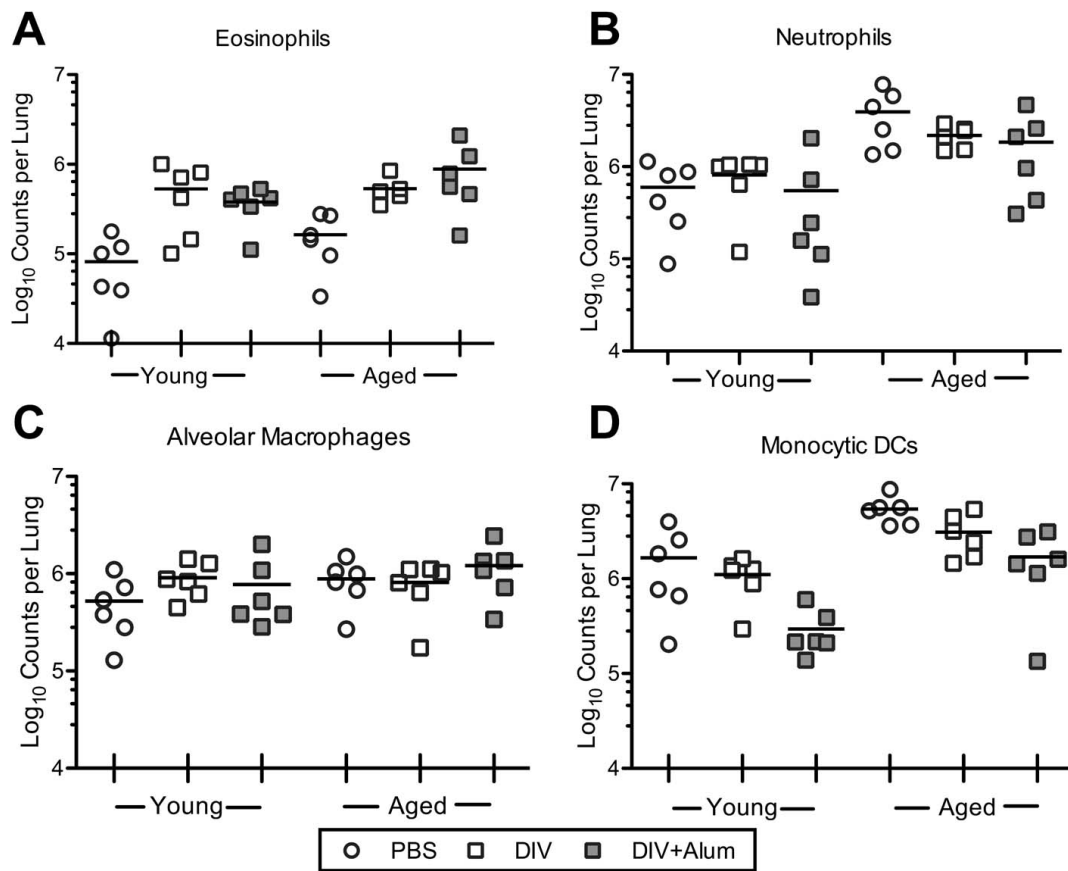


Figure 2.9: Flow cytometric analysis of additional lung immune cell populations in young and aged mice following immunization and subsequent lethal challenge.

Mice challenged with icHC/SZ/61/03-S were sacrificed 4 days post infection and lungs stained with an eight color panel. Each point represents the cell population for an individual mouse. A) Eosinophil counts for each of the vaccination groups (n=6 per group). Regardless of the age of the mice, the eosinophil counts were significantly increased in both DIV and DIV+alum immunized groups compared to mock-vaccinated ($F_{2,30}=15.81$, $p<1 \times 10^{-4}$). B) For neutrophil counts only age was a significant factor ($F_{1,30}=24.7150$, $p=2.525 \times 10^{-5}$). Alveolar macrophage counts were significantly affected by immunogen in young but not aged animals, with posthoc analysis indicating both DIV and DIV+alum significantly different from mock vaccinated ($F_{2,30}=3.5534$, $p=0.04121$). Monocytic dendritic cells (mDCs) were also significantly affected by age ($F_{1,30}=20.3622$, $p=9.193 \times 10^{-5}$) as well as immunogen ($F_{2,30}=9.5681$, $p=0.0006107$), with posthoc analysis indicating significant reductions in mDC counts in DIV+alum groups relative to both DIV and mock groups.

VACCINE INDUCED EOSINOPHILIA IS A COMMON FEATURE OF N PROTEINS ACROSS GROUP 2B CORONAVIRUSES

The data from our studies collectively demonstrated that eosinophilic infiltration occurs during DIV vaccination in both young and aged mice populations, irrespective of the adjuvant and the challenge virus used. Previous data from our laboratory has shown that vaccination with Venezuelan Equine

Encephalitis Virus Replicons (VRPs) expressing SARS N protein (VRP N) induces a similar eosinophilic phenotype while completely failing to protect against SARS CoV replication [88], suggesting that the eosinophilia may be driven by SARS N protein. To identify whether sequences intrinsic to SARS N protein or a N protein from a group 2b coronavirus closely related to SARS contribute to the induction of eosinophilia, we immunized mice with VRPs expressing SARS N, the N gene from a bat coronavirus BtCoV.279 (VRP 279 N), or an irrelevant antigen VRP HA (containing hemagglutinin gene from PR8 strain of influenza). The BtCoV.279 N gene shares 95% sequence homology with SARS N gene with conservation across all the major domains of N protein. Groups of mice immunized with 10^5 IU of VRP N and VRP 279N showed high antibody titers post boost (data not shown), and were challenged with 10^5 pfu of rMA15 GDO3-S. This virus causes 15% weight loss in infected young BALB/c mice by day 4 post infection [90]. Mice from all the groups showed 15% weight loss by day 4 post infection with virus titers ranging to 10^5 pfu (data not shown), indicating failure of N gene based vaccines to protect from virus replication. Histological analysis of congo red stained lung sections showed increased number of eosinophils proximal to airways in VRP N immunized mice compared to VRP HA immunized mice (Fig 10A). Interestingly, enhanced influx of eosinophils was also found in regions proximal to airways in lungs from mice immunized with VRP 279 N (Fig 10A). Blind scoring from lung sections indicated a median count of 25 eosinophils per region in VRP N and 279 N immunized groups, whereas the VRP HA group showed a median count of 3 per region (Fig 10B). These data clearly indicated that eosinophilia is driven by immune responses to sequences intrinsic to SARS nucleocapsid protein and is conserved in N proteins across group 2b coronaviruses.

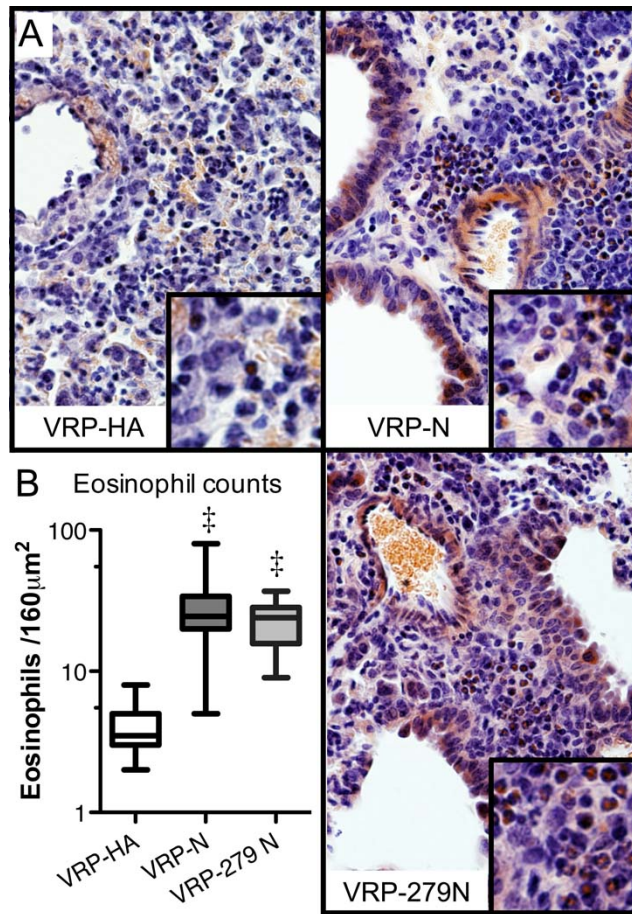


Figure 2.10: Eosinophilia influx is conserved across Group 2b N-proteins.

Young mice immunized with VRPs expressing the SARS N protein (VRP N), the N protein from another group 2b bat coronavirus, BtCoV.279 (VRP 279N) or an irrelevant antigen (VRP-HA) were challenged with icGD03 and lungs taken 4 days post-infection. A) Representative images of lung sections (400x) stained with Congo red. B) Both the SARS N and BtCoV.279 N proteins induce a significant eosinophilic inflammatory influx compared to the irrelevant antigen. (\ddagger $p < 0.0001$)

2.5. Discussion

Human coronaviruses HCoV 229E, HCoV OC43, and the SARS-CoV, each likely originating from animal reservoirs, have demonstrated the high proclivity for coronaviruses to cross the species barrier, adapt, and colonize the human host. Though not currently circulating in humans, SARS-CoV, like other zoonotic viruses, remains a significant re-emerging disease threat given its maintenance in animal reservoirs. The development of vaccines or therapeutics for SARS-CoV is complicated by several challenges: the presence of a large heterogeneous zoonotic reservoir of related strains, the resistance of highly susceptible aged populations to vaccination, and potential disease enhancing complications of the

vaccine formulations [88,95]. Though many experimental SARS vaccine formulations have been developed, whole inactivated virus vaccines have the advantage of large scale production, presentation of multiple epitopes, and conformation stability [83,85-89].

Aged populations are classically difficult to vaccinate, and suffer increased disease pathologies following infection with a variety of respiratory viruses including influenza virus, RSV, HCoV OC43, and the SARS-CoV [93]. Until recently, most published assessments of SARS-CoV vaccine efficacy utilized models capable of assessing only viral replication or antibody induction, and are routinely conducted in animal models that elide important human disease presentations [82,83,88,96-98]. While necessary, these assessments are incomplete, especially because more robust lethal challenge models have been developed that recapitulate severe end stage lung disease pathologies and allow assessment of the potential complications of senescence [41,99,100,106]. As shown here, a vaccine that appears protective in young animals is much less protective, and potentially pathogenic, in an aged animal model.

SARS-CoV emerged from a heterologous pool of closely related animal strains, suggesting that future outbreak emergences will likely involve strains with unique changes in the S glycoprotein. The viral strains used in this study represent a homologous lethal challenge virus (icMA15), as well as a nonlethal human heterologous virus (icGD03-S) and a lethal zoonotic virus (icHC/SZ/61/03-S), which allowed us to directly test whether DIV was capable of providing effective protection against heterologous viruses in both young and highly susceptible aged populations. Importantly, the DIV vaccine provided partial clinical protection against both homologous and heterologous challenge in young animals, and this protective effect was enhanced by alum adjuvant. By contrast, even the adjuvanted DIV vaccine failed to protect against virus-induced disease and viral replication following homologous or heterologous challenge in aged animals. Perhaps most importantly, though DIV+alum protected against viral replication, disease, and respiratory pathology following homologous viral challenge (icMA15) in young animals, which is consistent with prior reports [96-98], both DIV alone and DIV+alum failed to protect against respiratory pathology following homologous challenge in aged animals, and both vaccine formulations failed to protect against respiratory pathology following heterologous challenge in mice of any age (Fig 4,5). These results further demonstrate the difficulty in eliciting protective immune responses in highly susceptible elderly population

and indicate that in the face of a re-emergent SARS virus, likely antigenically heterologous from the 2002 outbreak strain, existing vaccine formulations are likely to fail to provide protective immunity.

In addition to the general failure of the DIV or DIV+alum vaccines to elicit protective immunity against heterologous SARS viruses or provide protection even against homologous viral challenge in aged animals, both the DIV and DIV+Alum vaccine formulations results in significantly enhanced immune pathology within the lungs compared to control animals. Although adjuvanted DIV protected young animals from morbidity and mortality following lethal challenges, the heterologous virus, icHC/SZ/61/03-S, induced a lung pathology more severe in vaccinated than in unvaccinated mice (Fig 4). This increased pathology was not correlated with weight loss or mortality through day four post-infection (Fig 3), but the increased immune infiltrate indicates the vaccine is not fully protective against heterologous challenges. Further, in aged animals recalcitrant to immunization, insufficient protective immunity correlated with a significantly increased immunopathology. Thus, evidence of enhanced disease subsequent to vaccination was evident in both heterologous challenge models and models of immune senescence.

In each of the experiments conducted here, immunization with the whole inactivated SARS vaccine induced increased inflammatory infiltrates and pulmonary eosinophilia upon subsequent challenge, demonstrating the potential for dangerous clinical complications. This is consistent with two prior studies of vaccine formulations incorporating SARS N, where N-specific immune responses resulted in enhanced eosinophilic immune pathology [88,95]. This pathologic signature is reminiscent of the two known human examples of vaccine-induced immunopathology, atypical measles and enhanced RSV. For both of these vaccine induced immunopathologies, infection subsequent to vaccination resulted in a failure to control viral replication, enhanced clinical disease, and a pathology characterized by increased complement deposition and inflammation, a skewing towards a Th2 responses, and eosinophilic influx [107]. Cytokine profiles of DIV+alum vaccinated and icHC/SZ/61/03-challenged mice showed increased levels of Th2 effector cytokines and eosinophil chemokines (IL-5, IL-13, and CCL11/eotaxin) compared to mock-vaccinated groups (Fig 8). In contrast, IFN- γ and IL-4 (Th1 and Th2 inducing cytokines) were unchanged at 2 and 4 days post-infection, likely because the peak mRNA levels for these inducing cytokines were earlier in the timecourse of infection.

As previous studies had indicated peak eosinophilia at four days post-infection, we assessed lung eosinophilia by both histopathology and flow cytometry at this timepoint, quantifying significant increases in the lungs of vaccinated mice following CoV challenge [88]. Eosinophilia was present independent of age and independent of the alum adjuvant, although adjuvant did increase the magnitude of the eosinophilic influx. DIV-induced eosinophilic influx was present even in the animals that were protected from morbidity and mortality. When this protection was absent, eosinophilic immunopathology was a dominant response more severe than the viral pathology seen in unvaccinated controls. The eosinophilia in clinically protected animals may thus serve as a marker for a potentially pathogenic immune responses. While recent studies have argued that eosinophils are not the primary mediators of RSV vaccine-induced immune pathology, they may contribute to increased airway hyperresponsive conditions, including asthma, and the pathophysiology of viral infections [108,109].

Only eosinophils were consistently and significantly increased in response to vaccination with DIV. By contrast, neutrophils and monocytic DC populations were significantly affected by age, and monocytic DCs were decreased as a function of vaccination. The greater population of neutrophils in aged animals following challenge, independent of vaccination, suggests that neutrophils may contribute to the increased severity of SARS-CoV pathogenesis in the aged. A pathogenic role for neutrophils in infection has been demonstrated for other respiratory viruses, including influenza, suggesting conserved mechanisms of enhanced respiratory pathology in the aged [110,111].

SARS-CoV targeted neutralizing antibodies are sufficient to provide complete immunity against lethal SARS challenges in multiple animal models, and show evidence of controlling disease severity in human infections [42,78,80,88,112-114]. Spike-specific antibodies are both neutralizing and protective up to one year post-vaccination in mice, while anti-nucleocapsid antibodies are neither neutralizing nor protective, and further appear detrimental to the longevity of protective antibodies [88,95]. This deleterious effect does not appear to be antibody mediated (ADE) since passive transfer was unable to replicate the immunopathology, though low post-transfer antibody titers preclude definitive exclusion of this potential mechanism [88,115].

While multiple major and minor SARS-CoV antigens are incorporated in DIV, the N protein is the most likely agent of eosinophilic immunopathology [116]. N is a strongly immunogenic protein [117-120],

is the most abundant protein in infection [116], and has been shown in prior studies to induce immunopathology when delivered in isolation [121]. This nucleocapsid-induced enhancement is not apparent in animals with appreciable levels of neutralizing antibodies, indicating that the induction of sufficiently neutralizing antibody responses can protect against SARS vaccine-induced immune pathology. However, the results presented here clearly demonstrate that in situations where individuals fail to mount protective anti-SARS responses, as is the case with either heterologous viral challenge or in immune senescence, the DIV vaccinated individuals are at significant risk for vaccine-induced immune pathology. With this in mind, it will also be important to determine the mechanisms by which N vaccination promotes immune pathology, with a key question being whether pathology is simply due to a non-protective response against N or if N vaccination actively skews the host immune response to promote immune pathology. Given that N has been shown to modulate innate immunity and act as an interferon antagonist, it is possible that N sufficiently alters the host immune response to induce a Th2 skew and subsequent inflammatory pathology [122]. Indeed, immunization with N appears to induce a Th2 skewing of the immune response regardless of adjuvant or formulation, suggesting the nucleocapsid protein alone may well be the defining factor in CoV vaccine induced enhancement (K. Long, D. Deming, R. Baric, and M. Heise, manuscript in progress) [88,95]. Therefore, additional studies are required to assess whether N's innate immunomodulatory activity is linked to the N vaccine induced immune pathology, and if so, whether this reflects a more general trait of viral interferon antagonists in modulating the downstream host adaptive immune response.

The major conclusion that can be drawn from these studies is that although DIV SARS vaccines do elicit protection under optimal conditions (homologous challenge in immunocompetent individuals), more stringent challenges reveal likely failures. If DIV vaccine approaches are to be used for SARS in the future, efforts must be made to improve the quality and magnitude of the vaccine-induced immune response while limiting the vaccine's capacity to induce immune pathology. The whole virus vaccine used in this study was doubly inactivated by UV irradiation and formalin [98]. Formalin-inactivated vaccines are suggested to skew the immune response towards a Th2 response, producing higher levels of IL-4 and increasing the relative contribution of IgG2a isotypes [123,124]. Previously, formalin inactivation leading to a disruption of fusion glycoproteins or addition of carbonyl groups had been blamed for the skewing of

FI-RSV immune responses [107,123]. However, recent studies suggest that inactivation by alternate methods still result in a Th2 skew and immunopathology, and that it is a failure of affinity maturation that results in non-protective responses and subsequent antibody-mediated enhancement [124,125]. Furthermore, the fact that the DIV vaccine did elicit neutralizing antibody responses and protection against homologous challenge in young animals suggests that the DIV-induced pathology did not simply represent a loss of antigenic epitopes. Therefore, we do not think the method of inactivation is necessarily responsible for immunopathology associated with DIV, but rather that any SARS vaccines that include the nucleocapsid protein should be investigated for challenge-induced enhancement.

The results presented here reinforce the need to find methods to enhance the protective S specific immune response while minimizing potentially pathologic anti-N response. Our observation that immunization with Bt.CoV 279N which has high sequence similarity with SARS N also induces eosinophilia, indicates that sequences intrinsic to N protein that are conserved across group 2b coronaviruses may drive this immune mediated pathology. The amino acids responsible for this response will need to be mapped. Assessment of N-induced immune pathology by sequentially divergent CoV N-proteins may allow the design of chimeric SARS CoVs that could serve as vaccines devoid of immune pathology. In both young and aged mice, adjuvanting with alum increases the immunogenicity of the DIV, concordant with many earlier studies using this adjuvant [98]. In young mice, approximately one-half the animals mounted neutralizing antibodies following DIV vaccination, and all achieved neutralizing titers when DIV was adjuvanted with alum (Fig 2). However, only half the aged mice were capable of mounting neutralizing antibody titers to DIV +alum, and none mounted such responses absent the adjuvant. Alum is one of the few adjuvants approved for use in human vaccine formulations and functions to stimulate Th2 immunity, a potentially confounding factor in the induction of immunopathology. We briefly assessed an alternative adjuvant VAP (VEE-adjuvanting particles), which is reported to stimulate Th1 immunity [124,126-128]. In contrast to reports of success in young mice, the VAP-adjuvanted formulation in aged mice ablated rather than enhanced the protective response to DIV; subsequently challenged mice showed morbidity and mortality rates comparable to unvaccinated controls (data not shown) [128,129]. While the mechanism of this ablation has not been defined, the VAP adjuvant likely functions through cross-presentation of exogenous antigens within antigen presenting cells, a process impaired in age-associated

immunosenescence [130]. VEE formulations incorporating the wild-type 3000 glycoprotein show better immunogenicity in aged animals, likely due to improved cross-presentation over the attenuated 3014 glycoprotein, suggesting that alternative VAP formulations may be more effective [90]. Therefore, if DIV approaches are to be considered for SARS or other respiratory coronaviruses, we feel that it will be important to rigorously test the vaccine and potential adjuvant in the aged mouse model to assess both efficacy and potential immune pathology in the face of immune senescence and/or heterologous viral challenges.

Emergent zoonotic viruses present novel and shifting targets for vaccine design. The clear deficiency of the doubly inactivated SARS vaccine against challenge models with divergent Spike glycoproteins highlights the need for vaccines that induce broadly neutralizing immune responses. Further, impartial conservation of viral antigens cannot be considered a benefit to vaccine formulations for coronaviruses when select immunogens induce detrimental immune responses upon challenge. The N-induced pathogenic responses appear to be masked by S-targeted neutralizing antibodies, but become dominant once the protective immunity wanes. In the case of SARS-like CoV, we cannot expect zoonotic variation to reduce specificity for N more readily than for S, as the S glycoprotein of multiple isolates shows greater sequence variation and readily evolves over the course of an epidemic [3,42,92]. Further, the conservation of N across Group2B coronaviruses, and the demonstrated conservation of N-induced immunopathology, raises the possibility that challenge with non-epidemic coronavirus strains may induce eosinophilic immunopathology in vaccinated populations. Despite the difficulty of vaccine design for zoonotic viruses such as coronaviruses, paramyxoviruses, filoviruses, etc, a growing pool of sequence data for zoonotic isolates, the rapidity of sequencing and isolation in the case of outbreaks, synthetic gene design, and the multiple vectored, inactivation, or antibody-generating platform technologies available ensure that vaccines can be readily formulated in the case of novel outbreaks [29]. The challenge for researchers and clinicians is to validate these vaccines in strong animal models and to confirm and enhance vaccine efficacy in aged individuals. Identifying the vaccine components that induce protective immunity in aging individuals will be essential to protecting this vulnerable population. The data presented herein indicate that SARS-CoV, coupled with a panel of heterologous zoonotic precursor viruses, represents a

tractable model system to evaluate the molecular mechanisms governing immunosenescence, and its impact on emerging virus pathogenesis and vaccine efficacy.

2.6. Contributions

This work was supported by grants from the National Institutes of Health, Division of Allergy and Infectious Diseases (AI075297, U54AI080680, U54 AI081680-01) and the UNC-CH Medical Science Training Program (T32GM008719 (MEB)).

We would like to thank Dr. Kanta Subbarao at the NIH for generously providing the icMA15 virus. We recognize the generous gift of the adjuvanted and unadjuvanted DIV from BEI. We would also like to thank Dr. Vineet Menachery for help in manuscript preparation.

CHAPTER 3: Iterative Development of Potent and Broadly Neutralizing Antibodies Targeting the Spike Receptor Binding Domain.

3.1. Overview

This chapter describes two collaborative projects between the Baric and the Georgiou or Marasco laboratories. Both projects are based on a single extensively characterized humanized monoclonal antibody (mAb), 80R, which was developed by the Marasco laboratory. 80R binds the receptor binding domain (RBD) of SARS-CoV spike glycoprotein (S) and is capable of neutralizing the epidemic strain of SARS-CoV, but is incapable of neutralizing heterologous human strains and is readily escaped by variants expressing a single substitution in the RBD. The Georgiou and Marasco laboratories independently generated 80R-derived mAbs intended to extend the breadth of neutralization and increase the barrier to viral escape. The Georgiou laboratory generated a series of 80R-derived single-chain fragment variable (scFv) by affinity maturation [131] while the Marasco laboratory generated their 80R-derived mAbs by using human antibody phage display libraries and panning against RBDs from either heterologous strains or escape mutants [132]. We worked in collaboration with these two laboratories to iteratively characterize each generation of antibodies by: determining their neutralization profiles on cell culture; assessing their ability to protect mice from lethal SARS-CoV challenge following passive transfer; generating, sequencing, and cloning SARS-CoV escape mutants; and by evaluating the virulence of the escape variants in mice. The highest affinity 80R derivative, SK4, was generated in the Georgiou laboratory. Neutralization escape from SK4 in cell culture required at least two concurrent substitutions in the S RBD, indicating a higher barrier to escape relative to the parent 80R, but SK4 was incapable of neutralizing viral variants bearing heterologous S from early epidemic or zoonotic strains [131]. The second and third generation mAbs designed to target heterologous and escape variant RBDs were broadly neutralizing: some neutralized every zoonotic, epidemic, and escape variant virus we tested. However, neutralization escape required only a single substitution in the S RBD and each of these mAbs readily selected for neutralization escape variants in cell culture. Concerningly, some of the resulting escape variants displayed increased pathogenesis in

murine models. These studies emphasize the utility of using infectious clone viruses, rather than pseudotyped viruses, and animal models that replicate human disease to extensively characterize the neutralization potential of nAbs. Further, these studies extend our characterization of the SARS-CoV RBD as an antiviral target. Specifically, it is apparent that mAbs targeting RBD present a low barrier to escape for the virus, and future development should include a cocktail of mAbs targeting different epitopes within the RBD; particularly if neutralization escape variants might exhibit enhanced pathogenesis. Future studies using a combination of broadly neutralizing and high affinity derivatives may provide more comprehensive neutralization profiles and escape-resistant cocktails.

3.2. Introduction

Advancements in antibody humanization technology triggered a surge in the development of therapeutic monoclonal antibodies, and although the vast majority of these products have been approved for use in cancer or autoimmunity, several mAbs targeting viruses have also been developed. More efficient antibody technologies, including isolation by phage display or B-cell immortalization and structure-guided mutagenesis, has led to the investigational development of Abs targeting a wide variety of viruses and with greater efficacy and breadth of neutralization [42,133-142]. In addition to the development of novel therapeutics, the characterization of nAbs has also provided insight into the role of Ab escape in viral evolution. For example, a panel of anti-hemagglutinin mAbs was used to demonstrate the stochastic escape patterns and seemingly limitless capacity of influenza virus to escape single mAbs with minimal fitness cost [143]. Additionally, characterization of mAbs and sera from convalescent SARS patients against panels of epidemic-associated spike glycoproteins provided strong evidence of antibody-directed evolution during the course of the SARS epidemic [42,64].

Currently, the anti-RSV monoclonal, palivizumab, remains the only approved direct-acting anti-viral mAb [144,145]. However, additional mAbs targeting rabies [146,147], HCV [148,149], HIV [149], and RSV [150,151], and mAbs targeting several other viruses, including CMV [152], influenza virus [153,154], Hendra virus [155], and Ebola virus [133] may also ultimately provide the basis for new options. The threat of highly pathogenic human coronaviruses, as evidenced by the SARS-CoV epidemic and the recent emergence of a novel coronavirus, MERS-CoV, has fueled extensive investigations into potential coronavirus therapeutics, including mAb-based options [156-158]. A substantial amount of effort has been

devoted to the production of a whole-inactivated anti-SARS-CoV vaccine in the event of a future outbreak, and the vaccine was able to protect against morbidity and mortality in non-human models of infection [159]. Unfortunately, the whole inactivated SARS-CoV vaccine has limited protection against heterologous strains and may actually enhance pathogenesis by induction of a nucleocapsid-specific cell-mediated immune response in the absence of a strong neutralizing antibody response, such as might occur in vaccinated people over time [88,159]. Monoclonal antibodies may offer advantages over vaccines, including relatively short production times, which would allow for rapid response to newly emergent viruses or antigenic variants, and potential uses for prophylaxis, such as in the case of a known or suspected exposure events, or as treatment therapy in the case of infection. Additionally, therapeutic antibodies would avoid the concerns of immune enhancement and reversion linked to inactivated or attenuated vaccines, respectively.

Of the four major structural proteins of SARS-CoV, which include the spike (S), envelope (E), nucleocapsid (N), and matrix (M) proteins, most characterized mAbs target S or N [117,160], the two most highly immunogenic viral proteins [161-163]. However, anti-S mAbs may be neutralizing while anti-N mAbs are not, and S has therefore been the preferred target for the development of antibody-based vaccines and therapies [164,165]. Further, anti-S antibody responses appear to be persistent and have been detected for up to three years post-exposure in human patients and one year post-vaccination in a mouse model, making it a particularly attractive target for vaccines [88,163]. The S1 domain of spike contains the RBD, and although antibodies can be targeted against the S2 domain, the S2 region is less immunogenic [162,166]. Indeed, anti-S1 antibodies isolated from patients infected by SARS-CoV predominated over their anti-S2 counterparts [162,164]. Anti-S2 antibodies are also less potently neutralizing [162,166], making it a less attractive target. Unsurprisingly, the RBD has become the preferred target and has led to a vastly larger proportion of anti-S1 mAbs than anti-S2 mAbs in the available repertoire [64,167].

One of the first and best-characterized anti-S mAbs is 80R, an IgG mAb isolated from a naïve human scFv lambda phage display library [168]. The 80R mAb binds the RBD and blocks interaction with the SARS-CoV receptor, angiotensin converting enzyme 2, ACE2 [169]. 80R neutralizes the virus, and can reduce viral replication in a 16-week old BALB/c mouse model of SARS-CoV infection [170]. The crystal structure of 80R in complex with the SARS-CoV RBD (pdb code 2GHW) demonstrated that 80R binds the

RBD in an epitope overlapping, but not identical to, the binding site for the ACE2 receptor, with 17 of the 29 RBD-80R contact residues shared with the RBD-hACE2 contact residues [171]. There are, however, limitations to the use of 80R as a therapeutic mAb. Sub-extinction levels of 80R in the presence of SARS-CoV routinely select for a substitution at residue D480 of S, either alanine, glycine, or tyrosine, and a substitution to alanine abolishes 80R binding while retaining binding to hACE2, effectively conferring viral escape from neutralization by the mAb [64,131,170]. Further, the 480G residue is present in late-phase independent emergence virus (GD03, 2003/04) and civet-associated SARS-CoV from the same outbreak period (2003-04), rendering these viruses resistant to 80R neutralization [64].

In an attempt to broaden neutralization of and prevent escape by SARS-CoV, we worked in collaboration with the Marasco and Georgiou laboratories to develop and test several 80R-derivative monoclonal antibodies. The Georgiou laboratory took the approach of developing a high affinity derivative of 80R. The 80R scFv was randomly mutagenized by error-prone PCR to generate a library of 1.6×10^8 independent transformants. Subsequent screening of this library using anchored periplasmic expression and decreasing concentrations of soluble RBD, mutagenized and rescreened the high affinity clones, and used site-directed mutagenesis on key binding residues to generate the RS2, SK4, and RSK scFvs, respectively [131,172]. Notably, studies of the high-affinity 80R derivatives were conducted with scFv rather than full IgG mAbs. These antibody fragments are fully capable of binding antigen, but the small size alters pharmacokinetics, allowing for more rapid tissue penetration but also rapid elimination by the kidney, complicating animal studies [173]. The original 80R antibody was reported to bind S with an equilibrium dissociation constant (KD) of 32 nM [168]. In contrast, the most affinity matured derivative, SK4, bound with an affinity 270-fold higher than the measured KD of the parent 80R scFv [131]. Here, we characterize the breadth and potency of these high affinity 80R derivatives by a series of neutralization assays with the epidemic strain, heterologous strains, and escape variants to other neutralizing scFv. Further, we selected escape mutants to both RSK and SK4 and used homology modeling of the antibody-RBD interface to explain the SK4's robust binding and escape-resistant phenotype [131].

The Marasco laboratory attempted to select for broadly neutralizing mAbs by sequentially panning human antibody phage display libraries against the RBDs of SARS-CoV strains that were homologous and heterologous to the epidemic strain. Initial attempts to develop a more broadly neutralizing mAb involved a

repeat of the initial panning of the Marasco laboratory's naïve library with two different panning targets: the RBD from the GD03 virus, which bears an S that is related to the civet-like virus strains and is heterologous to the epidemic strain, rather than the standard epidemic strain, Tor-2 (identical to Urbani in the RBD), and the Tor-2/Urbani RBD with the D480A substitution. The antibody resulting from panning with GD03 as a target, 11A, could neutralize GD03 but not Tor-2/Urbani. The antibody that bound the D480A-RBD could bind but not neutralize a SARS-CoV S-bearing pseudovirus [64]. In an alternative approach, the Marasco laboratory used structural biology to identify key residues of 80R that interacted with the RBD and used both chain shuffling of the Vkappa light chain and focused mutagenesis of the CDRL1 (aa161-164) to create 80R-cs and 80R-fm libraries. These libraries were panned against 4 RBD targets: Tor2, Tor2-D480A, Tor2-D480G, and GD03 [64]. Several of these second generation mAbs derived from these libraries were broadly neutralizing, but the most broadly neutralizing mAb was Fm6 [64]. Follow-up studies characterizing Fm6 and the other second-generation mAbs are described in Sui et al 2013, a manuscript in preparation with relevant extracts included below. This manuscript also describes the characterization of a third generation of mAbs, Y12 and Y112A, designed to be both broadly neutralizing and, by binding RBDs expressing the Fm6 escape substitution, capable of blocking a neutralization escape pathway.

3.3. Increased Antibody Affinity Confers Broad In Vitro Protection against Escape Mutants of Severe Acute Respiratory Syndrome Coronavirus¹

3.3.1. Overview

Even though the effect of antibody affinity on neutralization potency is well documented, surprisingly, its impact on neutralization breadth and escape has not been systematically determined. Here, random mutagenesis and DNA shuffling of the single-chain variable fragment of the neutralizing antibody 80R followed by bacterial display screening using anchored periplasmic expression (APEX) were used to generate a number of higher-affinity variants of the severe acute respiratory syndrome coronavirus (SARS-CoV)-neutralizing antibody 80R with equilibrium dissociation constants (KD) as low as 37 pM, a >270-fold improvement relative to that of the parental 80R single-chain variable fragment (scFv). As expected, antigen affinity was shown to correlate directly with neutralization potency toward the icUrbani strain of SARS-CoV. Additionally, the highest-affinity antibody fragment displayed 10-fold-increased broad neutralization in vitro and completely protected against several SARS-CoV strains containing substitutions associated with antibody escape. Importantly, higher affinity also led to the suppression of viral escape mutants in vitro. Escape from the highest-affinity variant required reduced selective pressure and multiple substitutions in the binding epitope. Collectively, these results support the hypothesis that engineered antibodies with picomolar dissociation constants for a neutralizing epitope can confer escape-resistant protection [131].

3.3.2. Introduction

It is well established that the potency of neutralizing antibodies for either viruses or bacterial toxins depends on affinity [150,174,175]. Surprisingly, engineering antibodies with increased affinity has not been investigated as a strategy for conferring broader protection as a means to hinder escape. A higher antigen affinity results from a higher $\Delta G_{\text{binding}}$. While antibody-antigen interactions are often dominated by

¹ Mridula Rani,^a Meagan Bolles,^f Eric F. Donaldson,^f Thomas Van Blarcom,^b Ralph Baric,^c Brent Iverson,^{a,c} and George Georgiou^{a,b,d}

Institute of Cellular and Molecular Biology,^a Department of Chemical Engineering,^b Department of Chemistry and Biochemistry,^c and Department of Molecular Genetics and Microbiology,^d The University of Texas at Austin, Austin, Texas, USA; Department of Epidemiology^e and Department of Microbiology and Immunology^f, University of North Carolina at Chapel Hill, Chapel Hill, North Carolina, USA
Copyright © American Society for Microbiology [Journal of Virology, September 2012, 86(17): 9113–9121 doi:10.1128/JVI.00233-12]

interactions with a binding “hot spot” on the antigen, a high $\Delta G_{\text{binding}}$ can also arise from additional interactions between the epitope and the paratope [176]. Accordingly, we hypothesized that increasing the affinity of 80R for the RBD can elicit broader neutralization [131]. Variants of the 80R scFv anti-body fragment exhibiting up to 280-fold-higher affinity for the RBD were generated by random mutagenesis and screening using Escherichia coli display by anchored periplasmic expression (APEX) [172]. As expected, in vitro neutralization potency against the icUrbani strain correlated directly with affinity. Importantly, neutralization of viruses containing the RBD D480A or D480Y mutation that evaded neutralization by 80R [170] also correlated with affinity. Only reduced selective pressure with lower concentrations of the high-affinity antibody led to the evolution of SARS-CoV escape mutants, which contained, in addition to D480Y or D480A, secondary amino acid substitutions within the 80R epitope.

3.3.3. Materials and Methods:

VIRUSES AND CELLS

Recombinant viruses icUrbani (AY278741), icGD03-MA and icHC/SZ/61/03 were propagated in Vero E6 cells [41,90,101]. Vero E6 was maintained in MEM media (Invitrogen, Carlsbad, CA) supplemented with 10% Fetal Clone II (Hyclone, South Logan, UT) and gentamycin / kanamycin (UNC Tissue Culture Facility). Growth curves were performed in Vero E6 with the different wild type or mutant recombinant-derived escape mutant viruses at a MOI of 0.1 for 1 hour and overlaid with medium. Virus samples were collected at various time points post infection and stored at -70°C until viral titers were determined by plaque assay.

Virus titers were determined as plaque forming units (PFU) by plating 6-well plates with 5×10^5 Vero E6 cells per well and inoculating cultures with 200 μl from the 10-fold serial dilutions. Cells were incubated with the virus for 1 h at 37°C and overlaid with 3 ml of 0.8% agarose in complete media. Plates were incubated for 2 days at 37°C and plaques were visualized by staining with neutral red for 3-6 hours. Virus concentration was calculated as PFU/ml. All virus work was performed in a Class II biological safety cabinet in a certified bio-safety level 3 laboratory containing redundant exhaust fans while wearing Tyvek suits and Powered Air Purifying Respirators.

ISOLATION OF ESCAPE MUTANTS UNDER NEUTRALIZING ANTIBODY SELECTIVE PRESSURE

1 x 10⁶ PFU of icUrbani were incubated with 20 µg of a neutralizing scAb (RSK, SK4 or 80R) in a 200µL volume for 30 min and then inoculated onto cells in the presence of the respective scAb antibody fragment at a concentration of 20 µg/ml. The development of cytopathic effect (CPE) was monitored over 72 hrs and progeny viruses harvested. Antibody treatment was repeated two additional times and more rapid CPE noted with each passage. The viruses from passage four were plaque purified in the presence of antibody and neutralization resistant viruses were isolated. The S glycoprotein genes from four individual plaques for each neutralization experiment were sequenced and the neutralization titers between wild type and antibody-resistant viruses were determined as described below.

In the experiment above, the SK4 scAb resulted in the extinction of parent viruses on three separate occasions. To increase the probability of escape mutant evolution, we incubated 1 x 10⁶ PFU of icUrbani with decreasing concentrations of SK4 ScAb antibody fragment (15, 10, 5 and 1 µg) for 30 minutes, and then infected cultures in the presence of 5 µg/ml SK4 antibody. Depending on treatment conditions, cytopathology was evident either within 48 h (5, 1 µg doses) or was minimal after 4 days (15 and 10 µg). Low dose SK4 treated progeny viruses (1 and 5 µg doses) were treated with 5 µg of SK4 for two passages, and then selected with one additional treatment of 10 and 15 µg doses, resulting in highly antibody resistant viruses that produced extensive CPE in cultures within 24-36 hours. High-dose treated stocks were passaged once in the absence of antibody (pass 2) to restore virus titers, and then reselected two times in the presence of 5µg antibody. Two final treatments of 10 and 15 µg of SK4 antibody resulted in highly resistant populations that rapidly produced CPE in culture. Two to four plaques were isolated from each treatment regimen (9 plaques total) in the presence of 20 µg SK4 antibody and the S glycoprotein gene was sequenced.

PLAQUE REDUCTION NEUTRALIZATION ASSAY (PRNT)

Each scAb in the panel (80R, RSK, RS2, and SK4) was serially diluted 1:2 in PBS starting at 30 µg/mL. Wild-type icUrbani, icGD03-MA and icHC/SZ/61/03 were diluted and approximately 100 PFU of each was added to the scAb dilution series for 30 minutes at 37°C. The percentage neutralization was calculated as 100 - (number of plaques with antibody / number of plaques without antibody) X 100. For 50% plaque reduction neutralization titers (PRNT50s) of single-substitution variants, the viruses were

diluted to 100 PFU and added to 2-fold serial dilutions of SK4 starting at 5 µg/ml. The single-substitution variants are escape mutants developed against mono-clonal antibodies, as previously described (L443R and T332I [62] and D480G [64]) or as described above (Y436H, Y442S, and N479I).

3.3.4. Results

SARS-CoV NEUTRALIZATION AND ESCAPE.

To evaluate the neutralizing ability of the purified 80R, SK4, and RSK scAbs, we conducted plaque reduction neutralization titer assays with each of the scAbs against SARS-CoV (icUrbani). As expected, the neutralization potencies of the antibodies increased according to affinity. Compared to 80R (IC₅₀, 0.722 µg/ml), both RSK and SK4 exhibited 10-fold-greater neutralization (IC₅₀, 0.069 µg/ml and 0.059 µg/ml, respectively) (Fig. 3). For antibodies 80R and RSK, in vitro neutralization escape mutants of the icUrbani strain emerged after three passages in cell culture, and four plaques for each antibody were picked for sequence analysis. Three of the four 80R escape mutants carried a mutation from aspartic acid to alanine at position 480 (D480A), and one had a mutation of aspartic acid to tyrosine (D480Y), replicating the D480 residue identified by previous selection with the full IgG version of this antibody [64,170]. In the case of the RSK antibody, three of the four escape variants had the D480Y mutation and one had a Y436H mutation (Table 2).

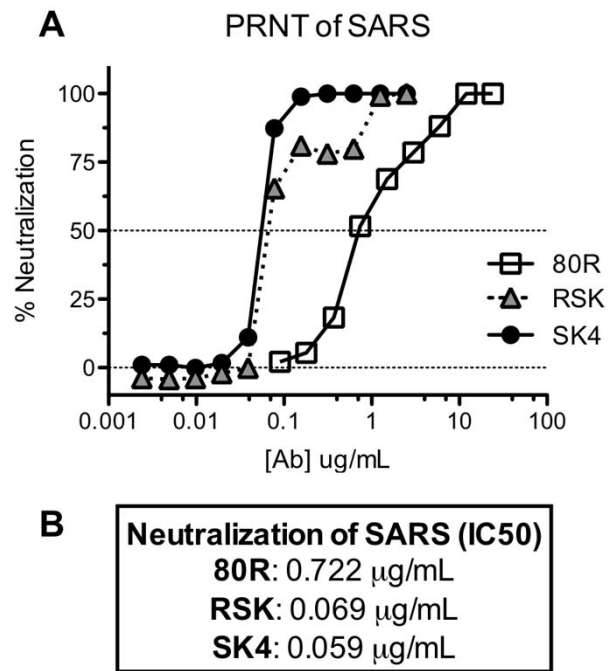


Figure 3.3.3: Neutralization activity of the SK4 and RSK scAbs in comparison to 80R.

Neutralization activity was tested by plaque reduction assay against icUrbani. Approximately 100 PFU of icUrbani was incubated with the scAb dilution series. The percentage neutralization was calculated as $[100 - (\text{number of plaques with antibody} / \text{number of plaques without antibody})] \times 100$.

Table 3.3.2: Amino acid changes in the RBD of spike protein found in the neutralization escape mutants.

| ScAb | Mutation(s) | No. of clones with mutation/ total sequenced |
|------|-------------|---|
| 80R | D480A | 3/4 |
| | D480Y | 1/4 |
| SK4 | N479I+D480Y | 9/9 |
| RSK | D480Y | 3/4 |
| | Y436H | 1/4 |

Importantly, the SK4 antibody exhibited very high neutralizing potency, and 20 μg was sufficient to completely extinguish 1×10^6 PFU of the parent virus, yielding no escape variants. Therefore, the initial concentration of SK4 scAb was decreased to reduce the selective pressure and was incrementally increased over multiple viral passages. A total of nine plaques were isolated from the final selection with 20 μg SK4 and sequenced.

All nine of the isolated escape mutants contained two mutations: N479I and D480Y (Table 2). Both D480 and N479 have been found to be highly adapted RBD residues that allow specific binding to hACE2, and mutations at these positions decrease their affinity for hACE2 and hence infectivity [177]. D480 has been shown to have a critical role in the binding of the parental antibody 80R to the RBD [170,171], and substitution to a tyrosine has been shown not to affect the binding of the RBD (and therefore the virus) to the human ACE2 receptor [178]. The mutation N479I had been found in bananin-resistant virus, and this position is found to correspond to a highly variable site in the RBD [179].

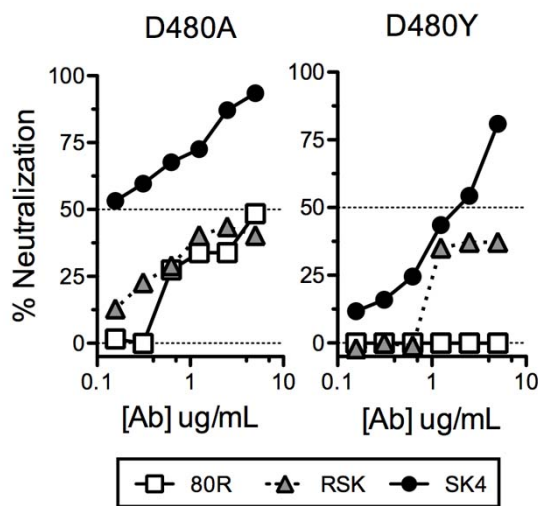


Figure 3.3.4: Cross neutralization studies of high-affinity scAbs with escape mutants with the D480A and D480Y mutations.

Cross neutralization studies with mutant viruses encoding either D480A or D480Y, which mediated escape from 80R and its derivatives, were performed with all three antibodies (Fig. 4). Importantly, SK4 successfully neutralized both escape mutants, suggesting an enhanced role for high affinity in overcoming the effect of D480 substitutions. We note, however, that none of the scAbs could neutralize the civet strain icHC/SZ/61/03 or the mouse- adapted variant of the human 03/04 strain, icGD03MA; the latter strain carries a Y436H mutation associated with increased mACE2 receptor usage [29] (data not shown). The spike proteins of GD03 MA and HC/SZ/61/03 each differ from that of the icUrbani strain at six other amino acid positions within the RBD (Table 3), and evidently, at least some of these are critical for antibody binding.

Table 3.3.3 Amino acid differences in the RBD of the spike protein

| Strain | Amino acid at position: | | | | | | |
|------------------------------------|-------------------------|-----|-----|-----|-----|-----|-----|
| | 344 | 360 | 436 | 472 | 479 | 480 | 487 |
| Urbani (human 02/03) | K | F | Y | L | N | D | T |
| HC/SZ/61/03 (civet) | R | S | Y | P | R | G | S |
| GD03MA (mouse-adapted human 03/04) | R | S | H | P | N | G | S |

To further assess the breadth of SK4 neutralization, we tested SK4 neutralization against several viruses that emerged as escape variants to other monoclonal antibodies reported earlier [62,64]. These viruses contained single substitutions in the RBD, both within and outside the 80R/SK4 interface. Two escape variants, L443R and T332I, were developed under selection with the broadly neutralizing antibodies s230.15 and s109.8, respectively [62]. Residue 443 is a contact interface site with ACE2 but not with 80R, while residue 332 does not directly interface with either 80R or ACE2. The escape variants Y436H, Y442S, N479I (data not shown), and D480G emerged following selection with 80R derivative antibodies and contain substitutions that interface with 80R and, except for D480G, also interface with the ACE2 receptor [171].

SK4 was capable of neutralizing all six of these antibody escape variants. Three of the escape variants, namely, Y436H, Y442S, and T332I, were neutralized with an efficacy comparable to that observed with icUrbani (IC50s of 0.049 $\mu\text{g/ml}$, 0.039 $\mu\text{g/ml}$, and 0.109 $\mu\text{g/ml}$, respectively, compared to 0.059 $\mu\text{g/ml}$ for icSARS) (Fig. 5). Importantly, SK4 neutralized three other escape variants, with IC50s lower than the IC50 displayed by 80R for icUrbani [0.234 $\mu\text{g/ml}$ (L443R), 0.432 $\mu\text{g/ml}$ (N479I), and 0.542 $\mu\text{g/ml}$ (D480G), compared to an IC50 of 0.722 $\mu\text{g/ml}$ for 80R with icUrbani]. Thus, viruses containing amino acid substitutions at either N479 or D480, which when combined mediated escape from SK4, were neutralized with a lower IC50 than that of 80R for icUrbani.

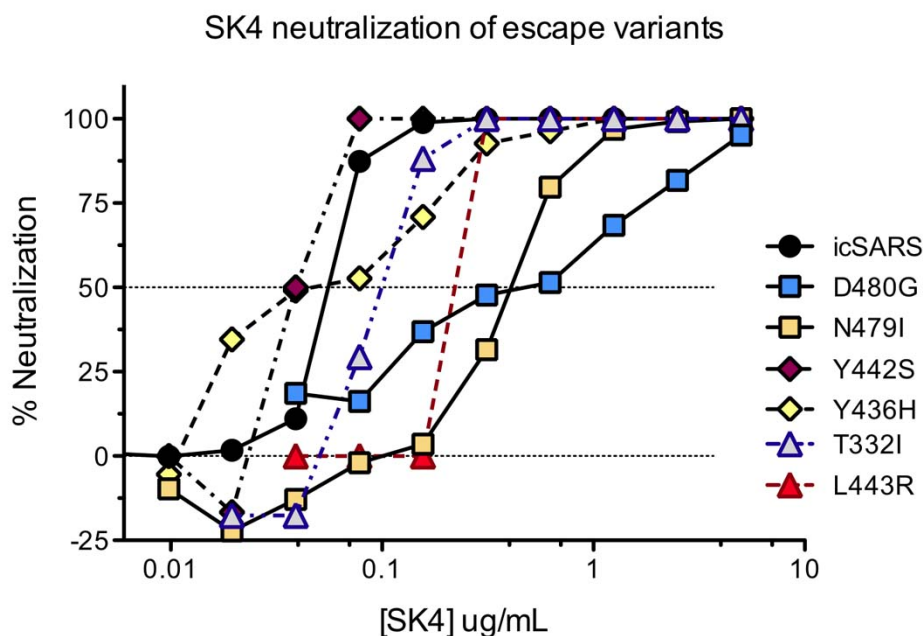


Figure 3.3.5: SK4 neutralization of escape variants.

Neutralization activity of SK4 was tested against escape variants, and the IC50s were compared to that of icUrbani.

3.3.5. Discussion

Individually, the substitutions N479I and D480G each cause a shift in neutralization that is nonetheless insufficient to escape SK4, reinforcing the necessity of double substitutions to escape the high-affinity neutralization by SK4. Additional substitutions either selected by 80R-derived antibodies or derived independently of 80R antibodies are also incapable of providing escape from SK4. It is worth noting, however, that while SK4 is capable of neutralizing each of the single-substitution spike variants we tested, it is unable to neutralize the more divergent spikes, i.e., those containing variants in six or seven positions relative to the icUrbani strain. This suggests that high-affinity neutralizing antibodies like SK4 would provide excellent resistance to escape and would be best paired with a broadly neutralizing antibody for a highly effective therapeutic cocktail.

Just as important as neutralization breadth, higher affinity appeared to suppress the formation of viral escape mutants. At a concentration of 80R that readily gave rise to escape mutants, incubation with the highest-affinity antibody, SK4, led to no CPE or viral plaques after multiple attempts. In order to

further understand the potential role affinity might play during simulated infection, the anti-RBD antibodies were intentionally used at sub-neutralizing concentrations in an effort to generate viral escape mutants. Sequencing revealed that the most common RBD mutation observed in the escape mutants generated by all antibodies was D480Y. For SK4, the highest-affinity antibody in the study, escape mutants could be generated only when the concentration of antibody was reduced further, and it required two mutations in the RBD: N479I and D480Y. The accumulation of two mutations for escape from the action of the neutralizing antibody would of course be expected to be a much more rare event, and thus the incidence of such escape variants in a therapeutic setting would likely be low. However, we do note that even SK4 failed to neutralize SARS-CoV HC/SZ/61/03 and GD03MA, presumably because the RBD in these strains contains multiple mutations that drastically alter the character of the binding epitope (Table 3).

In a recent study, Zhang et al. used a sequential antigen panning (SAP) method and successfully isolated broadly cross-reactive antibodies with two- to threefold lower IC₅₀s than the parent HIV-1-neutralizing antibody scFv X5 [180]. Upon further characterization, they found that the highly potent m9 antibody not only exhibited broad neutralizing activity but also suppressed the generation of escape mutants upon immune selection [181]. Additional studies on broadly neutralizing antibodies to HIV from memory B cells also suggest that affinity has an important role in breadth and potency of neutralization [182,183].

However, one needs to proceed with caution. In the case of motavizumab, a high-affinity variant of palivizumab (Synagis), a higher incidence of immunogenicity was seen in phase III clinical trials that led to discontinuation of its development as a therapeutic agent [142,183,184]. Collectively, our results together with evidence from earlier studies support the notion that very high-affinity neutralizing antibodies may be particularly useful in a therapeutic setting and suppress the emergence of escape variants.

3.4. Effects of Targeting Spike Protein Receptor Binding Domain on Neutralization Escape and Fitness of SARS-Coronavirus²

3.4.1. Overview

The receptor binding domain (RBD) of the spike (S) glycoprotein of SARS-CoV is a major target of protective immunity in vivo and a large number of neutralizing antibodies (nAbs) recognizing the RBD have been developed. Studies have shown that all nAbs against the RBD can select for neutralization escape mutants in vitro, however, the biological implications of targeted escape mutations on virus-receptor interactions and pathogenesis remain unclear. We have previously identified a panel of neutralizing human monoclonal nAbs against an epitope within the RBD, which is overlapping with the interaction interface of the RBD and its receptor, angiotensin 1 converting enzyme 2 (ACE2). We used focused mutagenesis, chain shuffling, and de novo panning to select for second and then third generation nAb variants with improved breadth, binding and neutralization activities. While most second and third generation nAbs showed broadened neutralization activity against a few strains, some were highly effective across a comprehensive panel of related SARS variants spanning different stages of an expanding epidemic. Further, while many of these nAbs effectively neutralized escape mutants derived from other RBD-targeting nAbs or the ancestral antibodies, they all selected for new escape mutations within a distinct binding tract along the RBD. Using this panel of mutants, we also extensively investigated their effects on receptor binding and virus fitness in vitro and in vivo. We note that while some of these nAbs had great potency and breadth, none of these nAbs blocked escape or significantly attenuated the virus. Further, a convergent combination of two nAbs targeting the same epitope did not prevent escape. These results suggest that the RBD epitope targeted by the studied antibodies is structurally flexible and can tolerate a large variety of mutations without

² Jianhua Sui^a, Meagan Bolles^b, Barry Rockx^{b,c}, Robert C. Liddington^d, Ralph S. Baric^b and Wayne A. Marasco^a

^aDepartment of Cancer Immunology and AIDS, Dana-Farber Cancer Institute; Department of Medicine, Harvard Medical School, Boston Massachusetts. ^bDepartments of Epidemiology and Microbiology and Immunology, University of North Carolina, Chapel Hill. ^cCurrent address: Rocky Mountain Laboratories, National Institute of Allergy and Infectious Diseases, National Institutes of Health, Hamilton, Montana.

^dInfectious and Inflammatory Disease Center, Stanford-Burnham Medical Research Institute, La Jolla, CA 92037, USA.

The following draft is scheduled for submission to JVI this year.

significantly altering structure or function. These studies imply that certain epitope(s) are highly plastic, allowing for ready selection of escape mutations that can further alter receptor binding and pathogenesis. A conserved epitope with more sophisticated function and structural constraint may provide an ideal escape-proof target and a divergent combination approach, targeting different epitopes, may be more effective in providing broad neutralization and prevention of escaping variants.

3.4.2. Introduction

Coronaviruses are important emerging human RNA viruses as exemplified by the global outbreak of severe acute respiratory syndrome (SARS) in 2002/2003 with 10% mortality rates, which were caused by a highly infectious betacoronavirus, the group 2b SARS Coronavirus (SARS-CoV) [185-189]. More recently, a new human group 2c betacoronavirus was detected in Saudi Arabia which caused similar acute respiratory disease syndromes and high mortality [158]. A wide range of other coronaviruses has also been detected in bats, including closely related bat SARS-like-CoVs, which likely served as precursor strains for the SARS-CoV outbreak [3,6,7,28,30,190]. SARS-like-CoVs and other coronaviruses circulating in bats may replicate, recombine and cross species barriers to reemerge as new human pathogens that cause severe respiratory diseases. Therefore SARS-CoV remains a warning for vigilance and a research model for developing better prevention and treatment strategies against novel emerging coronaviruses in the future. From therapeutic antibody and broadly effective vaccine standpoints, to be better prepared for potential reemergence of devastating virus in the future, it is not only important to develop broadly neutralizing antibodies (BnAbs) that could neutralize a broad spectrum of epidemic and precursor viruses, but also to uncover their escape mutant pathways and develop strategies that either prevent virus neutralization escape or select for escape pathways that attenuate virus virulence.

The characteristic surface Spike (S) protein of SARS-CoV is the major target for vaccines and therapeutic antibodies [191]. Numerous S-protein-specific neutralizing antibodies against the virus have been reported [78,80,164,166,168,169,192-196]. The majority of these nAbs recognize epitopes within the receptor binding domain (RBD) that is responsible for ACE2 receptor binding [78,80,164,165,168,169,194-196]. Evidence also points to the RBD as a major neutralizing epitope in vivo [162,163,197,198]. NAbs against S2 were seen during natural human infection with SARS-CoV, but there is a paucity of information

on their epitopes and potencies [120]. Human nAbs developed as potential therapeutics for the prophylaxis and treatment of SARS mainly targeted the RBD domain [78,80,164,168]. Studies have been conducted to assess anti-RBD nAbs for their breadth of protection against all relevant strains of SARS-CoV and neutralization escape variants [42,62]. Some antibodies neutralized multiple viral strains, however all nAbs tested, including strain-specific or broadly nAbs, selected for escape mutants. It remains unclear if escape-resistant epitopes on the RBD have not yet been identified or if the coronavirus RBD is generally a poor target for escape-resistant monoclonal antibody development.

We have previously developed a potent but strain specific human nAb 80R [168,170,171] that targets a conformationally sensitive neutralizing epitope located between amino acids 426-492 of the RBD, and later we reported that the neutralization activity of 80R was broadened to target a heterologous human variant virus, GD03, by antibody engineering [64]. A series of 80R derivative nAbs were developed through light chain shuffling and focused mutagenesis of CDR2 of the light chain variable region (VL-CDR2) [64]. In this study, we tested if convergent nAbs, designed to target the same or similar neutralizing epitope within the RBD, can prevent or attenuate viral escape mutants alone or in combination. We first examined if a second generation of nAbs, broadened from 80R's specificity to also target the GD03 spike, can more effectively neutralize a wide range of natural SARS-CoV strains and whether these antibodies can neutralize 80R's neutralization escape variants. We next analyzed virological outcome following focused antibody pressure on the 80R neutralization epitope – whether 80R derivatives alone or in combination with 80R can block neutralization escape pathway(s) or force viral attenuation pathway(s). Some of 80R derivative nAbs had great potency and breadth in neutralizing multiple viral strains, including the escape mutant viruses derived from other nAbs, however none of these second generation nAbs blocked escape or significantly attenuated the virus. Further, a combination of two of them also did not block escape. These results suggest this particular epitope targeted by 80R and its derivatives is structurally flexible, which is unlikely to be resistant to neutralization escape mutation(s). Ideally, a more conserved epitope with more sophisticated function and structural constraint should be targeted. Additionally, a divergent combination approach, targeting different epitopes, may be more effective in providing broad neutralization and prevention of escaping variants.

3.4.3. Materials and Methods

VIRUSES AND CELLS

The generation and characterization of each of the recombinant infectious clones (icSARS, icGD03, and icGD03-MA) have been described previously [90,101]. All work was performed in a Class II biological safety cabinet in a biosafety level 3 laboratory containing redundant exhaust fans. Personnel were equipped with powered air-purifying respirators with high-efficiency particulate air and organic vapor filters (3M, St. Paul, MN), wore Tyvek suits (DuPont, Research Triangle Park, NC), and were double gloved. Vero E6 cells were grown in minimal essential medium (MEM) (Invitrogen, Carlsbad, CA) supplemented with 10% Fetal Clone II (HyClone, South Logan, UT) and gentamicin-kanamycin (UNC Tissue Culture Facility). Viruses were propagated on Vero E6 cells in Eagle's MEM supplemented with 10% Fetal Clone II (Hyclone, South Logan, UT) and 1X Antibiotic-Antimycotic (Gibco, Grand Island, NY) at 37°C in a humidified CO₂ incubator. At 30 hours post infection, supernatant was clarified by centrifugation at 1600 rpm for 10 minutes, aliquoted, and frozen at -80°C until use. The viral titers of the stocks were determined on Vero E6 cells by plaque assay, as described elsewhere [41,42].

NEUTRALIZATION ASSAY WITH INFECTIOUS CLONE OF SARS-CoV (IC SARS-CoV) OR ESCAPE MUTANTS

Neutralizing titers were determined by either a microneutralization assay or a plaque reduction neutralization titer assay [41]. For the microneutralization assay, nAbs were serially diluted two-fold and incubated with 100 PFU of the different icSARS-CoV strains for 1 h at 37°C. The virus and antibodies were then added to a 96-well plate with 5×10^3 Vero E6 cells/well and 5 wells per antibody dilution. Wells were checked for cytopathic effect (CPE) at 4 to 5 days post infection, and the 50% neutralization titer was determined as the nAb concentration at which at least 50% of wells showed no CPE. For the plaque reduction neutralization titer assay, nAbs were serially diluted two-fold and incubated with 100 PFU of the different icSARS-CoV strains for 1 h at 37°C. The virus and antibodies were then added to a 6-well plate with 5×10^5 Vero E6 cells/well in duplicate. After a 1-h incubation at 37°C, cells were overlaid with 3 mL of 0.8% agarose in medium. Plates were incubated for 2 days at 37°C and then stained with neutral red for 3 h, and plaques were counted. The percentage of plaque reduction was calculated as $[1 - (\text{number of plaques with antibody} / \text{number of plaques without antibody})] \times 100$. All assays were performed in duplicate.

EXPRESSION AND PURIFICATION OF RBD OF SARS-CoV MUTANTS AND ACE2 PROTEINS FOR SPR ANALYSIS

Plasmids encoding the RBD (residues 318-510) fused C-terminally with a Fc tag of human IgG1 were constructed as described elsewhere [178,199]. Briefly, the RBDs of escape variants were amplified using the following primers encoding NheI and BspEI restriction sites (underlined), respectively: 5'-CCGTGCTAGCCAATATTACAAACTTGTGTCCTTTTGGAGAG-3' and 5'-ACATTCCGGAAACCGTGGCCGGTGCATTTAAAAGTTC-3'. The RBD amplicons were digested and ligated into the R5T3-Ig vector, after which RBD-Fc fusion proteins were produced by transfection of 293F cells (Invitrogen) and purified with Protein A-Sepharose affinity chromatography. Soluble human ACE2 protein corresponding to its N-terminal extracellular domain (aa18-740) [61] was kindly provided by Dr. Fang Li at University of Minnesota Medical School. For mouse ACE2 protein, its N-terminal extracellular domain (aa19-615) was cloned in pcDNA3.1 and fused with a His6-tagged at C-terminal, and the protein was produced by transfection of 293F cells and purified by IMAC chromatography.

SURFACE PLASMON RESONANCE (SPR) ANALYSIS

Binding of Abs to different RBDs were analyzed on a Biacore T100 (Biacore) at 25 °C, as described previously [64,153]. Anti-human IgG Fc antibody (Biacore) was covalently coated onto a CM5 sensor chip by amine-coupling using the coupling kit (Biacore). Abs were captured onto anti-human IgG Fc surfaces at the flow rate of 10 µl/min in HBS buffer (Biacore). ACE2 soluble protein was injected over each flow cell at the flow rate of 30 µl /min in HBS buffer at different concentrations ranges depending on binding affinity for each Ab. The highest concentration tested for mouse ACE2 reached 20 mM. A buffer injection served as a negative control. Upon completion of each association and dissociation cycle, surfaces were regenerated with 3M MgCl₂ solution. The association rates (k_a), dissociation rate constants (k_d), and affinity constants (KD) were calculated using Biacore T100 evaluation software. The goodness of each fit was based on the agreement between experimental data and the calculated fits, where the Chi² values were below 1.0. Surface densities of Abs were optimized to minimize mass transfer. All k_a , k_d , KD reported here represent the means and standard errors of at least two experiments.

ESCAPE MUTANT ANALYSIS

Neutralization-resistant SARS-CoV mutants were generated as described elsewhere [42]. In brief, 1×10^6 pfu of icUrbani, icGD03, or icGD03-MA were pre-incubated with 30 mg of a nAb in 100 mL of media at 37°C for 1 h and then inoculated onto 10^6 Vero E6 cells in the presence of the respective Ab at the same concentration. The development of cytopathic effect was monitored over 72 h, and progeny viruses were harvested. NAb treatment was repeated 2 additional passages, passage 3 viruses were plaque purified in the presence of Ab, and neutralization-resistant viruses were isolated. Experiments were performed in duplicate, and the S glycoprotein gene of individual plaques from each experiment was amplified by reverse-transcription-PCR into three products using primers S1f (5'-GTTGTCTTCCTATTCCTCTT-3'), S1r (5'-CTGCATAGACATTGGAGAAGC-3'), S2f (5'-CAGGAGATGTTGTGAGATTCC-3'), S2r (5'-GTGTGTTGCGATCCTGTTTCAG-3'), S3f (5'-CTACAGAAGTAATGCCTGTTTC-3'), and S3r (5'-GTGCAGTAATTGATCTTAGAG-3'), and sequenced. The neutralization titers of wild-type and nAb-resistant viruses were determined as described elsewhere [41,42].

ANIMAL STUDIES

Female BALB/c mice, young (10 weeks; Jackson Labs, Bar Harbor, ME) or aged (12 months of age, Harlan Labs, Indianapolis, IN) were acclimated for one week after shipping. All mice were housed under sterile conditions in individually ventilated Hepa-filtered Sealsafe cages using the SlimLine system (Tecniplast, Exton, PA). Experimental protocols were reviewed and approved by the Institutional Animal Care and Use Committee at the University of North Carolina, Chapel Hill. For prophylactic passive antibody protection studies, aged mice were injected intraperitoneally with 250 µg of mAb (80R, Fm6, or PBS) in 400 µL PBS 24 hours prior to infection. For all viral challenges, mice were anesthetized with a ketamine (1.3 mg/mouse)-xylazine (0.38 mg/mouse) mixture administered intraperitoneally in a 50-µl volume, and then intranasally inoculated with 10^5 pfu of icUrbani, icGD03, icGD03-MA, Fm6-escape mutant (Fm6-Esc), Fm39-Esc, Cs5-Esc, Y12-Esc, Y112A-Esc. After challenge, morbidity (weight) and mortality were assessed daily. On day 4 post-infection, mice were euthanized by isofluorane and one quarter of each mouse lung was taken for viral titer.

LUNG VIRAL TITERS

Lung tissue samples were weighed and stored in 1mL PBS at -80°C until time of titration. Tissue was thawed and homogenized with glass beads at 60 seconds at 6000 rpm in a MagnaLyser (Roche). The solution was centrifuged at 13,000 rpm under aerosol containment in a table top centrifuge for 5 min, the clarified supernatant was serially diluted in PBS, and 200- μ L volumes of the dilutions were placed onto monolayers of Vero E6 cells in six-well plates. Following 1 hour of incubation at 37°C, the cells were overlaid with 0.8% agarose-containing medium. Two days later, the plates were stained with neutral red and the plaques were counted.

STATISTICS ANALYSIS

Percentages of starting weights and viral titers were evaluated for statistically significant differences by unpaired t tests using GraphPad software.

3.4.4. Results

NEUTRALIZATION AND PASSIVE PROTECTION BY 80R-DERIVATIVE HUMAN MABS.

Previous studies had identified several broadly neutralizing mAbs, the most promising of which were capable of neutralizing spike-protein pseudotyped lentiviruses with Urbani, GD03, and the Urbani-D480G spikes [64]. In the most recent study, we further extended the neutralization profiles of four of the second generation nAbs, and noted that only Fm6 was capable of neutralizing every zoonotic spike variant and the escape variants generated with other nAbs [42]. We further evaluated Fm6 and compared it to 80R for its prophylactic effect in protecting SARS-CoV challenges in a senescent mouse model. Twelve-month-old BALB/c mice that received Fm6 at 12.5mg/kg intraperitoneally 24 hours prior to infection with Urbani or GD03 were protected against significant weight loss. For both Urbani and GD03 viral challenge groups, all five mice in each Fm6 treated groups had a more than 3-log reduction in viral titers in their lungs on day 4 after infection to below the assay limit. In contrast, animals that received PBS or 80R were not protected against weight loss and viral load in lungs after challenge with both viruses (Fig. 2). 80R has been previously shown to significantly reduce virus titers in lungs of young mice that were infected with Urbani virus [170]. SARS-CoV is more virulent in aged than in young mice, as evidenced by increased virus titers, more-severe disease outcomes, and higher mortality rates in aged populations similar to what has been reported for humans [200]. That Fm6 but not 80R protected aged mice from infection demonstrates Fm6 is

more potent than 80R, and further emphasizes the need to test potential therapeutics in the more stringent aged animal models of human disease.

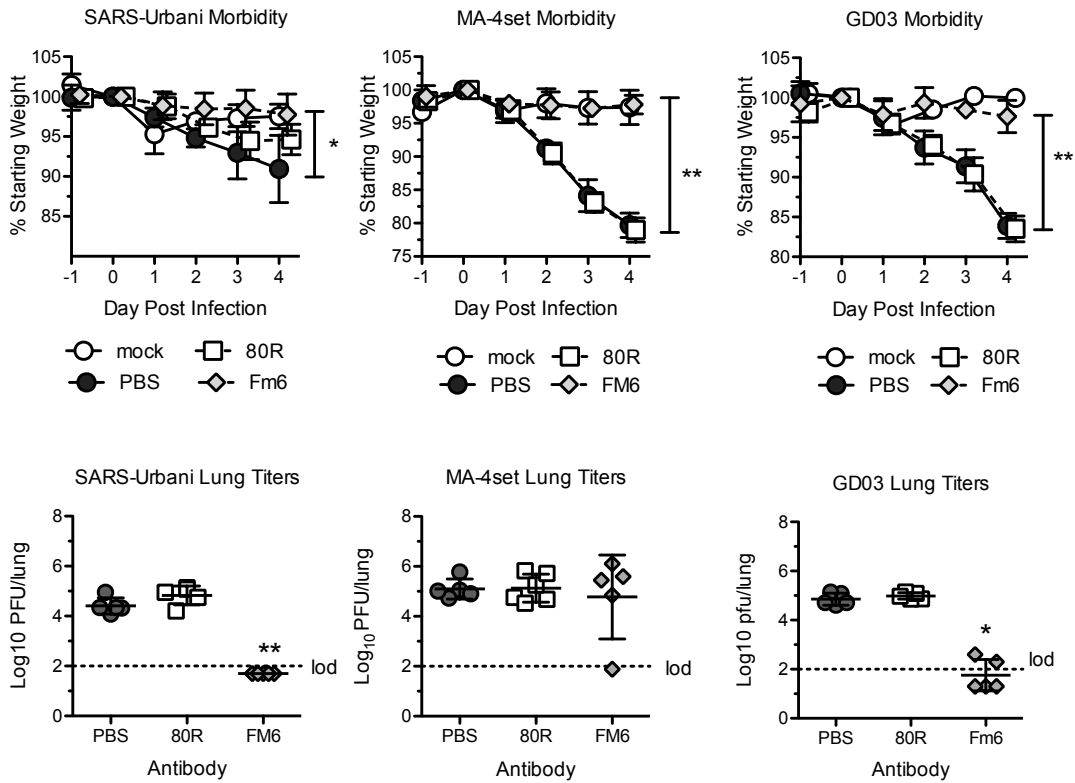


Figure 3.4.2. Prophylactic treatment of SARS-CoV infections in 12-month-old aged BALB/c mice by 80R and Fm6 nAbs.

Body weights of mice infected with icGD03 or icUrbani were measured daily after passive administration of 12.5 mg/kg (~250 mg/mice) nAbs. Lung tissues of mice infected with icGD03 or icUrbani were harvested on day 4 post-infection and assayed for infectious virus by a plaque assay using Vero E6 cells. Error bars, standard deviations (n= 5).

A THIRD GENERATION OF NABS DESIGNED TO PREVENT ESCAPE.

Despite the increased potency, Fm6 as well as the other 2nd generation nAbs all allowed for the generation of escape variants with single substitutions in the RBD, all at residues D480, N479, or Y436. In an attempt to prevent virus escape, a third generation of nAbs were generated by panning either a non-immune antibody phage display or a light chain shuffled 80R-vk-cs library with the Urbani RBD with the Y436H substitution [64]. Two nAbs were identified that could neutralize Urbani, GD03, D480G-, D480A-, or Y436H-variant spike pseudotyped viruses: Y12, from the non-immune library, and Y112A, from the 80R-vk-cs library. We evaluated the neutralization efficacy of these two nAbs, as well as Fm6

and 80R, by PRNT50 assays with Urbani, GD03, GD03-Y436H, the 80R-escape (D480G), and the Fm6-escape (Y436H) viruses. While both Y12 and Y112A were capable of neutralizing Urbani-Y436H and GD03-Y436H at comparable nAb concentrations, Y112A more potently neutralized Urbani, GD03, and the 80R-escape variant (Fig 4).

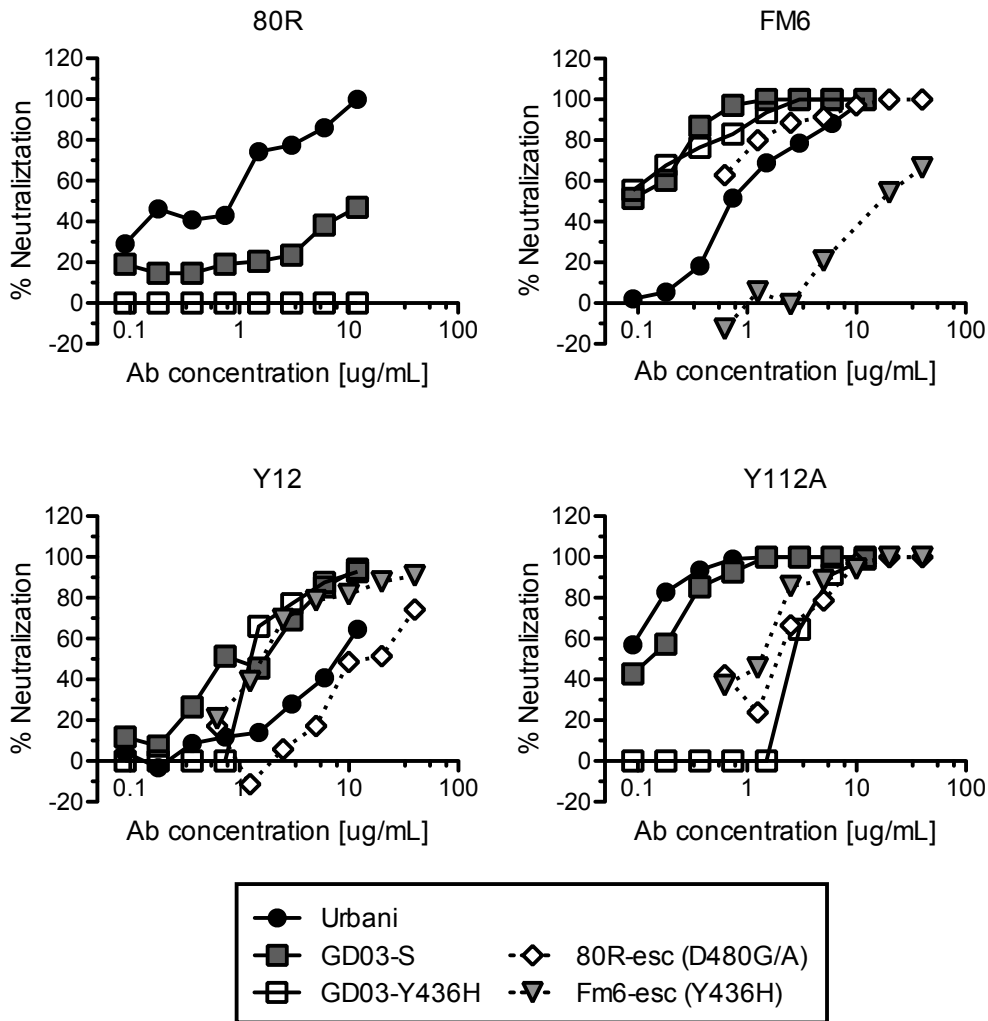


Figure 3.4.4. Broadly neutralization activity of nAbs, fm6 and Y112A.

Neutralization titers against five different SARS-CoVs or escape mutants were determined in a plaque reduction neutralization assay. Abs were serially diluted two-fold as indicated and 100 PFU of the different icSARS-CoV strains were used (see Materials and Methods). At the end of the assay, plaques were stained and counted for calculation of plaque reduction efficiency. Each data shown represent average of duplicate samples. GD03-MA is a mouse adapted strain encoding the 2004 human GD03 S protein with Y436H mutation in the RBD [90].

Y12, Y112A, AND COMBINATION OF 80R AND Fm6.

We next examined the escape profiles of a number of viral strains, including the 80R and Fm6 escape mutants, under the selection of Y12 and Y112A. A series of escape mutants were developed for all viruses tested for both second generation antibodies (Fig. 5A). Some of the escape substitutions had previously emerged following selection with other 80R derivative antibodies, suggesting that the RBD epitope targeted by the 80R derivatives has a limited set of residues sufficiently plastic to allow both nAb escape and continued stability/function. As neither Fm6, Y12, nor Y112A alone prevented viral escape, we next asked if a Convergent Combination Immunotherapy (CCI) approach, in which two nAbs are used directed against a similar epitope determinant, can prevent neutralization escape or seriously impact viral fitness. As shown in Fig 5a, the Urbani/D480G mutant virus selected by 80R Ab was no longer able to escape neutralization by Fm6, suggesting that the virus can only undergo one round of mutation when the virus was targeted by 80R and Fm6 sequentially. We therefore tested if the same evolutionary limitations exist when both antibodies are combined and used simultaneously. The result showed that the combination did not prevent the emergence of viral escape mutant(s), rather a resistant virus carrying N479T mutation was selected (Fig. 5A). Urbani-N479T is also an escape mutant of nAb fm39, which was not susceptible to either 80R or Fm6 in cross-neutralization studies (data not shown). Taken together, 80R and all its derivatives are selecting for slightly variant escape profiles along a similar track around the 80R epitope, and broadly acting escape mutation candidates exist at 5 or more positions along the interface between 80R and the RBD domain. These escape positions are either directly adjacent to or are the key contact residues for RBD binding to hACE2 (Fig. 5B).

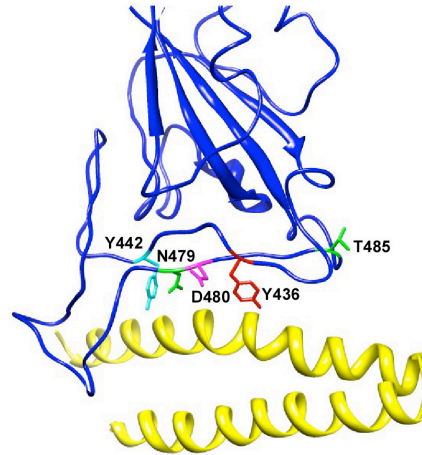
EFFECT OF ESCAPE MUTATIONS ON HUMAN ACE2 RECEPTOR BINDING AND IN VITRO VIRAL GROWTH.

In order to test if the escape mutants generated from the above studies alter virus entry and fitness, we determined binding affinity and kinetics between the RBDs of these escaping mutants and the soluble extracellular domain of human ACE2 (hACE2). Although most escape substitutions occur at positions in the RBD important for hACE2 binding [61], the majority did not significantly change the binding affinity (KD) and kinetics (K_a and K_d) to hACE2. The exception is Y12's escape mutation, Y442S, which had a ~6-fold slower K_d and a ~5-fold increased affinity (Fig. 5C). We further tested virus growth in Vero E6 cells, as the monkey homologue to hACE2 is identical across the interface with the SARS-RBD. Though

replication of all viruses was delayed early in infection as shown by a 1-2-log reduction in titer at 8 h after infection compared with wild-type icUrbani, all viruses reached comparable peak titers of 10^6 - 10^7 pfu/mL by 24 h after infection (Fig. 5D). These results indicate these escape mutants could efficiently grow in hACE2-expressing cells and suggest no loss in fitness despite the substitutions across the binding interface.

A

| Selection characteristic | Antibody | Virus under selection | Escape Substitution |
|--------------------------|----------|-----------------------|---------------------|
| parent antibody | 80R | Urbani | D480A/G |
| 1st generation | Fm6 | Urbani | Y436H |
| | cs5 | Urbani | N479I or D480Y |
| | fm39 | Urbani | N479T |
| convergent combination | 80R+Fm6 | Urbani | N479T |
| 2nd generation | Y12 | Urbani | Y442S |
| | Y112a | Urbani | D480A |
| | | Urbani-Y436H | D480G or Y436R |
| | | Urbani-D480G | D480V or T485A |



B

| Ab | Virus under selection | RBD binding with hACE2 | | | |
|-----------------|-----------------------|--------------------------------------|-----------------------------------|------------|-----------|
| | | Ka ($M^{-1}s^{-1} \times 10^5$) | Kd ($s^{-1} \times 10^{-2}$) | KD (nM) | |
| No Ab | Urbani-WT | WT | 6.2±0.9 | 4.0±0.1 | 65.0±10.9 |
| 80R | Urbani-WT | D480G | 5.4±1.1 | 7.4±4.1 | 139±21.5 |
| CS84 or CS5 | Urbani-WT | D480Y | 5.7±0.8 | 3.4±0.0 | 60.0±10.2 |
| 80R or Y112A | Urbani-WT | D480A | 4.7±0.3 | 3.8±0.3 | 81.0±0.5 |
| Y12 | Urbani-WT | Y442S | 5.0±0.0 | 0.7±0.0 | 13.0±0.0 |
| Fm6 | Urbani-WT | Y436H | 5.0±0.0 | 3.6±0.0 | 71.0±0.1 |
| CS5 | Urbani-WT | N479I | 4.1±0.3 | 1.9±0.0 | 46.3±0.3 |
| Fm6+80R or fm39 | Urbani-WT | N479T | 5.5±2.4 | 3.7±1.5 | 67.5±0.3 |
| Y112A | Urbani-Y436H | Y436H/D480G | 4.0±0.1 | 4.6±0.0 | 113.0±4.6 |

C

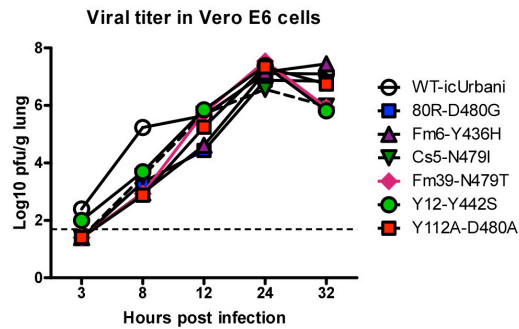


Figure 3.4.5. Locations of neutralization escape variant mutations on the structure of the SARS-CoV RBD and effects on the binding to human ACE and viral growth.

(A) Left, a list of all critical amino acid changes associated with escape mutation. Right, the locations of these amino acids on the structure of the SARS-CoV RBD (blue) bound to its receptor human ACE2 (yellow). (B) Binding affinity and kinetics measurement of the RBD of the escape mutations listed in panel A to human ACE2. Binding kinetics were evaluated using a 1:1 Langmuir binding model. Each ka, kd and KD value represents the mean and standard error of two to two independent experiments ran Biacore. (C) In vitro growth characteristics of neutralization escape mutant SARS-CoV. Cultures of Vero E6 were infected in duplicate with icUrbani WT and neutralization escape mutants as indicated at a multiplicity of infection (MOI) of 1, as described in Materials and Methods. Virus titers at different time points were determined by a plaque assay using Vero E6 cells. A dot line indicates the lowest detectable virus titer.

EFFECT OF ESCAPE MUTATIONS ON IN VIVO VIRUS GROWTH.

To assess the effect of antibody escape on viral pathogenesis, we infected 12-month aged Balb/c mice with two escape viruses, Cs5-escape (N479I) and Fm39-escape (N479T). These two escape viruses were attenuated, showing significantly less weight loss (less than 5%) compared with wild type Urbani virus (Fig. 6A), and the Cs5-escape (N479I) virus had a significant reduction in viral titer in the lungs. This may reflect the different effect of these mutations on binding to hACE2 and mACE2. SARS-CoV infection of murine cells is inefficient and limited by the very weak binding between RBDs and mACE2[201]. Consistently, by Biacore analysis we found that the binding affinity of the RBDs of wild type Urbani virus to mACE2 was very low (estimated to be lower than 20mM, hundreds fold less than to hACE2). Similarly, the RBDs from each of the Urbani escape mutants listed in Fig. 5C had binding affinities at this very low level and were not accurately measured due to high mACE2 concentrations required (data not shown). This is somewhat surprising, as at a minimum the Y436H mutant RBD should have improved interaction with mACE2 receptor as it is a mouse adapted mutation described in MA15 [57].

We further assessed the binding and pathogenesis of escape mutants of Y12 and Y112A generated on the GD03 and GD03-Y436H background (Fig. 6B). Two escape mutations, Y442L and S487T, selected on GD03-Y436H by Y12 and Y112A, respectively, increased the binding affinity to hACE2 about 4-fold compared with GD03-Y436H or wild-type GD03 to hACE2. For the Y112A-selected escape variant, increased binding to hACE2 is consistent with the association of S487T is an epidemic-associated sequence located at the interface with hACE2 [41]. Additionally, the Y442L substitution has been identified as a mouse-adapting substitution in the MA20 strain, predicted to increase interaction with mACE2 via Q34 [200]. Interestingly, both mutant viruses showed significantly increased in vivo growth in young mice with a more than 2-log increasing in viral titer in the lungs by day 4, compared with GD03-Y436H. The Y12 escape mutant showed more virulence than Y112A-escape: mice infected with the Y12 escape mutant virus lost up to 15% of their weight by day 4 after infection, whereas GD03-Y436H virus had less than 5% weight loss (Fig. 6C). In agreement with the greater in vivo weight loss of Y12 escape mutant (GD03-Y436H/Y442L), the binding affinity with mACE2 was the only measurable one among the many others under the same conditions examined by Biacore and Octet, reaching $KD \approx 400nM$. These results indicate

that the additional mutation of Y442L in GD03-Y436H increased binding affinity to both hACE2 and mACE2, increasing pathogenesis in a murine model.

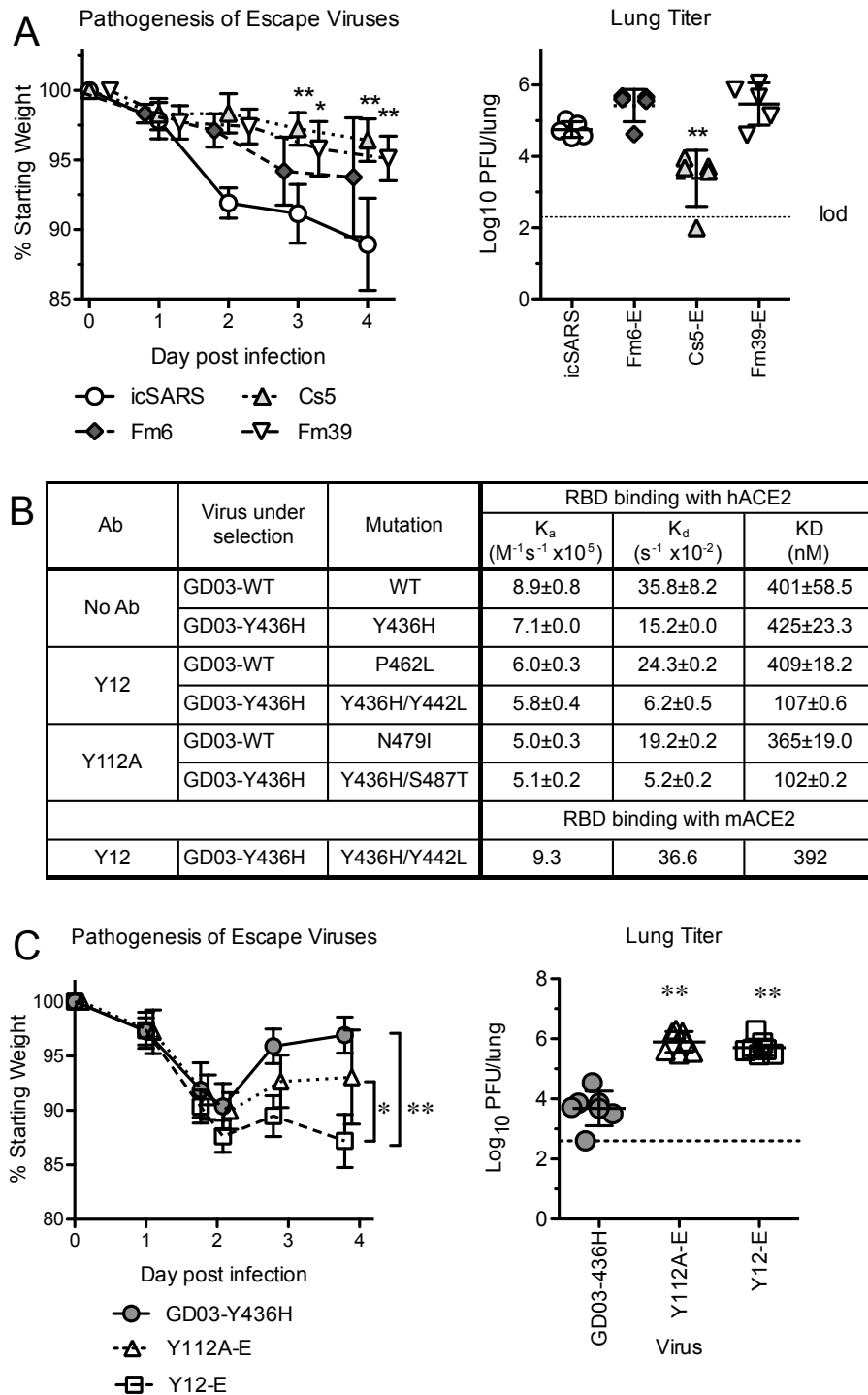


Figure 3.4.6. Effect of neutralization escape on in vivo replication.

(A) Escape mutants of cs5, cs39 and fm6 in aged mice (12-month). Left, weight loss. All the mice were inoculated with 10^5 pfu of viruses as indicated. Body weights of infected mice were measured on a daily

basis (5 mice per group). Weight changes are expressed as the mean percentage changes for infected animals relative to the initial weights at day 0. Right, lung titers. Lung tissues were harvested from infected mice on day 4 after infection and were assayed for infectious virus. Virus titers at different time points were determined by a plaque assay using Vero E6 cells. (B) A table lists escape mutants generated with icGD03 or icGD03-MA (Y436H) viruses for nAb Y12 and Y112A and the binding kinetics of the RBD of these escape mutants with human ACE2 and mouse ACE2. (C) Y12 escape mutants in young mice (10-week). The experiment was performed similarly as in panel A except the mice are 10-week young mice. Error bars denote standard deviations. * $p < 0.05$, ** $p < 0.01$, compared with the icUrbani-WT, by 2-way analysis of variance. A dot line indicates the lowest detectable virus titer.

3.4.5. Discussion

The 2002/2003 SARS-CoV epidemic and the recent identification of another novel coronavirus, MERS-CoV, in 2012, emphasizes the continued role of coronaviruses as emerging viral human pathogens [158]. Therapeutic monoclonal antibodies can provide immediate protection and have relatively swift production compared to vaccines, provided they can be designed to protect against the breadth and antigenic variation of a RNA virus. 80R was one of the first neutralizing monoclonal antibodies designed to target SARS-CoV, and the use of structural modeling in addition to iterative panning with variant S proteins has allowed us to develop of mAbs with increased breadth and potency [64,168]. Among the 80R derivatives generated previously [64], Fm6 is the most potent mAb with broadest neutralization activity in vitro (Fig. 1, 3 and 4) and protected aged mice from infection with two human strains, Urbani and GD03 (Fig. 2). However a Y436H escape mutation was developed when the epidemic SARS-CoV, Urbani virus, was placed under the selection of Fm6. A new nAb, Y12 and a 80R derivative nAb Y112A, were developed against the Y436H mutant using similar approaches we employed previously [64]. Both Y12 and Y112A also showed broadly neutralizing activities to other viral strains (Fig. 3C-D and Fig. 4); however they did not block escape. Detailed escape mutant profile analysis for 80R and all its derivatives showed that they selected for slightly variant escape profiles along a similar track around the 80R epitope at 5 positions along the interface between 80R and the RBD domain (Fig. 5A-B). Although these mutations are at positions either adjacent to or the key contact residues for binding to hACE2 receptor, most of them did not significantly affect hACE2 binding and virus growth in vitro.

Neutralization escape variants for Ab Cs5 and fm39, Urbani-N479I and Urbani-N479T respectively, showed significant attenuation in 12-month aged mice. This correlates with the low binding affinities to mACE2, and demonstrate the effect of binding affinity on pathogenesis. Growth in Vero E6 cells and the measured binding affinity to hACE2 indicate these mutations had different effects on bindings

to hACE2 and mACE2. The Fm6 neutralization escape substitution, Y436H, is identical to the sole Spike substitution in MA15, a mouse-adapted Urbani virus with six total substitutions conferring rapid lethality in young BALB/c mice [57]. However the Fm6 escape mutant, Urbani-Y436H showed only a slight increase in lung titer in aged mice, which is in agreement with a recent report that the Y436H mutation is necessary but not sufficient in contributing to the adaptation [200]. Though structural modeling suggests that the Y436H change may increase binding with D38 of mouse ACE2 via electrostatic interaction [200], this was not confirmed in our Biacore studies. The binding between wild-type and all the escape mutants studied here was very weak (<20nM), except one escape mutant that contains a double mutation of Y436H and Y442L in the RBD of GD03 virus. This double mutation dramatically increased the binding affinity of RBD to mouse ACE2, reaching 400nM, and is the only mutant with a binding affinity to mACE2 high enough to be measured in this study. Indeed, mice infected with this mutant virus exhibited up to 15% weight loss, significantly more virulent than the background GD03-MA virus with a single Y436H substitution (Fig. 6C). The Y442L change has also been reported to be associated with increased virulence of a mouse adapted MA-20 virus on the Urbani background [200]. These results demonstrate that a Y442L substitution improves binding to mouse ACE2 and directly contributes to the increased in vivo virulence. The S487T is known important for human adaption of SARS-CoV from civets [59]. While this substitution did not significantly increase weight loss in the GD03-Y436H background, it significantly increased viral lung titers by 4 days post-infection. Both the Y442L and the S487T substitutions increased binding affinity to human ACE2 by ~4-fold compared to the background GD03-Y436H and the wild-type GD03 strains. While many of the escape substitutions selected by nAbs either reduced or had no impact on binding and pathogenesis, it is notable that these two antibodies selected for escape variants that could increase pathogenesis in a mouse model. This emphasizes the importance of carefully characterizing the escape phenotypes of nAbs, particularly those targeting the RBD, and the need for further development of therapeutics with increased barriers to escape.

80R and all its derivative nAbs selected for slightly variant escape mutants along the interface of 80R and RBD, confirming that they all recognize a very similar epitope. These antibodies provided a unique toolset to test if a Convergent Combination Immunotherapy (CCI) approach in which two or more nAbs directed against a similar epitope can prevent neutralization escape. With the two antibodies we

tested, 80R and Fm6, different escape results were obtained depending on if they were used sequentially or simultaneously. When 80R was used first to select for the escape variant Urbani-D480G, no further escape mutant could be selected following Fm6 neutralization. However the same evolutionary constraint did not exist when both antibodies were used simultaneously; the virus took a new escaping pathway (N479T) to escape the neutralization of 80R and Fm6. Although this result suggests that combinational therapy against this particular epitope in the RBD may be possible when used strategically, it may not be practical for treating novel emerging viruses.

The RBDs of coronaviruses are typically virus specific and vary in length and sequence significantly, consistent with the structurally and functionally diverse receptor specificity. The C-terminal S2 domain is rather highly conserved and contains the functional elements required for membrane fusion that usually places strong evolutionary constraints on the sequence [202]. Our detailed escape studies focusing on a particular epitope in the SARS-CoV RBD demonstrate the difficulty of preventing escape with monoclonals targeting a single epitope. This is consistent with previous reports that escape mutants were generated for all the SARS-CoV RBD-specific nAbs tested [42,62]. Monoclonal Ab development for influenza has demonstrated that targeting of conserved epitopes can allow for broad neutralization profiles [153]. The S2 domain of the SARS-CoV Spike may be an ideal target for developing BnAbs with greater potency of neutralization, resistance to neutralization escape, and breadth (including new SARS-like-CoVs that might emerge).

On the other hand, a combination of nAbs targeting different neutralizing epitopes is likely a better strategy to provide broader protection and reduce the possibility of generating escaping variants. Fm6 cross-neutralized escape viruses generated by other broadly nAbs (Fig. 1B), including the escape variant of nAb S109.8 that recognizes an epitope distinct from the Fm6 epitope and not in direct contact with ACE2 [62]. Thus, Fm6 may be a good candidate for divergent combination with S109.8 to prevent escape and provide neutralization against a broader range of viruses. Of note, the approach we applied to broaden the activity of a primary strain-specific nAb is a valid strategy for developing BnAbs, as Fm6 was capable of neutralizing all epidemic and zoonotic SARS-CoV variants. However the breadth of activity does not necessarily ensure a high barrier to viral escape, and escape in epitopes critical for receptor binding may have significant implications for binding and pathogenesis. The selection of antibody escape variants with

altered receptor usage or increased pathogenesis in mice is not unique to SARS-CoV [203], and the role of antibody selection in the virulence profiles of respiratory viruses, particularly during emergence events, is worth further investigations.

3.4.6. Contributions

This work is supported by NIH U01-AI061318 and R01AI085524 to W.A.M.

MEB is supported by the UNC-CH Medical Science Training Program (T32GM008719).

CHAPTER 4: Structural Plasticity and Antibody Escape in the SARS-CoV Spike Receptor Binding Domain.¹

4.1. Overview

Human monoclonal antibody therapies have great potential for the rapid and effective treatment of newly emergent respiratory pathogens. The Spike glycoprotein (S) of SARS-CoV is highly immunogenic, and neutralizing antibodies targeting the receptor binding domain (RBD) of spike are highly enriched and encode a significant component of overall protective neutralizing antibody response following infection. However, the genetic mutability and plasticity of binding in the RBD allows for rapid escape from individual neutralizing antibodies (Ab). Previous studies have demonstrated that a single monoclonal Abs can induce one or more substitutions across the RBD, as well as antibody escape variants with increased pathogenesis in a mouse model. Therefore, we sought to identify combinations of escape substitutions that were deleterious to SARS-CoV viability in order to inform selection of combination antibody therapeutics. Using a database of over thirty known antibody-escape virus sequences, we used synthetic biology to generate nine of ten viable Combinatorial Escape Viruses (CEVs) incorporating multiple escape-conferring substitutions across the RBD. Our results illustrate the plasticity of the domain, identify combinations of escape substitutions which are mutually antagonist, identify potential escape resistant combinatorial antibody therapies, and describe the utility of predictive structural modeling. Further, assessing CEV neutralization by multiple independently derived mAbs demonstrated complex susceptibility phenotypes, and allowed us to map broader antibody binding tracts than indicated by single substitutions. Assessment of

¹ Meagan Bolles^a, Eric Donaldson^b, Jianhua Sui^c, George Georgio^d, Antonio Lanzavecchia^e, Wayne Marasco^c, Ralph Baric^{a,b}.

^aDepartment of Microbiology and Immunology and ^bDepartment of Epidemiology, University of North Carolina at Chapel Hill, Chapel Hill, North Carolina; ^cDepartment of Cancer Immunology and AIDS, Dana-Farber Cancer Institute; Department of Medicine, Harvard Medical School, Boston Massachusetts; ^dInstitute of Cellular and Molecular Biology, Department of Chemical Engineering, and Department of Molecular Genetics and Microbiology, The University of Texas at Austin, Austin, Texas, USA; ^eInstitute for Research in Biomedicine, Bellinzona, Switzerland.

The following manuscript is scheduled for submission this year.

the neutralization networks across the RBD and the plasticity of the domain have informed our efforts to develop both potent and broadly neutralizing cocktails of antibodies resistant to viral escape while neutralizing the broadest range of SARS-like natural and human isolates including mutant panels of RBD sequences described in nature.

4.2. Introduction

The importance of coronaviruses (CoV) as emerging zoonotic RNA viruses has been repeatedly emphasized over the past decade, particularly with the emergence of SARS-CoV in 2002/2003 and the recent human coronavirus MERS-CoV in 2012 [158]. Coronaviruses have an established potential for cross species transmission, with a minimal genetic barrier that allows the virus to quickly adapt to use novel species receptors as evidenced by the broad zoonotic reservoir and repeated incidents of introduction into human populations [36,55,204,205]. The spike glycoprotein is the primary determinant of coronavirus species specificity and tissue tropism, responsible for binding the host receptor, human angiotensin converting enzyme 2 (ACE2) for SARS-CoV [199]. Neutralizing antibodies targeting the spike glycoprotein (S) are critical for protection from SARS-CoV infection and passive transfer provides protection from virus replication and clinical disease in highly lethal animal models of human disease [42,163,206]. Further, anti-S antibodies are capable of providing selective pressure during interspecies transmission events, during which sequential changes may allow for altered binding to host receptors as well as resistance to neutralizing antibodies [22,42,64].

Despite a decade of investigation, no approved therapeutics exist for SARS-CoV and some existing vaccine formulations either fail to provide complete protection in aged animal models of human disease or induce a strong Th2 immune pathology [88,159,207]. As peak SARS-CoV titers in humans occur 10 days post infection, with contact patient tracing and quarantine the use of post-exposure prophylaxis may be a viable therapeutic option and strategy to limit transmission in an outbreak setting [74]. Further, passive transfer of convalescent human Abs was used in human patients during the 2003/2004 epidemic with some evidence of success [206]. The technology for the development of humanized monoclonal antibodies (hMAbs) has advanced substantially in past years and several hMAbs have been approved for human use [164,208-210]. Palivizumab, an anti-RSV antibody, is the only human

monoclonal approved for antiviral indications, although monoclonal therapeutics targeting HIV, HCV, CMV, and rabies are in development [146,147,151,211-214]. Combinatorial antibody therapeutics, cocktails of mAbs designed to recapitulate the polyclonal response while maintaining the safety profile of humanized mAbs, have experimentally demonstrated enhanced neutralization breadth and potency for several viruses, including HIV, rabies, ebola, and SARS-CoV [42,133,137,146,208].

The development of therapeutics targeting emergent coronaviruses is complicated by the heterogeneity of the viral zoonotic precursor strains worldwide and the rapid evolution that occurs in response to selection [28,36]. Our laboratories have isolated escape viruses to over 30 human monoclonal antibodies tested to date, including antibodies developed by B-cell immortalization or phage display, and modified by affinity maturation, diversifying selection, or structure-guided focused mutagenesis [42,62,64,131,132,164]. The vast majority of neutralizing antibodies target Spike at the interface with its receptor, with single substitutions within the receptor binding domain (RBD) providing escape from antibody neutralization. Notably, we have isolated an escape variant to almost every monoclonal antibody tested including a high affinity antibody that requires two coincident substitutions, suggesting a flexibility in the S-RBD along the interface with ACE2 and emphasizing a potential obstacle to monotherapy [42,131]. Most SARS-CoV antibody escape variants demonstrate modest, if any, reductions in cell culture growth at early timepoints, but in vivo studies of escape variants have shown reduced, unchanged, and even increased pathogenesis in mouse models, a phenomenon not unique to SARS-CoV [62,132,203]. These studies emphasize the necessity of designing mAb cocktails that cross neutralize each other's escape mutants, respectively and that select for mutation sets that are deleterious, leading to unfit progeny [42,135,136,215].

Given the apparent flexibility of the RBD and the occurrence of antibody escape variants that increase pathogenesis in a mouse model, we sought to identify combinations of escape substitution variants that were deleterious to SARS-CoV viability, thereby informing the selection of an appropriate combination antibody therapy. Rani et al. have demonstrated the ability of a single mAb to select for dual substitutions in the RBD of an escape variant, so we used structural bioinformatics to engineer and synthetic biology to construct 10 combinatorial escape viruses (CEVs) with 1 to 4 antibody-escape substitutions within the RBD. We sought to determine the limits of RBD plasticity, to assess whether

structural prediction could enrich the identification of deleterious substitution combinations, and to determine whether neutralization phenotypes remain stable in the context of additional escape substitutions. Using these approaches, we identified antibody cocktail combinations that selected for highly deleterious combinations of mutations while retaining the capacity to neutralize a wide range of different, human and animal SARS-like RBD sequence variants recorded in the SARS-CoV spike glycoprotein.

4.3. Methods

VIRUS CONSTRUCTION

The combinatorial escape viruses (CEVs) differ from the epidemic strain SARS Urbani at 1 to 4 residues in the receptor binding domain (RBD; amino acids 319-510). Further, five of the mouse-adapted substitutions of the MA15 virus are included in the mouse adapted SARS-CoV MA15 genomic backbone: H133Y nsp5, E269A nsp5, T67A nsp9, A4V nsp13, and E11K M, to allow assessment of functional fitness reductions and neutralization/passive protection in animal models of human disease. The Spike Y436H substitution (the sixth of the MA15 substitutions) is also one of the antibody escape substitutions, and as such is included only in those CEVs as an intended escape site. The RBD substitutions were initially purchased as synthetic constructs 600bp or 1200bp in length (Bio Basic Inc, Ontario, CA). CEV05 was ordered as a 1200bp cassette encoding nucleotides 22,227 through 24,422 with the mutation encoding K390Q. CEV05 served as the template for the nine other viruses, each ordered as 600bp constructs encoding nucleotides 22,413 through 23,024 with the appropriate mutations. The cassettes were designed such that Bsu36I and BtgI digestion sites bordered the 600bp fragment, and SalI and PstI sites bordered the 1200bp fragment (Fig. 1A). To construct the other viral clones, the 1200bp CEV05 fragment in puc57 was digested with Bsu36I and BtgI, and then a 600bp fragment derived from the remaining 9 constructs was ligated into the 1200bp-puc57 vector. The resulting 1200bp construct (SalI/PstI) was excised, purified, and ligated into a icUrbani-CoV E fragment (which had been similarly digested with SalI/PstI and the larger fragment excised). The E fragments, now encoding each of the unique CEV-specific RBD domains, was excised, purified, and ligated with the mouse-adapted SARS-CoV fragments to generate full-length CoV cDNAs from which infectious RNA transcripts were derived, as previously described [101]. RNA transcripts were electroporated into Vero E6 cells which were monitored for CPE and passaged twice to increase titer, and the sequence of the S glycoprotein verified for each mutant. Sequences of the stock viral

RNA was identical to input sequences across the length of the spike glycoprotein. CEV03 was constructed on three independent occasions, and no transfected cells developed CPE across two passages, despite the presence of subgenomic RNA following transfection. These data indicate that the CEV03 mutations were deleterious and likely deficient in receptor interactions and/or entry.

PREDICTIONS AND HOMOLOGY MODELING

Homology models were constructed from the structure of SARS-RBD bound to human ACE2 (PDB code 2AJF). Using RosettaBackrub 3.1 (<https://kortemmelab.ucsf.edu/backrub/>), we generated 10 models of each of the CEVs as well as models from single substitution variants alone [216]. This method by necessity excluded analysis of CEV9, since Rosetta 3.1 was incapable of calculating cysteine changes [216]. The lowest energy option, notably often very similar or identical to the next several lowest options, was used for modeling in Mac PyMol [217]. As an alternate modeling method, FoldX, a plugin for YASARA, was used to create 5 homology models for each of the CEVs using the “mutate multiple residues” option, with a “repaired” PDB and optimization of neighboring side chains [218,219]. The lowest energy PDB from each of the two methods was then “repaired” in FoldX, an energy minimization operation required for reliable energy calculations [218]. We then used FoldX to calculate the stability (free energy of unfolding (ΔG) for the object) and interaction energies (kcal/mol) between the two molecules in the object, the RBD and ACE2 (Fig. S1).

EXPRESSION AND PURIFICATION OF RBD OF SARS-COV MUTANTS AND ACE2 PROTEINS FOR SURFACE PLASMON RESONANCE (APR) ANALYSIS

Plasmids encoding the RBD (residues 318-510) fused C-terminally with a Fc tag of human IgG1 were constructed as described elsewhere [132,178,199]. Briefly, the RBDs of the CEVs were amplified using the following primers encoding NheI and BspEI restriction sites (underlined), respectively: 5'-CCGTGCTAGCCAATATTACAAACTTGTGTCCTTTGGAGAG-3' and 5'-ACATTCCGGAAACCGTGGCCGGTGCATTTAAAAGTTC-3'. The RBD amplicons were digested and ligated into the R5T3-Ig vector, after which RBD-Fc fusion proteins were produced in 293F cells (Invitrogen) and purified with Protein A-Sepharose affinity chromatography. Soluble human ACE2 protein corresponding to its N-terminal extracellular domain (aa18-740) was kindly provided by Dr. Fang Li at University of Minnesota Medical School [61].

Binding of hACE2 to different RBDs were analyzed on a Biacore T100 (Biacore) at 25 °C, as described previously [64,132,153]. Anti-human IgG Fc antibody (Biacore) was covalently coated onto a CM5 sensor chip with an Amine Coupling Kit (Biacore).. ACE2 soluble protein was injected over each flow cell at the flow rate of 30 μ l /min in HBS buffer at different concentrations ranges depending on binding affinity for each Ab. A buffer injection served as a negative control. Upon completion of each association and dissociation cycle, surfaces were regenerated with 3M MgCl₂ solution. The association rates (*ka*), dissociation rate constants (*kd*), and affinity constants (*KD*) were calculated using Biacore T100 evaluation software. The goodness of each fit was based on the agreement between experimental data and the calculated fits, where the Chi² values were below 1.0. Surface densities of Abs were optimized to minimize mass transfer. All *ka*, *kd*, *KD* reported here represent the means and standard errors of at least two independent experiments.

GROWTH CURVES

To access virus growth, VeroE6, DBT-humanACE2, or DBT-civetACE2 cell lines were infected with Epsilon (MA 5-set), icSARS, or CEVs1-10 at a multiplicity of infection (MOI) of 0.1 for 1 hour at 37°C. After inoculation, the cells were rinsed twice with DPBS and growth medium (MEM +10%FcII and 1% anti/anti) was added to the cultures. 100uL aliquots of cell medium were taken at 3, 8, 12, 24, and 32 hours post-infection, stored at -80°C, and titers later determined by plaque assay on VeroE6 cells. Growth curves were performed on at least two independent occasions, with consistent results, and the data shown is representative.

NEUTRALIZATION ASSAYS

Neutralization titers were determined by microneutralization, as described previously [42]. Briefly, mAbs were serially diluted twofold at twice the final concentration, and then incubated with an equal volume of 100pfu virus at 37°C for one hour. (Virus titers were determined by plaque assay.) The virus-antibody combination was then added to a 96-well plate with 5x10³ Vero E6 cells per well, with 5 replicates for each of 8 antibody dilutions. Virus was allowed to infect cells for 1 hour, 2xMEM was added to each well, and wells were checked for cytopathic effect for 3-5 days post-infection. Starting mAb concentrations were 20 μ g/mL, adjusted down to 5 or 2 μ g/mL as required for mAbs with lower EC50s (s227, s230). To determine the combination/competitive index, as described previously [136], a

microneutralization assay was conducted as described above with s227, s230, and s227+s230, with the following changes: total antibody concentrations started at 10µg/mL for each (i.e. 5 µg/mL of each antibody in the combination) and with 7 replicates for each of 12 antibody dilutions.

4.4. Results

CEV VIABILITY AND RECEPTOR BINDING.

Ten combinatorial escape viruses (CEV) were designed to encode multiple antibody escape substitutions within the receptor binding domain (RBD) (Figure 1). Substitutions incorporated into CEV originated from a broad panel of antibody escape substitutions previously selected by mAbs isolated by B-cell immortalization or phage display and derived from SARS patients or naïve libraries, respectively [164,168]. Subsequent analysis of a panel of antibodies from the immune population grouped the antibodies into 6 categories of neutralizing breadth, including antibodies that only neutralized the late phase Urbani strains to others that targeted, conserved broadly neutralizing epitopes encoded within animal and early/middle phase SARS-CoV strains[42]. Of these, we include escape variants from four groups (Groups I, II, IV, and VI), with particular emphasis on the four broadly neutralizing antibodies (s109.8, s215.17, s230.15, and s227.14) [42]. In addition, the 80R mAb was selected from a naïve library and extensively characterized; subsequent modifications by two laboratories have generated high affinity derivatives (Rs2 and SK4), a broadly neutralizing mAb designed with structure-guided focused mutagenesis (Fm6), and two re-selected to maintain breadth while neutralizing the Fm6-escape variant (Y12 and Y112A) [64,131,132] (Fig. 2A). Individually, the majority of the escape substitutions incorporated into the CEVs were associated with significantly delayed replication kinetics at early timepoints on VeroE6 cells, eventually achieving comparable peak titers by 36 hours after infection [62,132]. A similar trend, though not as pronounced, was seen for several escape viruses growing on hACE2-DBT cells [62]. It is not clear whether combinations of these escape mutations would select for synergistic or antagonistic alterations in virus receptor interactions and S glycoprotein function resulting in reduced virus fitness and/or viability. The antibody escape sites in the RBD cover six antibody-escape epitopes as determined by cross neutralization studies, five of which lie directly along the interface with the SARS-CoV receptor, hACE2 (Fig. 2B).

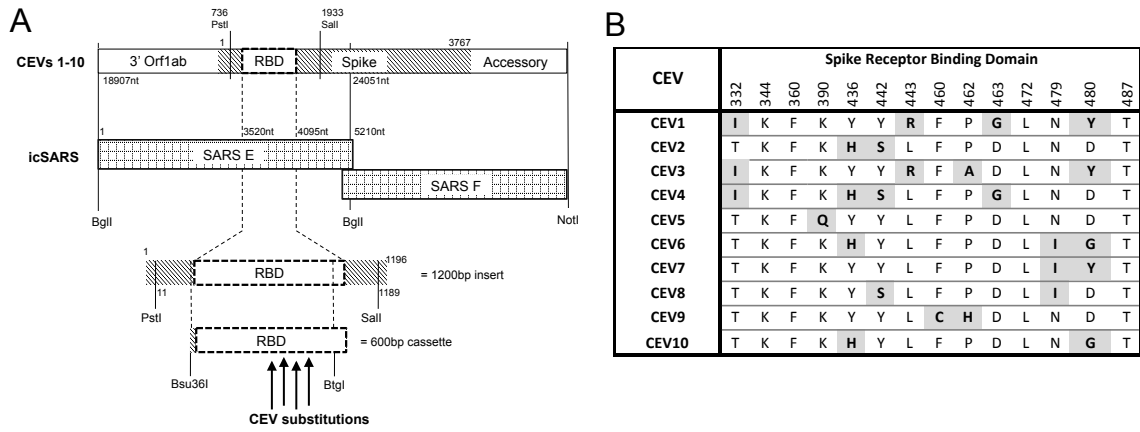


Figure 4.1: Combinatorial Escape Viruses.

A) Scheme for virus assembly from 600bp and 1200bp synthetic constructs. B) Amino acid sequence differences between the 10 CEVs and Urbani (WT).

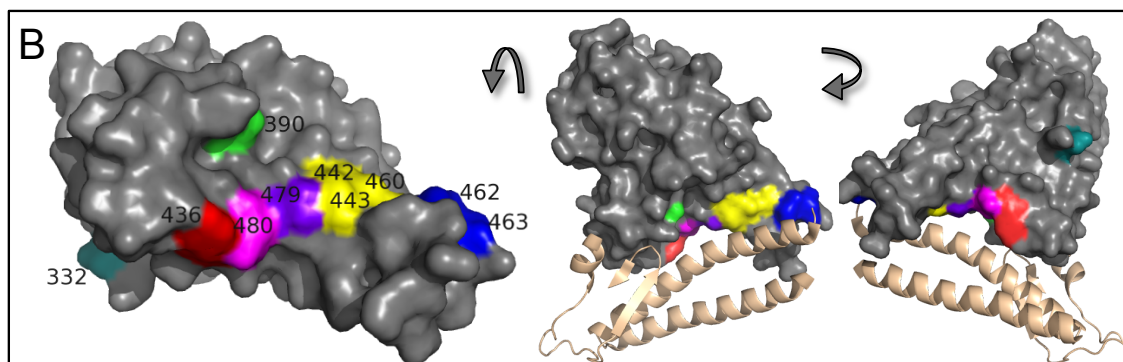
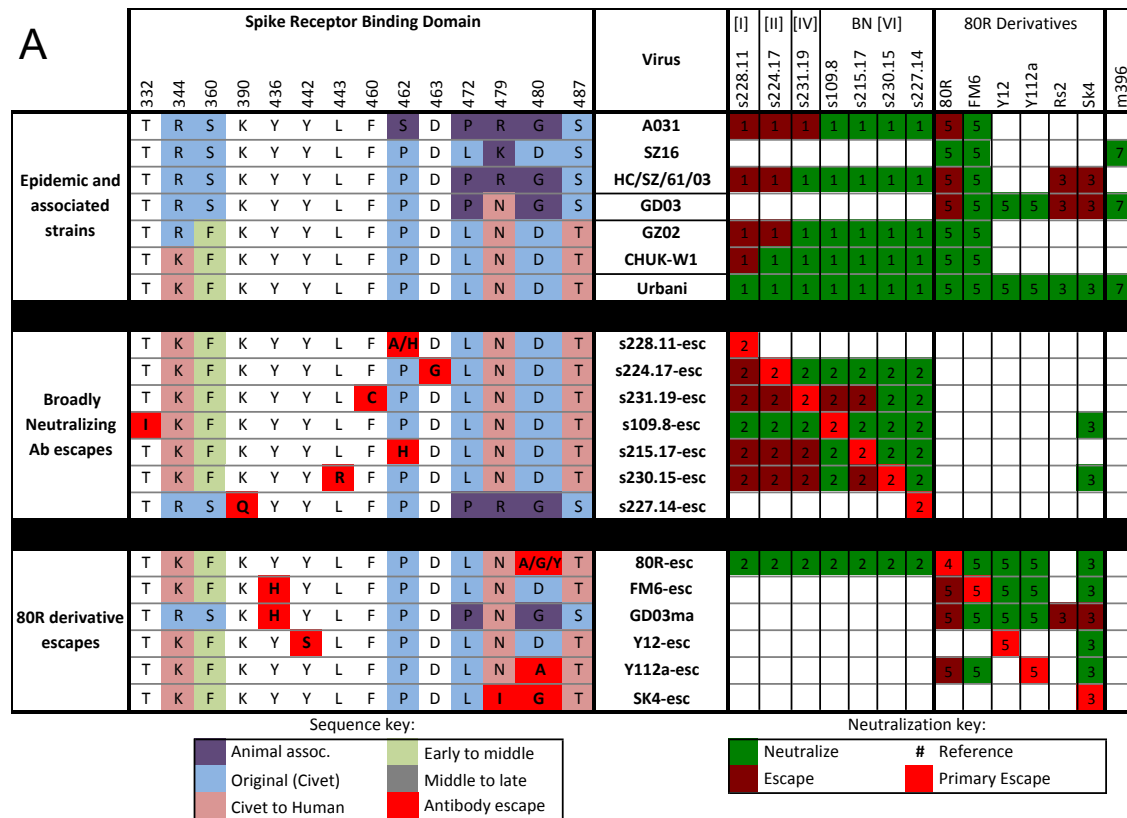


Figure 4.2: Panel of antibody-escape profiles.

A) Sequences and antibody neutralization profiles of epidemic strains and antibody escape viruses. References for neutralization phenotypes: 1=[42], 2=[62], 3=[131], 4=[64], 5=[132], 6=[80]. B) Antibody escape epitopes modified in CEVs, with residue numbers (relative to spike sequence) indicated on RBD (gray) on left. To right is same molecule, shown in complex with ACE2 interface with RBD. The D480 residue is shared by both the red (Y436) and purple (N479) epitopes, and CEV-6, CEV-7, and CEV-10 have multiple substitutions within these conjoined epitopes.

PREDICTIONS AND BINDING DATA FOR CEV RBDS INTERFACING WITH HUMAN ACE2.

For combinational therapy, a goal is to identify antibody combinations that select for combinations of deleterious escape mutations, perhaps by attenuating virus-receptor interactions. In our design of the ten

combinatorial escape viruses we used prior growth data for the individual escape substitutions, homology modeling, and FoldX differential energy calculations to predict which mutation combinations would most severely alter RBD-receptor stability and interaction energy between the two molecules, and therefore the viability of recombinant viruses. Based on previous growth analyses of single substitution escape variants, we predicted that the most impaired of the combinatorial escape viruses (CEVs) would include recombinant viruses, CEV-1, CEV-3, and CEV-4, because they all contained four substitutions across RBD, each of which were independently associated with reduced virus in growth on Vero cells. Additionally, CEV9 (P462H and F460C) was predicted to significantly alter the RBD backbone in one localized region, with P462H predicted to alter an essential aromatic stacking interaction and destabilize the local structure, potentially reducing viability (Fig. 2) [62]. Of the two substitutions incorporated into CEV-9 (blue in Fig. 2B), the P462H virus had no impact on virus growth while the F460C virus caused significantly reduced growth on both Veros and hACE2-DBTs, respectively [62]. Notably, a homology model generated in Rosetta Design predicted that the CEV9 combination would severely alter the local structure around residues 462 and 460, disrupting the cystine 467-474 bond (Fig. 3) and reducing stability of the RBD.

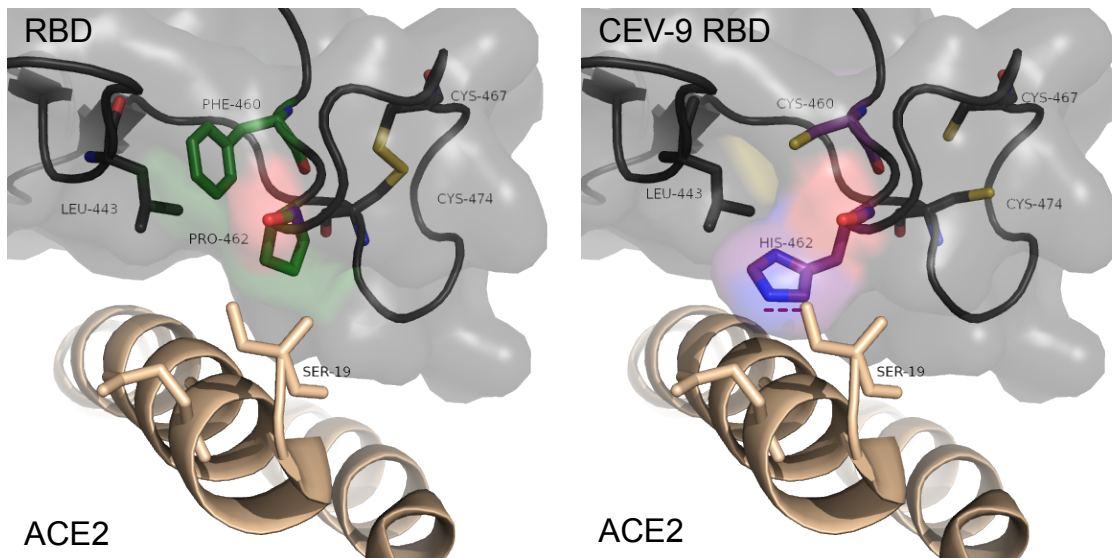


Figure 4.3: Predicted localized destabilization in CEV-9.

Rosetta design, which does not allow alterations to the backbone but rather creates homology models using side chain movement only, shows a disruption of the cystine 467-474 bond.

In an attempt to quantify predicted viability differences between CEVs, we generated two versions of homology models, both based off the crystal structure of the RBD in complex with ACE2 (PDB code 2AJF) [61]. We then used FoldX to calculate the predicted changes to stability and interaction energy between ACE2 and the RBDs [218]. In the first method, we used FoldX to generate 5 models from an energy minimized 2AJF structure, and in the second we generated 10 homology models using RosettaBackrub [216]. Using binding data and virus titer data on Veros for 6 single escape variants from a previous study [132], we evaluated the FoldX interaction energy and stability predictions for homology models generated by FoldX and RosettaBackrub. The Backrub-generated homology models were much more accurate than FoldX-generated models in predicting relative binding affinity and titer for the 6 single substitution variants (Fig. 10), therefore we extended this analysis to the combinatorial escape viruses.

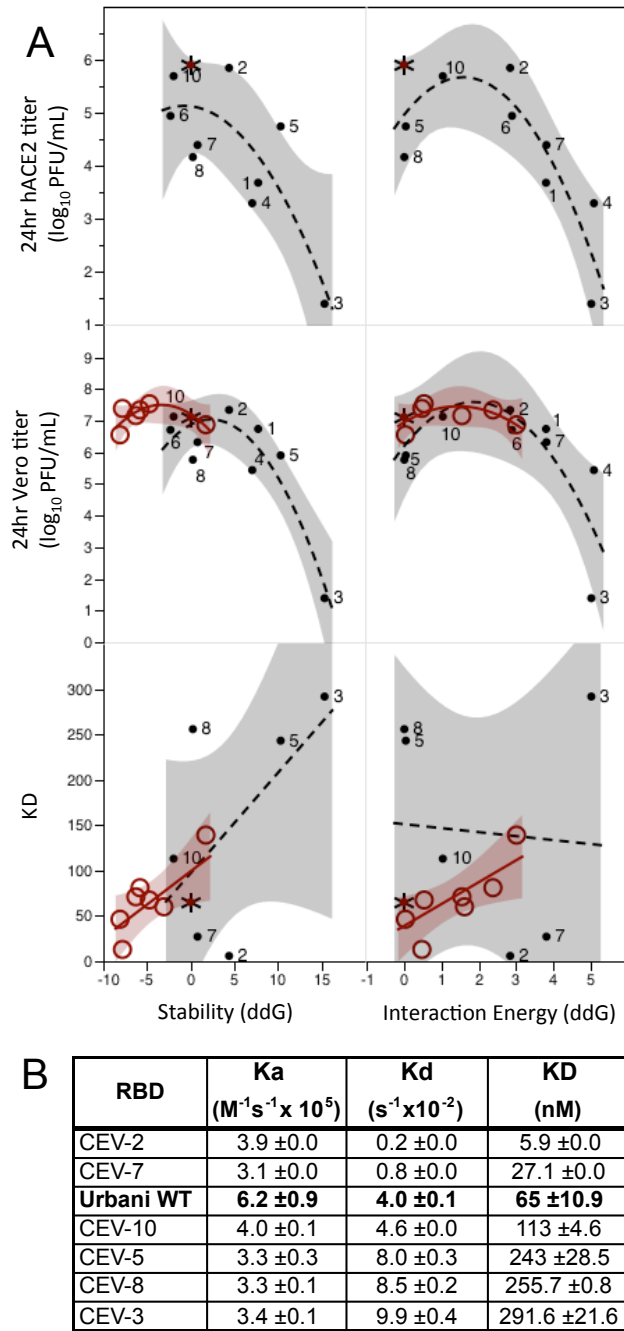


Figure 4.4: Predicting CEV viability

A) Predicted stability and interaction energy changes (ddG) for single escape variants (red, open circles) and combinatorial escape viruses (black, small circles) correlated to binding affinity (KD (nM)) and 24hr titers on hACE2 and vero cells. WT RBD is indicated by an asterisk. B) Binding data for a subset of CEVs.

As we expected, the CEV homology models were calculated to have a much broader range of stabilities and interaction energies (Fig. 4). For comparative purposes, the binding affinities of a subset of the CEV-RBDs were also determined in complex with the human ACE2 molecule (Fig. 4b). The

correlation of stability with binding affinity was markedly impaired for the 6 CEVs compared to the 6 single substitution variants, although both stability and interaction energy of the RBD did show an association with titers on humanACE2-DBTs and Veros. The FoldX analysis of backrub generated homology models ranked CEV3 as having the greatest increase in stability (ΔG) and interaction energy with ACE2 compared to the wildtype structure. Further, the binding affinity for CEV3 was the highest measured, suggesting that CEV3 was the least likely of the 10 CEVs to be viable. Indeed, despite three independent attempts no viable CEV-3 virus was recovered. Under identical conditions, the remaining nine other CEVs were viable, replicating to titers of between 1.2×10^6 and 3.4×10^7 pfu/mL.

CEV REPLICATION

We assessed growth curves for each of the nine viable CEVs on VeroE6, DBT-hACE2, and DBT-cACE2 cell lines. Growth curve titers for all 9 viable viruses were largely overlapping with the WT virus on Vero cells, with some delay at early timepoints (<10 hours post infection). All viruses grew to peak titers above $6.7 \log_{10}$ pfu/mL and within 1 log of the WT virus, which had a peak titer of $7.2 \log_{10}$ pfu/mL at 24 hours post infection. However, CEVs -4, -5, -7, -8, and -9 have some lag in titer, >0.7 log below WT at 24 hours post-infection, and CEV-4 is 1 log below WT at 24 hours post-infection.

We also assessed growth on delayed brain tumor (DBT) cells stably expressing either the human or civet ortholog of the ACE2 receptor (DBT-humanACE2 or DBT-civetACE2, respectively) [55]. The WT virus grew to $5.9 \log_{10}$ pfu/mL on hACE2-DBT cells, while CEV growth on hACE2-DBTs demonstrated greater variability than that seen on Vero cells. Five of the CEVs (left graphs, Fig. 5) are within 1 log of WT growth, although CEV-5 peaked early and declined and CEV7 was delayed in peak titer. The other four viruses, CEV-1, CEV-4, CEV-8, and CEV-9, showed impaired replication on hACE2-DBTs with peak titers below $4.2 \log_{10}$ pfu/mL. The civetACE2-DBT cells support lower replication of WT virus, as previously published [55], with peak titers of $\sim 4 \log_{10}$ pfu/mL. Only CEV2 had significantly increased replication on civetACE2-DBTs, with a peak titer of $5.4 \log_{10}$ pfu/mL. CEV-6 and CEV-10 had delayed growth kinetics, and CEVs -7, -1, and -4 demonstrated poor replication with peak titers below $2.9 \log_{10}$ pfu/mL.

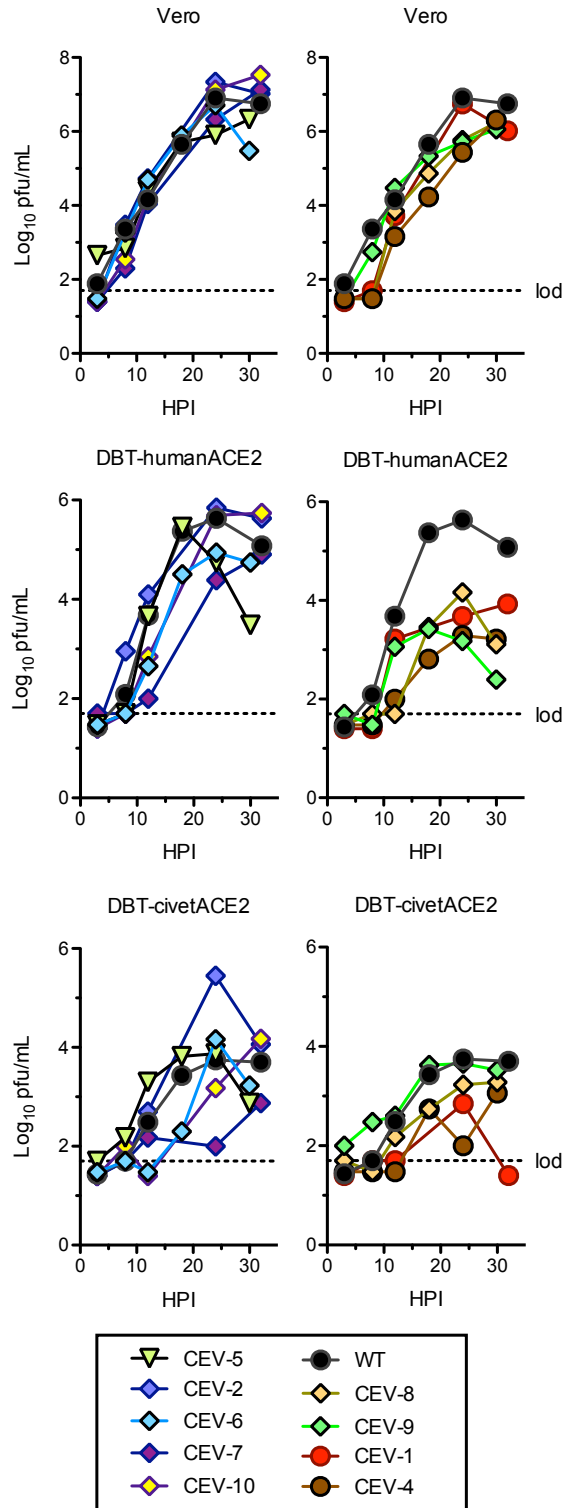


Figure 4.5: Growth curves to assess replication and virus production.

The 9 viable CEVs are shown in two groups, left are the 5 that grew to comparable titer on hACE2, right are the 4 that grew poorly on hACE2-DBTs. Growth curves are representative of two experiments.

CEV NEUTRALIZATION PHENOTYPES

To assess the effect of combinations of escape-associated substitutions we conducted microneutralization assays for the nine viable CEVs with seven representative monoclonal antibodies (Fig. 6) that include broadly neutralizing (Fm6, Y112A), high affinity (RS2, SK4) derivatives of 80R, as well characterized antibody derived from a naïve library. Additionally, we used the most potent broad neutralizing antibodies derived from immune B-cell clones (s227.14 and s230.15), and, m396, which was derived from a different library and has no known escape mutations [64,80,131,132,164]. Importantly, these antibodies select for escape mutants in different parts of the RBD and do not elicit any known cross escape phenotypes across the panel. Importantly, 80R and its derivatives and m396 structures in complex with ACE2 have been reported. Predicted neutralization phenotypes were constructed based on the inclusion or absence of a particular antibody's escape substitution within each of the viruses and structural predictions across the 80R and m396 interface.

Broadly Neutralizing Antibodies. The only monoclonal antibody capable of neutralizing all CEVs was s227.14, a broadly neutralizing antibody with no known escape variant in the SARS-CoV Urbani backbone. The only identified escape variant for s227.14 is a K390Q substitution selected on a civet virus backbone (HC/SZ/61/03) [42]. Incorporation of the K390Q substitution into the WT/Urbani backbone (CEV5) did not confer resistance to s227.14, thus this particular antibody's escape phenotype is dependent upon coordinated interactions with other residues encoded within the HC/SZ/61/03 backbone (Fig. 6).

| Virus | s230 | | s227 | | 80R | | FM6 | | Y112A | | RS2 | | SK4 | | m396 | |
|-------|--------------|-------------|--------------|-------------|--------------|-------------|--------------|-------------|--------------|-------------|--------------|-------------|--------------|-------------|--------------|-------------|
| | EC50 (ug/mL) | Fold Change |
| WT | 0.313 | | 0.156 | | 6.25 | | 2.5 | | 0.156 | | 0.625 | | <0.039 | | 2.5 | |
| CEV5 | <0.078 | 1 | <0.156 | <u>0.50</u> | 1.25 | 0.2 | 1.25 | 0.5 | 0.156 | 1.0 | 1.25 | 2 | <0.039 | 1 | 2.5 | 1.0 |
| CEV2 | <0.078 | 1 | 0.625 | 4 | 40 | <u>6.4</u> | >20 | <u>16</u> | >20 | 256 | >10 | 32 | 0.625 | 32 | 5 | 2.0 |
| CEV6 | 1.25 | 32 | 0.313 | 2 | >40 | <u>12.8</u> | >20 | <u>16</u> | >20 | 256 | >10 | <u>32</u> | >5 | <u>513</u> | 2.5 | 1.0 |
| CEV7 | 1.25 | 32 | 0.313 | 2 | >40 | <u>12.8</u> | 20 | 8 | >20 | 256 | >10 | <u>32</u> | >5 | <u>513</u> | >10 | 8.0 |
| CEV8 | 1.25 | 32 | 0.313 | 2 | 5 | <u>0.8</u> | >20 | 16 | 2.5 | 16 | >5 | 16 | 1.25 | 64 | 2.5 | 1.0 |
| CEV10 | <0.078 | 1 | 0.313 | 2 | >40 | <u>12.8</u> | >40 | <u>32</u> | >20 | 256 | >10 | 32 | >5 | 513 | 2.5 | 1.0 |
| CEV9 | >10.0 | 513 | <0.078 | 0.25 | 5 | 0.8 | 5 | 2 | <0.156 | 0.5 | 0.625 | 1 | 0.15625 | 8 | 2.5 | 1.0 |
| CEV1 | >10.0 | <u>513</u> | 0.313 | 2 | >40 | <u>12.8</u> | 5 | 2 | >20 | 256 | >10 | 32 | 0.625 | 32 | 2.5 | 1.0 |
| CEV4 | 0.313 | 8 | 0.313 | 2 | >40 | <u>12.8</u> | >20 | <u>16</u> | 20 | 128 | >10 | 32 | 1.25 | 64 | >10 | 8.0 |

Figure 4.6: CEV neutralization results.

EC50 values and fold change relative to WT for 7 monoclonal antibodies. Neutralization of CEVs by monoclonal antibodies representing broadly neutralizing 80R derivatives, affinity matured 80R derivatives, BN mAb from a human immune library, and m396 (from a non-immune human scFv library). Fold change is calculated as 2x upper limit of detection viruses not neutralized at the highest mAb concentration tested. Underlined fold-change values indicate viruses containing escape substitutions relevant to the mAb being tested.

S230.15 is another broadly neutralizing mAb with an escape substitution, L443R, identified following selection after SARS-CoV Urbani infection. Notably, CEV-6, CEV-7, CEV-8, and CEV-9 demonstrated significant resistance to s230.15 despite lacking any changes at the known escape site. Notably, cross-neutralization studies with viruses incorporating the individual substitutions of CEV-9 (F460C, P462H) had been readily neutralized by s230.15, while substitutions incorporated in CEV-6, CEV-7, and CEV-8 (Y436, D480, N479, and Y442) had not been assessed individually [62]. All four demonstrated EC50 values more than 32-fold higher than required to neutralize the WT virus. Due to the low EC50 for WT (0.313 $\mu\text{g}/\text{mL}$), even a 32-fold rightward shift (to 1.25 $\mu\text{g}/\text{mL}$) may indicate continued neutralization within physiologically relevant concentrations for CEV-6, CEV-7, and CEV-8. In contrast, CEV-9 was not neutralized at the highest concentration tested, 10 $\mu\text{g}/\text{mL}$. Therefore, we can extend the proposed footprint for mAb s230.15 from the single escape substitution, L443R (purple, Fig. 7), to include the domain covered by CEV-9, (green, Fig. 7), and the overlapping domain altered in CEV-6, CEV-7, and CEV-8 (blue, Fig. 7). We note that these escape-associated sites form a contiguous predicted epitope on the RBD surface along the interface with ACE2, and although speculative, these data suggest that these sites define the effective binding track for S230.15.

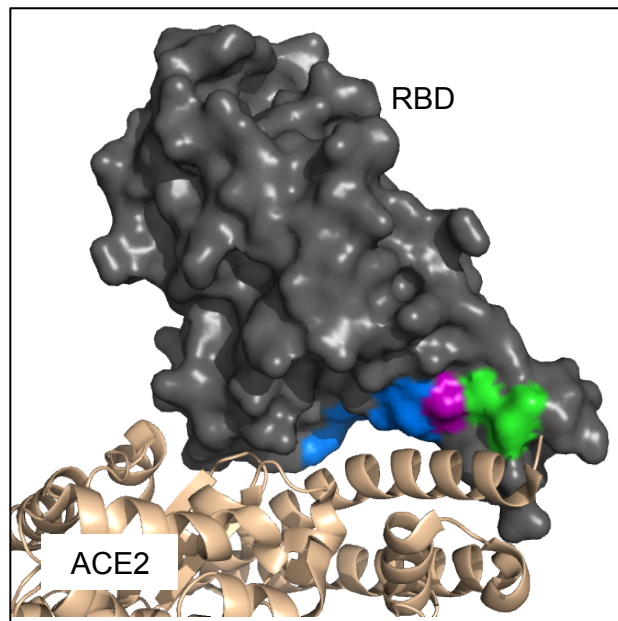


Figure 4.7: Expanded binding tract for mAb s230.15.

The primary escape site for s230.15 is L443R (purple). CEV-9 completely escaped neutralization by s230.15 with two substitutions, F460C and P462H. These substitutions form a contiguous epitope along the interface with hACE2. Blue is >32-fold shift (Y436, D480, N479, Y442). Yellow-orange is known escape

site (L443). Green is sites included in CEV-9, full escape (F460, P462). Unlikely that backbone of structure will remain with loss of the disulfide bond between cysteine(C) 474 and C467, but suggests combination of altered disulfide bonding and P463A substitution would substantially alter this epitope.

80R-Derivative Antibodies. The 80R antibody and its derivative antibodies likely interface along an overlapping footprint in the SARS RBD [132]. Several CEVs with combinations of substitutions around the 80R binding site allowed for escape from the 80R derivative antibodies. Escape studies of 80R repeatedly select for substitutions at residue 480, but cross neutralizations have extended the functional 80R epitope to include substitutions at residues 436 and 479 [132]. Notably, the 80R derivatives Y112A, RS2, and SK4 were incapable of neutralizing several viruses with substitutions in the 80R escape epitope, regardless of whether individual substitutions alter derivative antibody neutralization phenotypes. For example, Y112A selects for escape at N479I and can neutralize both the Y436H and the D480G escape mutant viruses. Surprisingly, CEV10, which combines Y436H and D480G, is completely resistant to Y112A neutralization. CEV-2, CEV-10, CEV-1, and CEV-4 were also highly resistant to neutralization by Y112A, Rs2, and SK4. However, the presence of a substitution at 436, 479, or 480 in a CEV does not unequivocally provide escape from 80R and other 80R-derived antibodies. In an example of a novel susceptibility phenotype, CEV8 is neutralized by 80R despite the presence of the N479I substitution. These novel escape and susceptibility phenotypes emphasize the plasticity of the RBD and the complexity of antibody binding epitopes. Substitutions within the epitope shift the susceptibility to neutralization by 80R-derivative antibodies, and further substitutions, both within the epitope and outside it, can push the virus to complete escape or generate novel susceptibilities.

The Fm6 and Sk4 antibodies are either broadly neutralizing and/or high affinity derivatives of 80R, respectively. Targeting the same epitope, the Fm6 phenotype was largely predictable; it failed to neutralize every CEV containing the Y436H substitution. One exception that was unexpectedly resistant to Fm6 neutralization, CEV-8 (Y442S, N479I), has 2 substitutions, each individually associated with escape from other 80R-derivative Abs, Y12 and Sk4, respectively [131,132]. The 80R binding tract therefore offers several residues at which the tolerance for 80R-derivative Ab binding may be shifted, and accumulations of substations in this region may allow escape phenotypes not predicted by selection from a clonal laboratory stock. In contrast to the predictability of Fm6, the majority of the CEVs escaped neutralization by the high affinity single chain Ab SK4. In a previous study, SK4 was capable of

neutralizing eight escape viruses with single substitutions across the RBD, but incapable of neutralizing the icHC/SZ/61/03 or GD03MA viruses, each containing six substitutions compared to the Urbani RBD [131]. The escape of 4 CEVs predicted to be neutralized suggests that the high affinity Ab has less tolerance for broad changes in the binding epitope.

M396 – a distinct epitope. The monoclonal antibody m396 was included in the neutralization screen as its interaction domain is known and distinct from 80R; so no known neutralizing epitopes were included in the CEV design. The m396 antibody-RBD interface overlaps the hACE2-RBD interface, with RBD residues I489 and Y491 predicted to contribute strongly to m396-binding [80]. CEV-5 had a substitution K390Q that was flanked by the m396 binding domain, was strongly neutralized by m396, while two alternate CEVs (CEV-4 and CEV-7) were highly resistant to m396 neutralization (Fig. 6). To determine whether we inadvertently incorporated an escape mutation into CEVs -4 and -7, we used m396 to select for escape variants, using wildtype SARS-CoV. After 3 passages under increasing antibody concentration m396, escape viruses were selected that grew to high titer in the presence of 20µg/ml of m396. Five escape viruses were sequenced, each with a single substitution in the RBD: R395S (1), R395T (2), and D392E (2). Note that D392A was shown to have no significant effect on binding to ACE2 [220], and the homology analysis of D392E suggests increased steric hinderance is cause of escape (Fig. 8C). R395A was shown to reduce binding, and analysis of a homology model suggests that R395T results in the loss of polar contact with m396-D95 (Fig. 8D). Notably, neither of these substitutions are incorporated into any of the CEVs, suggesting that resistance to m396 demonstrated by CEV-4 and CEV-7 are conferred by more general changes to the topology of the RBD. (Fig. 8A).

ASSESSING THE COMPETITIVE INDEX OF A PROPOSED COMBINATION THERAPY.

The mAbs s227.14 and s230.15 were the two most potent of the group 6 broadly neutralizing antibodies in a previous study, and s227.14 neutralizes all native variants and CEVs tested to date [42,62]. Additionally, s230.15 selects for escape variant L443R which is incorporated in both CEV3 and CEV1, a non-viable and attenuated CEV, respectively. Despite evidence of competitive binding to immobilized SARS-CoV spike glycoprotein [42], s227.14 and s230.15 did not display any evidence of antagonism in a co-neutralization assay (Fig. 9a). Combination index (CI) calculations for s227.14 and s230, based on microneutralizations conducted in septuplet, indicate non-competitive neutralization for the two

monoclonal antibodies (Fig. 9b). This suggests a cocktail of s227.14 and s230.15, two broadly neutralizing antibodies with non-competitive interaction, would prevent escape or select for attenuated escape variants.

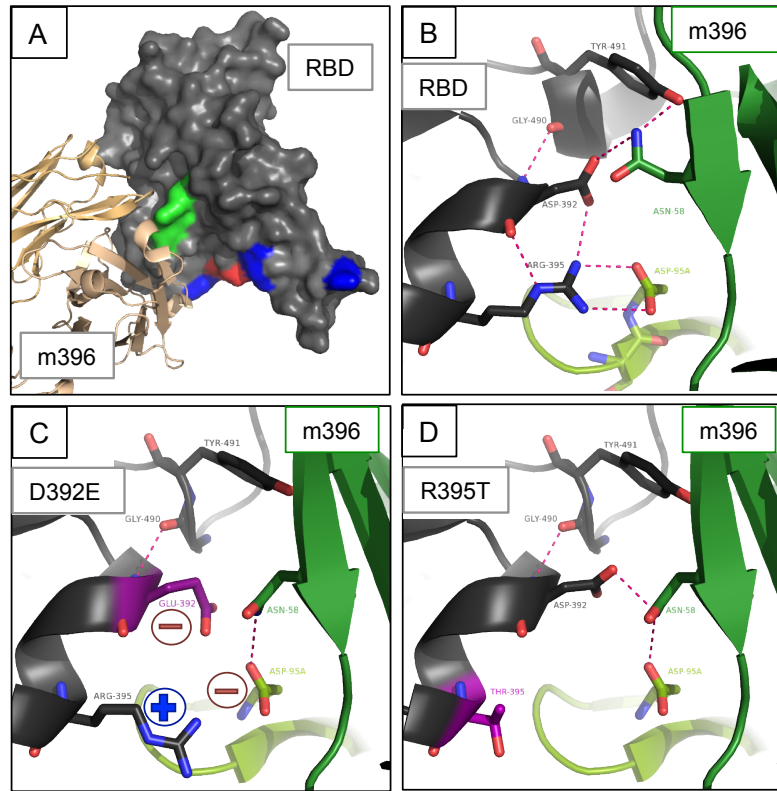


Figure 4.8: Mechanisms of escape from m396.

A) Topology of escape variants to m396. Single m396 escape residues, D392 and R395, are shown in green. Combinatorial m396 escape virus residues are shown in blue (CEV-4) and red (CEV-7). B) The interface between SARS RBD (gray) and m396 (green) includes multiple polar interactions and an electrostatic interaction between R395(RBD) and D95(m396). C) The D392E substitution associated with m396 escape increases steric hindrance at the RBD-mAb interface, introduces a negative charge, and alters the orientation of R395, breaking multiple polar bonds. D) The R395T substitution breaks the electrostatic interface between N95 and R395.

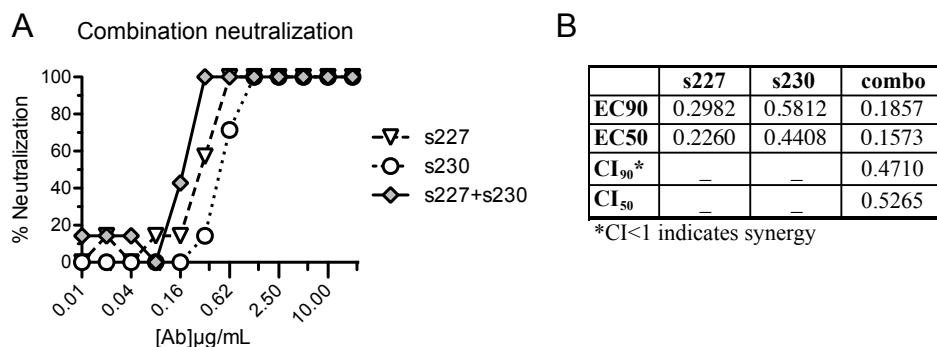


Figure 4.9: Co-neutralization with s227.14 and s230.15.

Despite evidence of competitive binding to immobilized SARS-CoV spike glycoprotein [42], s227.14 and s230.15 did not display any evidence of antagonism in a co-neutralization assay. B) Combination index (CI) calculations for s227.14 and s230, based on microneutralizations conducted in septuplet, indicate non-competitive neutralization for the two monoclonal antibodies [136].

4.5. Discussion

Group 2b betacoronaviruses demonstrate remarkable diversity in the spike glycoprotein, and not surprisingly, animal and human SARS-CoV spike glycoproteins were demonstrated to evolve rapidly during the 2003/04 epidemic, perhaps from immune mediated host shifting [36,42]. Further, the epidemic strain of SARS-CoV (Urbani) readily evolved mutations that diminished neutralization phenotypes from 38 of the 39 monoclonal antibodies (mAb) tested in our laboratory, including the evolution of rare adjacent mutation sets in key residues that engage the human RBD receptor [131]. Given these findings, it seems likely that single monoclonal antibody therapies may fail in an outbreak setting, despite improvements in selection, structure-based design, and manufacturing of therapeutic over the past decade [138,221,222]. For viruses that evolve quickly like influenza, HIV and noroviruses, efforts have focused on identifying mAbs with broad neutralization phenotypes capable of neutralizing antigenically diverse viruses while preventing viral escape. Several groups have noted the possibility of using a therapeutic cocktail of two or more mAbs to prevent escape [131,132,210]. In this work we describe the construction and characterization of 10 combinatorial escape viruses (CEVs) designed to incorporate up to four antibody-escape associated substitutions within the receptor binding domain. We generated these 10 CEVs in order to aid in the rational selection of broadly neutralizing mAbs cocktails that simultaneously minimize the likelihood of viral escape while ensuring that any escape mutants that might emerge would be less fit than other

circulating strains. In parallel, we sought to assess our ability to use available structure-based predictive tools to assist in therapeutic design. This platform approach may be broadly applicable to other important human pathogens.

In this manuscript, we develop a genetic approach to evaluate coordinated interactions of escape mutations with the goal of identifying antibody combinations that select for substitution sets that are highly deleterious or lethal, assessments based on *in vitro* replication and *in vivo* pathogenic features. We identify one combination of substitutions, CEV3 (T332I, L443R, P462A, and D480Y), which was not viable despite three independent attempts to grow the virus. In addition, while all viable CEVs grew within one log of the peak WT titer on VeroE6 cells, there were significant delays and limitations to peak titers on hACE2-DBTs cells. The limited replication of CEV-1, CEV-4, CEV-8, and CEV-9 on hACE2-DBTs likely reflects the fitness cost of the combined escape substitutions, either by altered binding to hACE2 on a cell line with altered receptor density, or by destabilization of the structure. Primate and human ACE2 protein sequences are identical across the region that interacts with the RBD, but the expression levels of ACE2 on the hACE2-DBT cells is higher than on Vero cells when assessed with a polyclonal antibody against the hACE2 ectodomain [55]. It is possible that high level receptor expression may establish a dominant negative effect on virus replication by preventing S incorporation into mature virions, thus, it is possible that some CEVs encode defects which are receptor concentration dependent [223]. Additional differences in host cell environments, including proteases like TMPRSS2 and Cathepsin L which are involved in Spike processing during entry, may also contribute to these differences in CEV relative peak titers between cells lines [224]. It is notable, however, that nine of the ten CEVs were viable in cell culture, replicating to comparable titers on Vero E6 cells, indicating a broad flexibility in the RBD for several coincident changes.

We used the extensive structural data available for the SARS-CoV RBD to generate homology models for each of the CEVs by two different programs, FoldX and Rosetta Backrub [216,218]. Rosetta Backrub has the capacity to allow for small changes in backbone of a protein model, but cannot change cysteine residues (and therefore could not model CEV-9). FoldX, in addition to generating homology models, can calculate (or predict?) free energy (“stability”) and the energy differences between two interacting molecules in a model (as in between the RBD and hACE2). The approach has been previously

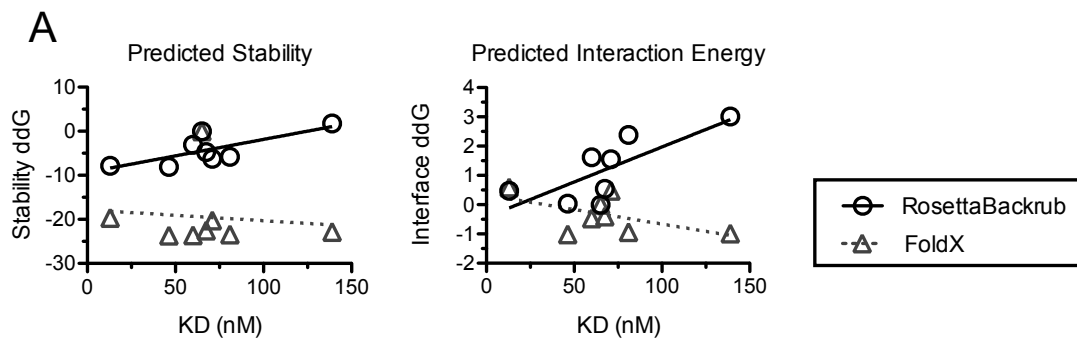
used to calculate stability changes for influenza escape mutants to oseltamivir [225,226]. By correlating changes in stability and interaction energies for single escape substitutions in the RBD with binding affinity and titer data, we assessed the accuracy of stability and interaction energy predictions calculated by the FoldX program for CEV models generated by either FoldX or Rosetta Backrub (Fig. S1) [132]. Backrub-generated models were noticeably better correlated to binding affinity for single escape variants. Perhaps not too surprisingly, the accuracy of both models was negatively affected by the multiple substitutions incorporated into the CEVs. Nonetheless, both binding data and prediction programs suggested that CEV-3 was the least stable of the viruses generated, a prediction borne out by the failure to generate a viable CEV-3 virus. Further advances in protein prediction, particularly for the more complicated problem of multiple substitutions, are necessary before these programs can be expected to reliably predict virus viability and receptor usage, but with greater sample sizes we are coming closer to identifying those thresholds.

By using a panel of human monoclonals from natural infections or phage libraries, one intended application of the CEVs was to test the preservation of escape phenotypes in the context of other substitutions within the RBD, mimicking sequential RBD changes in response to selective pressure. In general, the CEVs tested here were resistant to antibody neutralization when the correlated escape mutant was present in a particular RBD, thus the incorporation of other mutations did not appear antagonize/synergize this phenotype in this study. In parallel, CEVs were generally, but not always neutralized when a particular monoclonal antibodies escape substitution was absent. However, with the exception of s227, each tested mAb had at least one novel escape or susceptibility, and which increased our mapping of the putative interaction domain on the RBD (Fig. 1). For example the identification of novel substitutions that prevented mAb s230.15 neutralization, allowed us to predict a putative neutralization footprint for this mAb along the RBD-ACE2 receptor binding interface. Also, we note that mAb s227.14 was capable of neutralizing all nine CEVs including CEV-5, which contained the K390Q substitution that provided escape in the HC/SZ/61/03 backbone, indicating the reliance of this escape site on the other coordinated substitutions in the HC/SZ/61/03 sequence for escape.

The non-viable CEV (CEV-3) and four others with impaired growth on hACE2 (CEVs -8, -9, -1, -4) provided suggestions for which mAbs would perform most effectively in mAb combination therapies. The neutralization of all CEVs, zoonotic, and epidemic viruses enhances the appeal of s227.14 as

therapeutic cocktail component, in addition to the apparently increased barrier to virus escape. The s230.15 escape substitution is present in both CEV1 and 3, both of which are replication impaired and attenuated in vivo. In addition, the s215.17 escape substitution (P462H) is unique to CEV-9, and displays reduced growth phenotypes on hACE2 cells, and the P462A substitution (escape from s228.11) is uniquely in CEV-3, and should be further explored in future studies. Briefly assessing the feasibility of a mAb cocktail comprising two of these broadly neutralizing mAbs, we found that S227.14 does not compete with s230.15 in competitive neutralization studies, and propose this combination as an effective, escape-resistant mAb cocktail.

The vast majority of unpredicted neutralization phenotypes for the CEVs were novel escape phenotypes. These studies indicate that while a mAb may uniformly select for a single substitution when selected from a homogeneous starting population, such as a clonal laboratory virus stock, there are multiple substitutions across the antibody binding tract capable of allowing escape. Characterizations of antibody-induced antigenic drift in human influenza A virus have similarly demonstrated the persistent capacity for viral escape from a monoclonal antibody selection [143]. Our studies emphasize the structural plasticity of the Spike RBD, as multiple antibody-escape substitutions within the same epitope or in multiple epitopes across the receptor interface are viable. This structural plasticity in the RBD allows for rapid escape from antibody selection and, as the possibility of enhanced pathogenesis and simultaneous dual substitutions have already been demonstrated, it emphasizes the importance of robust characterizations of potential monoclonal antibody therapeutics. The 9 viable CEVs are powerful tools for assessing available structural prediction models, the plasticity of the RBD, the complex coordination between neutralization epitopes, and the impact of RBD substitutions on receptor binding and pathogenesis. Our characterization of the viability and neutralization phenotypes of these CEVs has allowed us to expand the predicted binding tract of broadly neutralizing antibodies and explore the functional impacts of multiple antibody escape substitutions. Further, the non-viable CEV and altered growth characteristics induced by select antibody combinations will better inform our efforts to develop both potent and broadly neutralizing cocktails of antibodies resistant to viral escape.



B

| | Stability Backrub Repaired | Stability Backrub Average | Stability FoldX Minimum | Stability FoldX Average | Interface Backrub Repaired | Interface Backrub Average | Interface FoldX Minimum | Interface FoldX Average |
|---|----------------------------|---------------------------|-------------------------|-------------------------|----------------------------|---------------------------|-------------------------|-------------------------|
| Is slope significantly non-zero? | | | | | | | | |
| F | 7.282 | 0.1756 | 0.07186 | 1.057 | 8.208 | 1.18 | 2.574 | 4.596 |
| DFn, DFd | 1.000, 6.000 | 1.000, 6.000 | 1.000, 6.000 | 1.000, 6.000 | 1.000, 6.000 | 1.000, 6.000 | 1.000, 6.000 | 1.000, 6.000 |
| P value | 0.0356 | 0.6897 | 0.7976 | 0.3435 | 0.0286 | 0.3191 | 0.1598 | 0.0758 |
| Deviation from zero? | Significant | Not Significant | Not Significant | Not Significant | Significant | Not Significant | Not Significant | Not Significant |
| Goodness of Fit | | | | | | | | |
| R square | 0.5483 | 0.02844 | 0.01184 | 0.1498 | 0.5777 | 0.1643 | 0.3002 | 0.4337 |
| Sy.x | 2.597 | 1.482 | 8.617 | 1.903 | 0.7828 | 0.7624 | 0.5808 | 0.7167 |

Figure 4.10: Summary of prediction methodologies.

KD values from single substitution escape variants [132] were compared to the predicted destabilization (Stability ddG compared to the wildtype structure, 2AJF) and interaction energy differences (Interface ddG) calculated in FoldX for homology models generated by either the FoldX “mutate multiple residues” function or by Rosetta Backrub [218,227]. Notably, the repaired structure of the lowest energy Rosetta backrub models showed a significant, non-zero, positive slope when both the calculated stability and interaction energy differences were graphed against the measured KD for the single substitution escape variant RBDs. For this reason, the repaired PDB of the lowest energy Rosetta backrub homology model was used for further analyses of predicted CEV viability. Linear regression calculations were conducted in Prism.

CHAPTER 5: Discussion and Future Directions.

5.1. Summary

The studies described in this dissertation were designed to assess immunization and therapeutic strategies for SARS-CoV, and, by extension, to enhance our characterization of the receptor binding domain of spike (S), a key neutralization target for SARS-CoV therapeutics. We make use of robust animal models that accurately replicate human disease and technologies that allow for the rapid generation, modification, and characterization of antibodies. In addition, the SARS-CoV infectious clone allows us to utilize SARS-CoV strains with heterologous S proteins and to generate novel viruses from synthetic constructs. The study of SARS-CoV and the potential therapeutics to target coronaviruses has taken on new urgency following the recent isolation and characterization of a novel human betacoronavirus, MERS-CoV [158,228]. Our studies of SARS-CoV have provided a valuable foundation for the rapid characterization of novel coronaviruses and anti-coronavirus therapeutics.

The experiments described in Chapter 2 explored the limitations of a doubly inactivated SARS-CoV vaccine (DIV), identifying a vaccine-induced immunopathology and emphasizing the importance of rigorous challenge viruses and animal models that accurately recapitulate age-associated lung pathology. Collaborations between the Baric laboratory and two other laboratories are described in Chapter 3, in which we assessed multi-generational monoclonal antibodies designed to be broadly neutralizing or escape resistant. Through this iterative assessment, we noted the flexibility of the receptor binding domain (RBD) of S and extended our characterization of this region as an antiviral target. Building from a database of escape substitutions in the RBD, we engineered ten recombinant Combinatorial Escape Viruses (CEVs) designed to assess the plasticity of the S-RBD, the utility of predictive modeling, and the neutralization networks across the RBD. Assessment of the neutralization networks across the RBD will inform our efforts to develop both potent and broadly neutralizing cocktails of antibodies resistant to viral escape. These tools will assist in the development of predictive tools and standardized platforms for combination mAb immunotherapies for emergent viruses.

5.2. SARS-Coronavirus whole inactivated vaccine studies

In our characterization of the protection and immune response to a doubly inactivated whole virus vaccine (DIV), we, like others, note that DIV can protect young mice from a homologous SARS-CoV challenge [98]. By extending our analysis to include the aged BALB/c model, as well as highly lethal homologous and heterologous challenge viruses, we noted the limited protection and possible enhanced disease in these more rigorous model systems. Specifically, we observed an enhanced immune infiltrate in the lungs of vaccinated aged animals or animals challenged with a heterologous strain. This immune enhancement appears to be Th2 skewed, with an increase in the numbers of eosinophils in the lungs of vaccinated animals as well as a significant increase in Th2-associated cytokines and chemokines. The Th2 skewing of vaccine responses in addition to the eosinophilic influx is reminiscent of other known vaccine-induced immunopathologies. These studies raised significant concerns about using whole inactivated virus vaccines in an aged population, which is both more susceptible to SARS-CoV and more difficult to vaccinate [90].

Future studies of the eosinophilic immunopathologic reaction following vaccination will seek to identify the targeted viral components as well as the host immune components that mediate this response. Venezuelan equine encephalitis virus replicon particles (VRPs) expressing the nucleocapsid protein (N) or the spike (S) were evaluated as vaccine candidates, demonstrating that VRP-S vaccines were protective. Notably this study also found that VRP-N vaccines induced a non-protective, eosinophilic inflammatory response following either homologous or heterologous challenge [88]. A vaccinia virus vaccine formulation expressing the SARS-CoV structural proteins similarly found the nucleocapsid protein to be responsible for a severe pneumonia [95]. In contrast, an evaluation of a recombinant spike and two whole inactivated virus vaccinations demonstrated an eosinophilic immunopathology for each of the formulations, suggesting the alternate hypothesis that the spike protein was responsible for the immunopathology [207]. However, the recombinant spike vaccine formulation induced significantly less eosinophilic infiltration than the whole inactivated vaccines, and lungs were assessed on day 2 post-infection, a timepoint which only displayed minimal eosinophilic infiltration following VRP vaccinations [88,207]. We expect that future studies will assess the immune responses to vaccination and challenge using recombinant S and N proteins in order to assess the effect of antigen and formulation on vaccine-induced enhancement. Identification of the viral

components and vaccine formulations that drive immunopathological responses to challenge will allow for rational design of safe and efficacious vaccines.

DIV vaccinations induced a Th2-biased immune response, including a skewing of IgG subtypes from IgG2a (Th1-associated) to IgG1 (Th2-associated) post-vaccination and a significant increase in IL-5 and IL-13 (Th2-associated cytokines) post-challenge. Interleukin(IL)-4 is a critical determinant in the development of Th2 responses, which are generally non-protective in viral infections [229]. Notably, if the nucleocapsid or another viral protein is responsible for triggering Th2-type responses independent of vaccine formulation, it is possible that innate Th2 responses may play a role in naïve SARS-CoV infections. Increased Th2 cytokines (IL-4, IL-5, and IL-10) were associated with fatal human cases of SARS [230]. Further, SARS-CoV was disproportionately lethal in individuals over 50 years of age, a population with enhanced Th2 responses [73,231-234]. Finally, a systems analysis of C57BL/6 mice infected with lethal and sublethal doses of SARS-CoV using the WGCNA (weighted gene correlation network analysis) approach grouped host responses into 24 groups of transcripts (modules) with co-regulated behavior, of which only one module displayed dose-response kinetics [235]. Two targets in this module, IL-4R α and IL-13R α 1, were listed in a prioritized ranking at positions 24 and 57, among approximately 700 genes hypothesized to be significant. These two genes form the Type II IL-4 receptor, and IL-4R α is a necessary component of the Type I IL-4 receptor, suggesting a role for IL-4 signaling in lethal SARS infection [229,236]. Ongoing studies are designed to explore the role of Th2 responses in naïve SARS-CoV infections and vaccine challenges by modulating both the host environment and through the use of recombinant viral immunomodulators.

5.2.1. Ongoing studies

One method of assessing the role of Th2 signaling in vaccination and lethal infection is to utilize knockout mouse lines with deficiencies in IL-4 signaling, the key cytokine in the development of Th2 responses. A preliminary assessment of the role of IL-4 signaling in lethal SARS-CoV infections utilized a trio of knockout mouse lines on the BALB/cJ background: IL-4 $^{-/-}$, IL-4R $\alpha^{-/-}$, and STAT6 $^{-/-}$. IL-4 is the key regulator in the development of Th2 responses, the IL-4R α subunit is required for IL-4 signaling through both Type I and Type II receptors (and additionally blocks IL-13 signaling through the Type II receptor), and the STAT6 transcription factor mediates IL-4 and IL-13 signaling. The IL-4 $^{-/-}$ and STAT6 $^{-/-}$

mice display an increased weight loss phenotype following MA15 challenge compared to the BALB/cJ controls, suggesting a protective role for IL-4 signaling in SARS-CoV infections. The IL-4R α ^{-/-} mice displayed modestly different weight loss profiles depending on the provider (Jackson Laboratory compared to Taconic Farms). However, any potential phenotype for IL-4R α ^{-/-} is complicated by small sample size of the Jackson IL-4R α ^{-/-} mice (n=3) and the lack of an appropriate control for the Taconic mice, which have not been backcrossed to the congenic BALB/cJ strain since 2000 (Taconic customer service, personal communication). We expect that future studies of IL-4 signaling in SARS-CoV will backcross commercially-available strains with their congenic controls, and then utilize these IL-4-signaling deficient mice to assess the role of Th2 signaling in vaccine-enhancement or naïve SARS-CoV challenges.

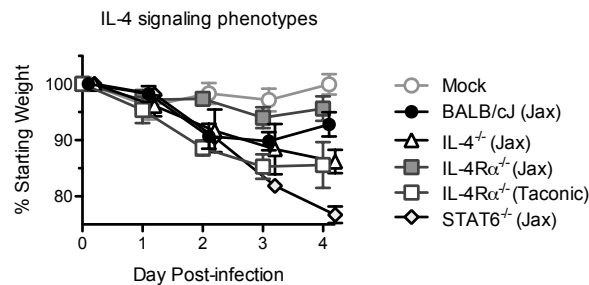


Figure 5.1 IL-4 signaling phenotypes following lethal MA15 SARS-CoV infection.

10 week old mice were infected with 10^5 pfu of MA15, which causes 10% weight loss and recovery in BALB/cJ mice. Jax = Jackson Laboratory; Taconic = Taconic Farms Inc. IL-4^{-/-} = BALB/c-Il4^{tm2Nnt}/J (n=5); IL-4R α ^{-/-} = BALB/c-Il4ra^{tm1Sz}/J (Jackson n=3; Taconic n=5), and STAT6^{-/-} C.129S2-Stat6^{tm1Gru}/J (n=5).

An alternate mechanism of modulating IL-4 signaling in SARS-CoV infections independent of host genetic factors takes advantage of the soluble IL-4R α (sIL-4R α), a naturally occurring isoform which is capable of binding and inhibiting IL-4 in a species-specific manner [237-239]. We introduced three soluble IL-4R α genes into the mouse-adapted SARS-coronavirus genome in place of the accessory proteins ORF7a/b, as previously described [240]. The three soluble IL-4R α sequences are derived from the BALB/c mouse, the C57BL/6 mouse, and the Rattus norvegicus genomes. IL-4 signaling through the IL-4 receptor is heavily species specific, so while the two mouse IL-4 receptors have small differences in binding affinity to BALB/c or C57BL/6 IL-4, the rat sIL-4R α virus will serve as a negative control for mouse pathogenesis studies and none of the three receptors will be capable of binding human IL-4 [239,241]. We anticipate that

expression of sIL-4R α will attenuate IL-4 signaling pathways and allow us to directly modulate, and therefore assess, the role of IL-4 signaling in SARS-CoV infections.

5.3. Live attenuated vaccine studies

Despite the relative ease of production, the whole inactivated virus vaccines assessed to date display limited protection from heterologous challenges or in aged animal models, and may induce nonprotective or enhancing immune responses in subsequent viral challenges [159]. In contrast to whole inactivated virus formulations, we recently demonstrated that a live-attenuated low-fidelity strain of SARS-CoV provided protection in both aged and immunocompromised mouse models with no evidence of reversion to virulence [242]. This live-attenuated formulation takes advantage of the nsp14 3'→5' exoribonuclease (ExoN), a protein required for high-fidelity replication and conserved across the coronavirus family [13]. We demonstrated that inactivation of the ExoN function in the mouse-adapted SARS-CoV (MAwt) background resulted in a virus (MA-ExoN) with attenuated pathogenesis in both young (10 week) and aged (14 month) BALB/c mice, with viral titers cleared by day 4 post-infection. Additionally, MA-ExoN did not revert to virulence or lose the attenuator phenotype after either 8 passages in aged BALB/c mice or after persistence for 30 days in SCID mice. Vaccination of aged mice with both low (102.5 pfu) and high (104 pfu) doses of MA-ExoN provided complete protection from a lethal challenge of MAwt, with no detectable titers at 2 days post-infection and high serum neutralization of the challenge virus.

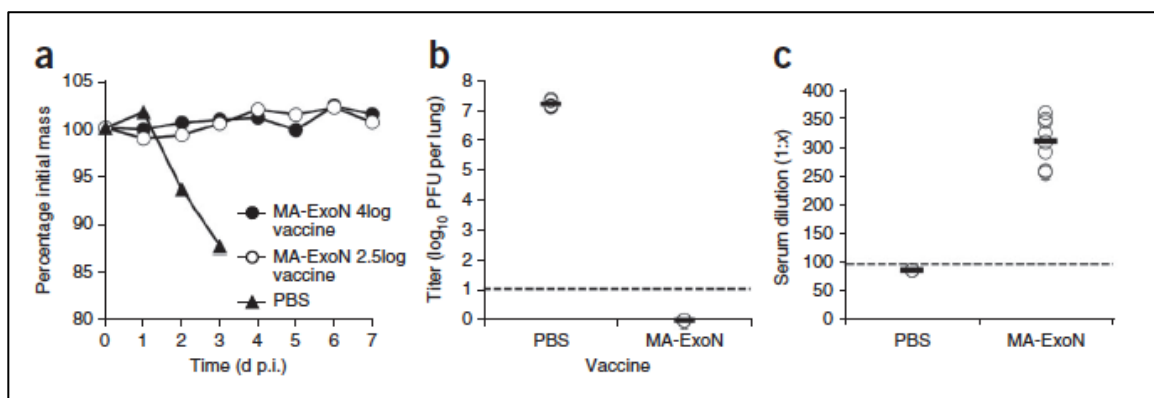


Figure 5.2: MA-ExoN vaccination protects from lethal challenge.

(a,b) Low-passage MA-ExoN and mock (PBS) vaccinations of 12-month-old female BALB/c mice followed by lethal challenge with MAwt. (a) Weight loss in challenged mice. Dark circles, 104 PFU MA-ExoN vaccination; white circles, 102.5 PFU MA-ExoN vaccination; dark triangles, PBS vaccination. Error bars indicate s.d. (b) Lung titers at day 2 after challenge. ExoN was given at a 2.5 log (102.5 PFU)

vaccination. The mean titer is indicated by a bar in each group. **(c)** Fifty-percent plaque reduction neutralization titer (PRNT50) assay using sera from PBS-vaccinated and MA-ExoN-vaccinated mice to neutralize MAwt. Reciprocal dilutions capable of effecting 50% plaque reduction are shown by circles; mean reciprocal dilutions are indicated by a bar for each group. The limit of detection for each assay, if given, is indicated by a dashed line. **Determination of viral neutralization antibody titers in mouse sera:** Mouse sera were heat inactivated for 30 min at 55 °C and then serially diluted to 1:100, 1:200, 1:400, 1:800 and 1:1,600 in PBS to a volume of 125 µl. Next, 125 µl of PBS containing low-concentration MAwt (40 PFU) or high-concentration MAwt (240 PFU) was added to each serum dilution. The virus-serum mixtures were incubated at 37 °C for 30 min. After incubation, virus titers of the mixtures were determined by plaque assay as described [101]. We then calculated the PRNT50 values, the serum dilutions at which plaque formation was reduced by 50% relative to that of virus stock not treated with serum.

5.4. Iterative development and characterization of anti-spike antibodies

Monoclonal antibodies have immense potential for the treatment of emergent viruses as they provide immediate protection, can be rapidly generated to respond to shifts in antigenicity, and can be readily used in hard-to-vaccinate populations, such as the elderly. In Chapter 3, we describe a series of collaborative experiments iteratively characterizing anti-RBD single chain fragment variable (scFv) and monoclonal antibodies (mAbs) designed to broadly and potently neutralize SARS-CoV and variants of the epidemic strain. We identified antibodies that were either escape resistant, requiring the virus adopt multiple concurrent substitutions to resist neutralization, or were broadly neutralizing, capable of preventing replication for viruses expressing the S proteins from zoonotic and human strains sampled from throughout the course of the epidemic. However, no single Ab was both escape resistant and broadly neutralizing, and escape variants to some of the broadly neutralizing antibodies displayed enhanced pathogenesis in mice. These studies extended our understanding of the RBD as an anti-viral target of neutralizing antibodies, deeply characterized the 80R epitope through the use of multiple derivative antibodies, and identified potential risks of single antibody therapy targeting a receptor binding epitope. Importantly, these studies established a platform of antibody development targeting a key neutralizing epitope of a betacoronavirus spike (S) protein, and will provide tools for the development of therapeutics for emergent coronaviruses.

The development of multiple derivative Abs targeting the same 80R epitope allowed for us to test whether a convergent combination of mAbs could prevent viral escape. Selecting an 80R-escape virus (D480G substitution) followed by selection with the broadly neutralizing Fm6 mAb led to extinction of the virus, while co-selection with both 80R and Fm6 readily generated an escape virus with a single

substitution, N479T. The successful escape from a combination protocol demonstrates that the RBD is sufficiently plastic to allow escape from multiple antibodies targeting the same epitope, although this may be a limitation of using two antibodies with only minor differences in the binding interface with the RBD. Additionally, the failure of the sequential antibody selection protocol, despite the success of the combination protocol, suggests that the viral extinction may have resulted from a starting population with limited diversity, rather than an intrinsic inability of the RBD to accommodate both the 80R-escape (D480G) and Fm6-escape (Y436H) substitutions. Several of the combinatorial escape viruses described in Chapter 4, including CEV-6, CEV-7, and CEV-10, demonstrate that a combination of these two escape substitutions are viable. Additionally, the high affinity scFv Ab Sk4 provided direct evidence that the RBD can accommodate multiple substitutions in response to antibody pressure, selecting for an escape virus with two substitutions, N479I and D480Y. It is notable, however, that two antibodies targeting a highly overlapping epitope, as when the antibodies are derived from the same parent antibody, allowed for a single substitution to provide escape from both antibodies. We anticipate that future studies will characterize divergent combination therapeutic cocktails, combinations of mAbs which target distinct non-overlapping regions of the RBD or that target both the RBD and a conserved region of the S2 domain.

The escape variants to second and third generation 80R-derivative mAbs demonstrated enhanced pathogenesis in mice, providing direct evidence that antibody pressure on the receptor interface can select for enhanced receptor-binding and emphasizing the importance of extensively characterizing antibody escape variants. These studies emphasize that mAbs targeting the RBD present a low barrier to escape for the virus, and future development should include a cocktail of mAbs targeting different epitopes within the RBD; particularly if neutralization escape variants might exhibit enhanced pathogenesis. These studies of multiple generations of antibodies and antibody escape variants, demonstrating dual substitutions, substitutions at contact interface sites, and altered pathogenesis profiles, prompted us to evaluate the plasticity of the RBD and the predictability of neutralization phenotypes with the generation of combinatorial escape viruses (CEVs).

5.5. Combinatorial Escape Viruses

Neutralizing antibodies against SARS-CoV largely target the receptor binding domain (RBD) of the Spike glycoprotein. Escape from antibody neutralization is associated with single substitutions, dual

substitutions, or even changes in contact interface sites along the RBD. The studies described in Chapter 4 assess the plasticity of the RBD, evaluate available tools for predicting stability of the variant viruses, and explore the interplay between multiple escape-associated substitutions. Detailed characterizations of antibody neutralization tracts will assist in the rational selection of combinatorial antibody therapeutics.

We note that the microneutralizations required much higher antibody concentrations than in some initial neutralizations of pseudovirus infections (i.e. 60ng/mL for 80R to neutralize a Tor2-pseudovirus, vs 6.25ug/mL to neutralize Urbani, which has the same RBD as Tor2) [168]. Further, the competitive index for the mAb combination s227.14+s230.15 suggested no antagonism between the two antibodies (Figure 4.9), despite evidence of competition in a bioassay incorporating biotinylated antibodies and immobilized S-glycoprotein [42]. In contrast, the competition assays described here were conducted with live virus and unmodified antibodies. These assay differences in calculated EC₅₀ and IC₅₀ values may be the result of structural display differences between immobilized S, pseudovirus, and live virus, emphasizing that the method of S presentation can vary between assays with measurable differences in outcome. Similarly, despite the concerning claims of enhancement of GD03 pseudovirus infection by anti-epidemic antibodies [243], no evidence of antibody-induced enhancement was demonstrated in subsequent studies with live virus, emphasizing the limitation of pseudotype assays and encouraging the use of live virus for verification where possible [88].

5.5.1. Future directions and ongoing studies

The 9 viable CEVs are powerful tools for assessing available structural prediction models, the plasticity of the RBD, the complex coordination between neutralization epitopes, and the impact of RBD substitutions on receptor binding and pathogenesis. Our initial characterizations of the viruses are described in the above manuscript, but ongoing studies will likely explore the pathogenesis of the viruses and conduct more detailed fitness evaluations. Additionally, as these studies identify candidate mAbs for use in antibody cocktails, we will utilize a diversified viral stock generated from the low-fidelity MA-ExoN attenuated vaccine strain to select for rare escape variants. These studies will extend our understanding of the functional impacts of antibody escape on the RBD and spike, and will better inform our efforts to develop both potent and broadly neutralizing cocktails of antibodies resistant to viral escape.

PATHOGENESIS STUDIES

Preliminary pathogenesis analyses were conducted with four of the CEVs in young BALB/cJ mice. Numbers were small (n=3 per group), but CEV-7 may have an increased pathogenesis compared to the MA15 5-set backbone strain. Future studies will utilize mouse lines with enhanced weight loss in order to better identify attenuated strains, and will expand the numbers and add additional characterizations, including lung viral titer.

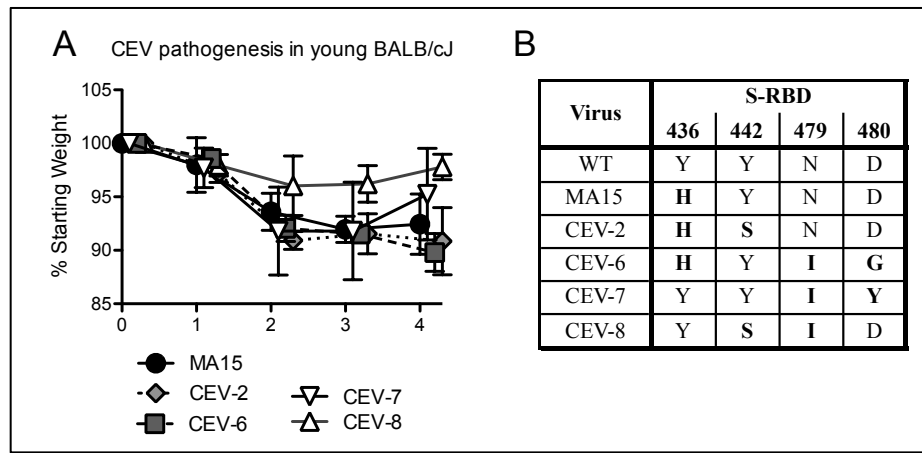


Figure 5.3 Morbidity of 4 CEVs in young mice.

Young BALB/cJ mice, 10 weeks of age, from Jackson Labs were infected with 10^5 pfu of MA15, CEV-2, CEV-6, CEV-7, or CEV-8 (n=3 per group). MA15 contains 6 substitutions across the genome that confer lethality in young BALB/c mice, one of which is the Y436H substitution in S. CEVs were constructed on a 5-set MA15 backbone, including the Y436H substitution causes ~10% weight loss, as do the two CEVs containing the Y436H substitution, CEV-2 and CEV-6. CEV-8 displays an attenuated weight loss phenotype, as expected, but CEV-7 may have an enhanced weight loss phenotype comparable to the viruses containing the Y436H substitution.

FITNESS CHARACTERIZATIONS.

Initial characterizations of CEV growth phenotypes on three cell types (Vero E6, humanACE2-DBT, and civetACE2-DBT cells) demonstrated that the 9 viable viruses grew to comparably high titer on Veros. Growth on humanACE2-DBTs differentiated 4 attenuated viruses from the 5 viruses that grew to peak titers comparable to wildtype. The Vero (African green monkey) ACE2 molecule is identical to human ACE2 across the RBD binding domain, but ACE2 expression is more highly expressed on hACE2-DBTs, leading us to hypothesize that some of the CEVs encode S-RBDs with receptor concentration dependent attenuation [223]. A more detailed fitness analyses would be required to identify any CEVs with

impaired fitness relative to wildtype. A full analysis of relative fitness will require competitive coinfections and passage, which anticipate will be conducted in future experiments for select viruses of interest. It is likely that even fitness-impaired viruses will evolve compensatory mutations during in vitro or in vivo passage. However, the mutation frequency of coronaviruses is lower than other viruses due to ExoN, a 3' to 5' exonuclease activity that functions in a likely RNA proof-reading complex [13].

Finally, most attempts to generate escape variants from a two-antibody cocktail extinguish the virus, but we hypothesize that utilizing a highly diverse viral swarm, rather than the limited variation of a clonal lab stock, will allow us to accurately identify possible escape substitutions. We proposed that the s227.14 + s230.15 combination will be both broadly neutralizing and resistant to escape, as both are broadly neutralizing, they do not appear to compete in co-neutralization assays, and s227.14 does not have any known escape substitutions on the epidemic (Urbani) backbone. The highly diverse viral swarm we propose as the starting stock is an amplified viral stock from the lung of a SCID mouse persistently infected with MA-ExoN for 30 days [242]. SCID mice do not clear the MA-ExoN virus, and plaques sequenced from the MA-ExoN persistently infected mice had a 9.6-fold higher mutation accumulation compared to the MAwt virus, including mutations in the S gene. We propose that the use of this diversified viral stock will allow us to select rare escape variants to a broadly neutralizing cocktail (s227.14+230.15), a convergent cocktail (Fm6+Sk4), and the individual antibodies s227.14 and s230.15. These studies will identify key residues in the binding epitopes of broadly neutralizing antibodies, and will demonstrate robust models for assessing antibody neutralization strategies.

5.6. SARS-Coronavirus

The study of SARS-CoV and the potential therapeutics to target coronaviruses has taken on new urgency following the recent isolation and characterization of a novel human betacoronavirus, Middle East Respiratory Syndrome Coronavirus (MERS-CoV) [158]. This new CoV shares many similarities to SARS-CoV, including clinical presentation, classification as a member of the betacoronavirus genus, and a presumed bat reservoir [158,228]. Importantly, the decade of study on SARS-CoV has provided a valuable foundation for the rapid characterization of novel coronaviruses and potential therapeutics. For example, the receptor for MERS-CoV has been identified, and evidence that anti-S antibodies are neutralizing is already accumulating [244]. Antibody generation and characterization has advanced to the point that

several antiviral monoclonal antibodies are on a promising path towards approval. We anticipate that monoclonal antibodies neutralizing the spike of MERS-COV, and cocktails capable of neutralizing both MERS-CoV and SARS-CoV, will be rapidly generated and characterized. Additionally, bioinformatics analyses are exponentially improving, and homology modeling is being used to predict promising antibody binding sites [245]. Finally, the utility of coronavirus infectious clones in combination with increasingly cost-effective synthetic biology allows for the rapid generation and characterization of recombinant coronaviruses. This rapid and rational production can allow for the generation of viruses designed to elucidate viral pathogenesis mechanisms, to iteratively inform structural biology predictions, or to generate vaccines informed by conserved coronavirus features.

REFERENCES

1. Cleri DJ, Ricketti AJ, Vernaleo JR (2010) Severe acute respiratory syndrome (SARS). *Infect Dis Clin North Am* 24: 175–202. doi:10.1016/j.idc.2009.10.005.
2. Pepin KM, Lass S, Pulliam JRC, Read AF, Lloyd-Smith JO (2010) Identifying genetic markers of adaptation for surveillance of viral host jumps. *Nat Rev Microbiol* 8: 802–813. doi:10.1038/nrmicro2440.
3. Lau SKP, Woo PCY, Li KSM, Huang Y, Tsoi H-W, et al. (2005) Severe acute respiratory syndrome coronavirus-like virus in Chinese horseshoe bats. *Proc Natl Acad Sci USA* 102: 14040–14045. doi:10.1073/pnas.0506735102.
4. Drexler JF, Gloza-Rausch F, Glende J, Corman VM, Muth D, et al. (2010) Genomic characterization of severe acute respiratory syndrome-related coronavirus in European bats and classification of coronaviruses based on partial RNA-dependent RNA polymerase gene sequences. *J Virol* 84: 11336–11349. doi:10.1128/JVI.00650-10.
5. Gloza-Rausch F, Ipsen A, Seebens A, Göttsche M, Panning M, et al. (2008) Detection and prevalence patterns of group I coronaviruses in bats, northern Germany. *Emerging Infect Dis* 14: 626–631.
6. Poon LLM, Chu DKW, Chan KH, Wong OK, Ellis TM, et al. (2005) Identification of a novel coronavirus in bats. *J Virol* 79: 2001–2009. doi:10.1128/JVI.79.4.2001-2009.2005.
7. Li W, Shi Z, Yu M, Ren W, Smith C, et al. (2005) Bats are natural reservoirs of SARS-like coronaviruses. *Science* 310: 676–679. doi:10.1126/science.1118391.
8. Tang X, Zhang J, Zhang S, Wang P, Fan X, et al. (2006) Prevalence and Genetic Diversity of Coronaviruses in Bats from China. *J Virol* 80: 7481–7490. doi:10.1128/jvi.00697-06.
9. Pfefferle S, Oppong S, Drexler JF, Gloza-Rausch F, Ipsen A, et al. (2009) Distant relatives of severe acute respiratory syndrome coronavirus and close relatives of human coronavirus 229E in bats, Ghana. *Emerging Infect Dis* 15: 1377–1384.
10. Woo PCY, Lau SKP, Huang Y, Yuen K-Y (2009) Coronavirus diversity, phylogeny and interspecies jumping. *PLoS Pathog* 5: e1000896. doi:10.1371/journal.ppat.1000896.
11. Deming D, Baric RS (2008) Genetics and Reverse Genetics of Nidoviruses. *Nidoviruses*.
12. Duffy S, Shackelton LA, Holmes EC (2008) Rates of evolutionary change in viruses: patterns and determinants. *Nat Rev Genet* 9: 267–276. doi:10.1038/nrg2323.
13. Eckerle L, Becker M, Halpin R, Li K, Venter E, et al. (2010) Infidelity of SARS-CoV Nsp14-exonuclease mutant virus replication is revealed by complete genome sequencing. *PLoS Pathog* 6: e1000896.
14. Denison MR, Graham RL, Donaldson EF, Eckerle LD, Baric RS (2011) Coronaviruses: An RNA proofreading machine regulates replication fidelity and diversity. *RNA Biol* 8: 270–279.
15. Fu K, Baric RS (1994) Map locations of mouse hepatitis virus temperature-sensitive mutants: confirmation of variable rates of recombination. *J Virol* 68: 7458–7466.
16. Holmes EC (2009) *The evolution and emergence of RNA viruses*. Oxford University Press, USA.

17. Pasternak A, Spaan W, Snijder E (2006) Nidovirus transcription: how to make sense...? *J Gen Virol* 87: 1403–1421. doi:10.1099/vir.0.81611-0.
18. Rest JS, Mindell DP (2003) SARS associated coronavirus has a recombinant polymerase and coronaviruses have a history of host-shifting. *Infect Genet Evol* 3: 219–225.
19. Vijgen L, Keyaerts E, Moës E, Thoelen I, Wollants E, et al. (2005) Complete genomic sequence of human coronavirus OC43: molecular clock analysis suggests a relatively recent zoonotic coronavirus transmission event. *J Virol* 79: 1595–1604. doi:10.1128/JVI.79.3.1595-1604.2005.
20. Kocherhans R, Bridgen A, Ackermann M, Tobler K (2001) Completion of the porcine epidemic diarrhoea coronavirus (PEDV) genome sequence. *Virus Genes* 23: 137–144.
21. Zhang XM, Herbst W, Kousoulas KG, Storz J (1994) Biological and genetic characterization of a hemagglutinating coronavirus isolated from a diarrhoeic child. *J Med Virol* 44: 152–161.
22. Song H-D, Tu C-C, Zhang G-W, Wang S-Y, Zheng K, et al. (2005) Cross-host evolution of severe acute respiratory syndrome coronavirus in palm civet and human. *Proc Natl Acad Sci USA* 102: 2430–2435. doi:10.1073/pnas.0409608102.
23. Zheng B-J, Wong KH, Zhou J, Wong KL, Young BWY, et al. (2004) SARS-related virus predating SARS outbreak, Hong Kong. *Emerging Infect Dis* 10: 176–178. doi:10.3201/eid1002.030533.
24. Guan Y, Zheng BJ, He YQ, Liu XL, Zhuang ZX, et al. (2003) Isolation and characterization of viruses related to the SARS coronavirus from animals in southern China. *Science* 302: 276–278. doi:10.1126/science.1087139.
25. Lau SKP, Poon RWS, Wong BHL, Wang M, Huang Y, et al. (2010) Coexistence of different genotypes in the same bat and serological characterization of Rousettus bat coronavirus HKU9 belonging to a novel Betacoronavirus subgroup. *J Virol* 84: 11385–11394. doi:10.1128/JVI.01121-10.
26. Vijgen L, Keyaerts E, Moës E, Maes P, Duson G, et al. (2005) Development of one-step, real-time, quantitative reverse transcriptase PCR assays for absolute quantitation of human coronaviruses OC43 and 229E. *J Clin Microbiol* 43: 5452–5456. doi:10.1128/JCM.43.11.5452-5456.2005.
27. Quan P-L, Firth C, Street C, Henriquez JA, Petrosov A, et al. (2010) Identification of a severe acute respiratory syndrome coronavirus-like virus in a leaf-nosed bat in Nigeria. *MBio* 1. doi:10.1128/mBio.00208-10.
28. Vijaykrishna D, Smith G, Zhang J, Peiris J, Chen H, et al. (2007) Evolutionary Insights into the Ecology of Coronaviruses. *J Virol* 81: 4012–4020. doi:10.1128/jvi.02605-06.
29. Becker MM, Graham RL, Donaldson EF, Rockx B, Sims AC, et al. (2008) Synthetic recombinant bat SARS-like coronavirus is infectious in cultured cells and in mice. *Proc Natl Acad Sci USA* 105: 19944–19949. doi:10.1073/pnas.0808116105.
30. Anderson L, Tong S (2010) Update on SARS research and other possibly zoonotic coronaviruses. *International Journal of Antimicrobial Agents* 36 Suppl 1: S21–S25. doi:10.1016/j.ijantimicag.2010.06.016.
31. Donaldson EF, Haskew AN, Gates JE, Huynh J, Moore CJ, et al. (2010) Metagenomic analysis of the viromes of three North American bat species: viral diversity among different bat species that

- share a common habitat. *J Virol* 84: 13004–13018. doi:10.1128/JVI.01255-10.
32. Lau SKP, Li KSM, Huang Y, Shek C-T, Tse H, et al. (2010) Ecoepidemiology and complete genome comparison of different strains of severe acute respiratory syndrome-related *Rhinolophus* bat coronavirus in China reveal bats as a reservoir for acute, self-limiting infection that allows recombination events. *J Virol* 84: 2808–2819. doi:10.1128/JVI.02219-09.
 33. Ren W, Qu X, Li W, Han Z, Yu M, et al. (2008) Difference in receptor usage between severe acute respiratory syndrome (SARS) coronavirus and SARS-like coronavirus of bat origin. *J Virol* 82: 1899–1907. doi:10.1128/JVI.01085-07.
 34. Hou Y, Peng C, Yu M, Li Y, Han Z, et al. (2010) Angiotensin-converting enzyme 2 (ACE2) proteins of different bat species confer variable susceptibility to SARS-CoV entry. *Arch Virol*. doi:10.1007/s00705-010-0729-6.
 35. Li W, Wong S-K, Li F, Kuhn JH, Huang I-C, et al. (2006) Animal origins of the severe acute respiratory syndrome coronavirus: insight from ACE2-S-protein interactions. *J Virol* 80: 4211–4219. doi:10.1128/JVI.80.9.4211-4219.2006.
 36. Graham RL, Baric RS (2010) Recombination, reservoirs, and the modular spike: mechanisms of coronavirus cross-species transmission. *J Virol* 84: 3134–3146. doi:10.1128/JVI.01394-09.
 37. Yu M, Tachedjian M, Cramer G, Shi Z, Wang L-F (2010) Identification of key amino acid residues required for horseshoe bat angiotensin-I converting enzyme 2 to function as a receptor for severe acute respiratory syndrome coronavirus. *J Gen Virol* 91: 1708–1712. doi:10.1099/vir.0.020172-0.
 38. Janies D, Habib F, Alexandrov B, Hill A, Pol D (2008) Evolution of genomes, host shifts and the geographic spread of SARS-CoV and related coronaviruses. *Cladistics* 24: 111–130.
 39. Yuan J, Hon C-C, Li Y, Wang D, Xu G, et al. (2010) Intraspecies diversity of SARS-like coronaviruses in *Rhinolophus sinicus* and its implications for the origin of SARS coronaviruses in humans. *J Gen Virol* 91: 1058–1062. doi:10.1099/vir.0.016378-0.
 40. Consortium TCSME (2004) Molecular evolution of the SARS coronavirus during the course of the SARS epidemic in China. *Science* 303: 1666–1669.
 41. Rockx B, Sheahan T, Donaldson E, Harkema J, Sims A, et al. (2007) Synthetic reconstruction of zoonotic and early human severe acute respiratory syndrome coronavirus isolates that produce fatal disease in aged mice. *J Virol* 81: 7410–7423. doi:10.1128/JVI.00505-07.
 42. Rockx B, Corti D, Donaldson E, Sheahan T, Stadler K, et al. (2008) Structural basis for potent cross-neutralizing human monoclonal antibody protection against lethal human and zoonotic severe acute respiratory syndrome coronavirus challenge. *J Virol* 82: 3220–3235. doi:10.1128/JVI.02377-07.
 43. Peng G, Sun D, Rajashankar KR, Qian Z, Holmes KV, et al. (2011) Crystal structure of mouse coronavirus receptor-binding domain complexed with its murine receptor. *Proc Natl Acad Sci USA*. doi:10.1073/pnas.1104306108.
 44. Schwegmann-Wessels C, Herrler G (2006) Sialic acids as receptor determinants for coronaviruses. *Glycoconj J* 23: 51–58. doi:10.1007/s10719-006-5437-9.
 45. Schultze B, Krempf C, Ballesteros ML, Shaw L, Schauer R, et al. (1996) Transmissible gastroenteritis coronavirus, but not the related porcine respiratory coronavirus, has a sialic acid

- (N-glycolylneuraminic acid) binding activity. *J Virol* 70: 5634–5637.
46. Zeng Q, Langereis M, van Vliet A, Huizinga E, de Groot R (2008) Structure of coronavirus hemagglutinin-esterase offers insight into corona and influenza virus evolution. *Proceedings of the National Academy of Sciences* 105: 9065.
 47. de Haan CAMC, Li ZZ, Lintelo te EE, Bosch BJB, Haijema BJB, et al. (2005) Murine coronavirus with an extended host range uses heparan sulfate as an entry receptor. *J Virol* 79: 14451–14456. doi:10.1128/JVI.79.22.14451-14456.2005.
 48. Jeffers SA, Tusell SM, Gillim-Ross L, Hemmila EM, Achenbach JE, et al. (2004) CD209L (L-SIGN) is a receptor for severe acute respiratory syndrome coronavirus. *Proc Natl Acad Sci USA* 101: 15748–15753. doi:10.1073/pnas.0403812101.
 49. Zhou Y, Lu K, Pfefferle S, Bertram S, Glowacka I, et al. (2010) A single asparagine-linked glycosylation site of the severe acute respiratory syndrome coronavirus spike glycoprotein facilitates inhibition by mannose-binding lectin through multiple mechanisms. *J Virol* 84: 8753–8764. doi:10.1128/JVI.00554-10.
 50. Bosch BJ, Bartelink W, Rottier PJM (2008) Cathepsin L functionally cleaves the severe acute respiratory syndrome coronavirus class I fusion protein upstream of rather than adjacent to the fusion peptide. *J Virol* 82: 8887–8890. doi:10.1128/JVI.00415-08.
 51. Shulla A, Heald-Sargent T, Subramanya G, Zhao J, Perlman S, et al. (2011) A transmembrane serine protease is linked to the severe acute respiratory syndrome coronavirus receptor and activates virus entry. *J Virol* 85: 873–882. doi:10.1128/JVI.02062-10.
 52. Glowacka I, Bertram S, Müller MA, Allen P, Soilleux E, et al. (2011) Evidence that TMPRSS2 activates the severe acute respiratory syndrome coronavirus spike protein for membrane fusion and reduces viral control by the humoral immune response. *J Virol* 85: 4122–4134. doi:10.1128/JVI.02232-10.
 53. Zhang C-Y, Wei J-F, He S-H (2006) Adaptive evolution of the spike gene of SARS coronavirus: changes in positively selected sites in different epidemic groups. *BMC Microbiol* 6: 88. doi:10.1186/1471-2180-6-88.
 54. Xu L, Zhang Y, Liu Y, Chen Z, Deng H, et al. (2009) Angiotensin-converting enzyme 2 (ACE2) from raccoon dog can serve as an efficient receptor for the spike protein of severe acute respiratory syndrome coronavirus. *J Gen Virol* 90: 2695–2703. doi:10.1099/vir.0.013490-0.
 55. Sheahan T, Rockx B, Donaldson E, Corti D, Baric R (2008) Pathways of cross-species transmission of synthetically reconstructed zoonotic severe acute respiratory syndrome coronavirus. *J Virol* 82: 8721–8732. doi:10.1128/JVI.00818-08.
 56. Day CW, Baric R, Cai SX, Frieman M, Kumaki Y, et al. (2009) A new mouse-adapted strain of SARS-CoV as a lethal model for evaluating antiviral agents in vitro and in vivo. *Virology* 395: 210–222. doi:10.1016/j.virol.2009.09.023.
 57. Roberts A, Deming D, Paddock CD, Cheng A, Yount B, et al. (2007) A mouse-adapted SARS-coronavirus causes disease and mortality in BALB/c mice. *PLoS Pathog* 3: e5. doi:10.1371/journal.ppat.0030005.
 58. Pacciarini FF, Ghezzi SS, Canducci FF, Sims AA, Sampaolo MM, et al. (2008) Persistent replication of severe acute respiratory syndrome coronavirus in human tubular kidney cells selects for adaptive mutations in the membrane protein. *J Virol* 82: 5137–5144.

doi:10.1128/JVI.00096-08.

59. Li W, Zhang C, Kuhn J, Moore M, et al. (2005) Receptor and viral determinants of SARS-coronavirus adaptation to human ACE2. *EMBO J* 24: 1634–1643. doi:7600640 [pii]10.1038/sj.emboj.7600640 [doi].
60. Sheahan T, Rockx B, Donaldson E, Sims A, Pickles R, et al. (2008) Mechanisms of Zoonotic Severe Acute Respiratory Syndrome Coronavirus Host Range Expansion in Human Airway Epithelium. *J Virol* 82: 2274–2285. doi:10.1128/jvi.02041-07.
61. Li F, Li W, Farzan M, Harrison SC (2005) Structure of SARS coronavirus spike receptor-binding domain complexed with receptor. *Science* 309: 1864–1868. doi:10.1126/science.1116480.
62. Rockx B, Donaldson E, Frieman M, Sheahan T, Corti D, et al. (2010) Escape from human monoclonal antibody neutralization affects in vitro and in vivo fitness of severe acute respiratory syndrome coronavirus. *J INFECT DIS* 201: 946–955. doi:10.1086/651022.
63. Watabe T, Kishino H (2010) Structural considerations in the fitness landscape of a virus. *Mol Biol Evol* 27: 1782–1791. doi:10.1093/molbev/msq056.
64. Sui J, Aird D, Tamin A, Murakami A, Yan M, et al. (2008) Broadening of neutralization activity to directly block a dominant antibody-driven SARS-coronavirus evolution pathway. *PLoS Pathog* 4: e1000197. doi:10.1371/journal.ppat.1000197.
65. Wu K, Li W, Peng G, Li F (2009) Crystal structure of NL63 respiratory coronavirus receptor-binding domain complexed with its human receptor. *Proc Natl Acad Sci USA* 106: 19970–19974. doi:10.1073/pnas.0908837106.
66. Vaughn EM, Halbur PG, Paul PS (1994) Three new isolates of porcine respiratory coronavirus with various pathogenicities and spike (S) gene deletions. *J Clin Microbiol* 32: 1809–1812.
67. Gallagher TM, Parker SE, Buchmeier MJ (1990) Neutralization-resistant variants of a neurotropic coronavirus are generated by deletions within the amino-terminal half of the spike glycoprotein. *J Virol* 64: 731–741.
68. Rowe CL, Baker SC, Nathan MJ, Fleming JO (1997) Evolution of mouse hepatitis virus: detection and characterization of spike deletion variants during persistent infection. *J Virol* 71: 2959–2969.
69. Qu X-X, Hao P, Song X-J, Jiang S-M, Liu Y-X, et al. (2005) Identification of two critical amino acid residues of the severe acute respiratory syndrome coronavirus spike protein for its variation in zoonotic tropism transition via a double substitution strategy. *J Biol Chem* 280: 29588–29595. doi:10.1074/jbc.M500662200.
70. Tang X, Li G, Vasilakis N, Zhang Y, Shi Z, et al. (2009) Differential stepwise evolution of SARS coronavirus functional proteins in different host species. 9: 52. doi:1471-2148-9-52 [pii]10.1186/1471-2148-9-52 [doi].
71. Wu K, Chen L, Peng G, Zhou W, Pennell CA, et al. (2011) A Virus-binding Hotspot on Human Angiotensin-converting Enzyme 2 is Critical for the Binding of Two Different Coronaviruses. *J Virol*. doi:10.1128/JVI.02274-10.
72. Booth C, Matukas L, Tomlinson G, Rachlis A, Rose D, et al. (2003) Clinical Features and Short-term Outcomes of 144 Patients With SARS in the Greater Toronto Area. *JAMA* 289: 2801–2809. doi:10.1001/jama.289.21.JOC30885.

73. Donnelly CA, Ghani AC, Leung GM, Hedley AJ, Fraser C, et al. (2003) Epidemiological determinants of spread of causal agent of severe acute respiratory syndrome in Hong Kong. *Lancet* 361: 1761–1766. doi:10.1016/S0140-6736(03)13410-1.
74. Peiris JSM, Chu CM, Cheng VCC, Chan KS, Hung IFN, et al. (2003) Clinical progression and viral load in a community outbreak of coronavirus-associated SARS pneumonia: a prospective study. *Lancet* 361: 1767–1772.
75. Yip CW, Hon CC, Shi M, Lam TT-Y, Chow KY-C, et al. (2009) Phylogenetic perspectives on the epidemiology and origins of SARS and SARS-like coronaviruses. *Infect Genet Evol* 9: 1185–1196. doi:10.1016/j.meegid.2009.09.015.
76. Normile D (2005) Researchers Tie Deadly SARS Virus to Bats. *Science* 309: 2154–2155. doi:10.1126/science.309.5744.2154.
77. Stockman LJ, Bellamy R, Garner P (2006) SARS: systematic review of treatment effects. *PLOS medicine* 3: e343. doi:10.1371/journal.pmed.0030343.
78. Greenough TC, Babcock GJ, Roberts A, Hernandez HJ, Thomas WD, et al. (2005) Development and characterization of a severe acute respiratory syndrome-associated coronavirus-neutralizing human monoclonal antibody that provides effective immunoprophylaxis in mice. *J INFECT DIS* 191: 507–514. doi:10.1086/427242.
79. Subbarao K, McAuliffe J, Vogel L, Fahle G, Fischer S, et al. (2004) Prior infection and passive transfer of neutralizing antibody prevent replication of severe acute respiratory syndrome coronavirus in the respiratory tract of mice. *J Virol* 78: 3572–3577.
80. Zhu Z, Chakraborti S, He Y, Roberts A, Sheahan T, et al. (2007) Potent cross-reactive neutralization of SARS coronavirus isolates by human monoclonal antibodies. *Proc Natl Acad Sci USA* 104: 12123–12128. doi:10.1073/pnas.0701000104.
81. Lin J-T, Zhang J-S, Su N, Xu J-G, Wang N, et al. (2007) Safety and immunogenicity from a phase I trial of inactivated severe acute respiratory syndrome coronavirus vaccine. *Antivir Ther (Lond)* 12: 1107–1113.
82. Roberts A, Lamirande EW, Vogel L, Baras B, Goossens G, et al. (2010) Immunogenicity and protective efficacy in mice and hamsters of a β -propiolactone inactivated whole virus SARS-CoV vaccine. *Viral Immunol* 23: 509–519. doi:10.1089/vim.2010.0028.
83. Netland J, Dediego ML, Zhao J, Fett C, Alvarez E, et al. (2010) Immunization with an attenuated severe acute respiratory syndrome coronavirus deleted in E protein protects against lethal respiratory disease. *Virology* 399: 120–128. doi:10.1016/j.virol.2010.01.004.
84. Roberts A, Lamirande EW, Vogel L, Jackson JP, Paddock CD, et al. (2008) Animal models and vaccines for SARS-CoV infection. *Virus Res* 133: 20–32. doi:10.1016/j.virusres.2007.03.025.
85. Martin JE, Louder MK, Holman LA, Gordon IJ, Enama ME, et al. (2008) A SARS DNA vaccine induces neutralizing antibody and cellular immune responses in healthy adults in a Phase I clinical trial. *Vaccine* 26: 6338–6343. doi:10.1016/j.vaccine.2008.09.026.
86. Yang Z-Y, Kong W-P, Huang Y, Roberts A, Murphy BR, et al. (2004) A DNA vaccine induces SARS coronavirus neutralization and protective immunity in mice. *Nature* 428: 561–564. doi:10.1038/nature02463.
87. Bisht H, Roberts A, Vogel L, Bukreyev A, Collins PL, et al. (2004) Severe acute respiratory

- syndrome coronavirus spike protein expressed by attenuated vaccinia virus protectively immunizes mice. *Proc Natl Acad Sci USA* 101: 6641–6646. doi:10.1073/pnas.0401939101.
88. Deming D, Sheahan T, Heise M, Yount B, Davis N, et al. (2006) Vaccine efficacy in senescent mice challenged with recombinant SARS-CoV bearing epidemic and zoonotic spike variants. *PLOS medicine* 3: e525. doi:10.1371/journal.pmed.0030525.
 89. Enjuanes L, Dediego ML, Alvarez E, Deming D, Sheahan T, et al. (2008) Vaccines to prevent severe acute respiratory syndrome coronavirus-induced disease. *Virus Res* 133: 45–62. doi:10.1016/j.virusres.2007.01.021.
 90. Sheahan T, Whitmore A, Long K, Ferris M, Rockx B, et al. (2011) Successful Vaccination Strategies that Protect Aged Mice from Lethal Influenza and Lethal Heterologous SARS-CoV Challenge. *J Virol* 85. doi:10.1128/JVI.01805-10.
 91. Marshall E, Enserink M (2004) Caution urged on SARS vaccines. *Science* 303: 944–946. doi:10.1126/science.303.5660.944.
 92. Hou Y-X, Peng C, Han Z-G, Zhou P, Chen J-G, et al. (2010) Immunogenicity of the spike glycoprotein of Bat SARS-like coronavirus. *Virology* 25: 36–44. doi:10.1007/s12250-010-3096-2.
 93. Goodwin K, Viboud C, Simonsen L (2006) Antibody response to influenza vaccination in the elderly: a quantitative review. *Vaccine* 24: 1159–1169. doi:10.1016/j.vaccine.2005.08.105.
 94. McElhaney JE, Hooton JW, Hooton N, Bleackley RC (2005) Comparison of single versus booster dose of influenza vaccination on humoral and cellular immune responses in older adults. *Vaccine* 23: 3294–3300. doi:10.1016/j.vaccine.2005.01.080.
 95. Yasui F, Kai C, Kitabatake M, Inoue S, Yoneda M, et al. (2008) Prior immunization with severe acute respiratory syndrome (SARS)-associated coronavirus (SARS-CoV) nucleocapsid protein causes severe pneumonia in mice infected with SARS-CoV. *J Immunol* 181: 6337–6348.
 96. He Y, Zhou Y, Siddiqui P, Jiang S (2004) Inactivated SARS-CoV vaccine elicits high titers of spike protein-specific antibodies that block receptor binding and virus entry. *Biochem Biophys Res Commun* 325: 445–452. doi:10.1016/j.bbrc.2004.10.052.
 97. See RH, Petric M, Lawrence DJ, Mok CPY, Rowe T, et al. (2008) Severe acute respiratory syndrome vaccine efficacy in ferrets: whole killed virus and adenovirus-vectored vaccines. *J Gen Virol* 89: 2136–2146. doi:10.1099/vir.0.2008/001891-0.
 98. Spruth M, Kistner O, Savidis-Dacho H, Hitter E, Crowe B, et al. (2006) A double-inactivated whole virus candidate SARS coronavirus vaccine stimulates neutralising and protective antibody responses. *Vaccine* 24: 652–661. doi:10.1016/j.vaccine.2005.08.055.
 99. Roberts A, Paddock C, Vogel L, Butler E, Zaki S, et al. (2005) Aged BALB/c mice as a model for increased severity of severe acute respiratory syndrome in elderly humans. *J Virol* 79: 5833–5838. doi:10.1128/JVI.79.9.5833-5838.2005.
 100. Vogel LN, Roberts A, Paddock CD, Genrich GL, Lamirande EW, et al. (2007) Utility of the aged BALB/c mouse model to demonstrate prevention and control strategies for severe acute respiratory syndrome coronavirus (SARS-CoV). *Vaccine* 25: 2173–2179. doi:10.1016/j.vaccine.2006.11.055.
 101. Yount B, Curtis KM, Fritz EA, Hensley LE, Jahrling PB, et al. (2003) Reverse genetics with a

- full-length infectious cDNA of severe acute respiratory syndrome coronavirus. *Proc Natl Acad Sci USA* 100: 12995–13000. doi:10.1073/pnas.1735582100.
102. Sheahan T, Deming D, Donaldson E, Pickles R, Baric R (2006) Resurrection of an “extinct” SARS-CoV isolate GD03 from late 2003. *Adv Exp Med Biol* 581: 547–550. doi:10.1007/978-0-387-33012-9_100.
 103. LoBue AD, Thompson JM, Lindesmith L, Johnston RE, Baric RS (2009) Alphavirus-adjuvanted norovirus-like particle vaccines: heterologous, humoral, and mucosal immune responses protect against murine norovirus challenge. *J Virol* 83: 3212–3227. doi:10.1128/JVI.01650-08.
 104. Thompson JM, Whitmore AC, Konopka JL, Collier ML, Richmond EMB, et al. (2006) Mucosal and systemic adjuvant activity of alphavirus replicon particles. *Proc Natl Acad Sci USA* 103: 3722–3727. doi:10.1073/pnas.0600287103.
 105. Meyerholz DK, Griffin MA, Castilow EM, Varga SM (2009) Comparison of histochemical methods for murine eosinophil detection in an RSV vaccine-enhanced inflammation model. *Toxicol Pathol* 37: 249–255. doi:10.1177/0192623308329342.
 106. Rockx B, Baas T, Zornetzer GA, Haagmans B, Sheahan T, et al. (2009) Early upregulation of acute respiratory distress syndrome-associated cytokines promotes lethal disease in an aged-mouse model of severe acute respiratory syndrome coronavirus infection. *J Virol* 83: 7062–7074. doi:10.1128/JVI.00127-09.
 107. Polack FP (2007) Atypical measles and enhanced respiratory syncytial virus disease (ERD) made simple. *Pediatr Res* 62: 111–115. doi:10.1203/PDR.0b013e3180686ce0.
 108. Castilow EM, Legge KL, Varga SM (2008) Cutting edge: Eosinophils do not contribute to respiratory syncytial virus vaccine-enhanced disease. *J Immunol* 181: 6692–6696.
 109. Ishioka T, Kimura H, Kita H, Obuchi M, Hoshino H, et al. (2011) Effects of respiratory syncytial virus infection and major basic protein derived from eosinophils in pulmonary alveolar epithelial cells (A549). *Cell Biol Int* 35: 467–474. doi:10.1042/CBI20100255.
 110. Malcolm KCK, Kret JEJ, Young RLR, Poch KRK, Caceres SMS, et al. (2011) Bacteria-specific neutrophil dysfunction associated with interferon-stimulated gene expression in the acute respiratory distress syndrome. *PLoS ONE* 6: e21958–e21958. doi:10.1371/journal.pone.0021958.
 111. Narasaraju TT, Yang EE, Samy RPR, Ng HHH, Poh WPW, et al. (2011) Excessive Neutrophils and Neutrophil Extracellular Traps Contribute to Acute Lung Injury of Influenza Pneumonitis. *Am J Pathol* 179: 12–12. doi:10.1016/j.ajpath.2011.03.013.
 112. Bossart KN, Zhu Z, Middleton D, Klippel J, Cramer G, et al. (2009) A neutralizing human monoclonal antibody protects against lethal disease in a new ferret model of acute nipah virus infection. *PLoS Pathog* 5: e1000642–e1000642. doi:10.1371/journal.ppat.1000642.
 113. Cameron MJ, Ran L, Xu L, Danesh A, Bermejo-Martin JF, et al. (2007) Interferon-mediated immunopathological events are associated with atypical innate and adaptive immune responses in patients with severe acute respiratory syndrome. *J Virol* 81: 8692–8706. doi:10.1128/JVI.00527-07.
 114. Zhang J-S, Chen J-T, Liu Y-X, Zhang Z-S, Gao H, et al. (2005) A serological survey on neutralizing antibody titer of SARS convalescent sera. *J Med Virol* 77: 147–150. doi:10.1002/jmv.20431.

115. Ubol S, Halstead SB (2010) How Innate Immune Mechanisms Contribute to Antibody-Enhanced Viral Infections. *Clinical and Vaccine Immunology*: 1–24. doi:10.1128/CVI.00316-10.
116. Neuman BW, Adair BD, Yoshioka C, Quispe JD, Orca G, et al. (2006) Supramolecular architecture of severe acute respiratory syndrome coronavirus revealed by electron cryomicroscopy. *J Virol* 80: 7918–7928. doi:10.1128/JVI.00645-06.
117. Chen Z, Pei D, Jiang L, Song Y, Wang J, et al. (2004) Antigenicity analysis of different regions of the severe acute respiratory syndrome coronavirus nucleocapsid protein. *Clin Chem* 50: 988–995. doi:10.1373/clinchem.2004.031096.
118. Chow SCS, Ho CYS, Tam TTY, Wu C, Cheung T, et al. (2006) Specific epitopes of the structural and hypothetical proteins elicit variable humoral responses in SARS patients. *J Clin Pathol* 59: 468–476. doi:10.1136/jcp.2005.029868.
119. Peng H, Yang L-T, Wang L-Y, Li J, Huang J, et al. (2006) Long-lived memory T lymphocyte responses against SARS coronavirus nucleocapsid protein in SARS-recovered patients. *Virology* 351: 466–475. doi:10.1016/j.virol.2006.03.036.
120. Zhong X, Yang H, Guo Z-F, Sin W-YF, Chen W, et al. (2005) B-cell responses in patients who have recovered from severe acute respiratory syndrome target a dominant site in the S2 domain of the surface spike glycoprotein. *J Virol* 79: 3401–3408. doi:10.1128/JVI.79.6.3401-3408.2005.
121. Zhu YG, Qu JM (2009) Differential characteristics of the early stage of lung inflammation induced by SARS-CoV Nucleocapsid protein related to age in the mouse. *Inflamm Res* 58: 312–320. doi:10.1007/s00011-009-8062-9.
122. Kopecky-Bromberg SA, Martínez-Sobrido L, Frieman M, Baric RA, Palese P (2007) Severe acute respiratory syndrome coronavirus open reading frame (ORF) 3b, ORF 6, and nucleocapsid proteins function as interferon antagonists. *J Virol* 81: 548–557. doi:10.1128/JVI.01782-06.
123. Moghaddam A, Olszewska W, Wang B, Tregoning JS, Helson R, et al. (2006) A potential molecular mechanism for hypersensitivity caused by formalin-inactivated vaccines. *Nat Med* 12: 905–907. doi:10.1038/nm1456.
124. Tsunetsugu-Yokota Y, Ato M, Takahashi Y, Hashimoto S-I, Kaji T, et al. (2007) Formalin-treated UV-inactivated SARS coronavirus vaccine retains its immunogenicity and promotes Th2-type immune responses. *Jpn J Infect Dis* 60: 106–112.
125. Delgado MF, Coviello S, Monsalvo AC, Melendi GA, Hernandez JZ, et al. (2009) Lack of antibody affinity maturation due to poor Toll-like receptor stimulation leads to enhanced respiratory syncytial virus disease. *Nat Med* 15: 34–41. doi:10.1038/nm.1894.
126. HogenEsch H (2002) Mechanisms of stimulation of the immune response by aluminum adjuvants. *Vaccine* 20: S34–S39.
127. Takasuka N, Fujii H, Takahashi Y, Kasai M, Morikawa S, et al. (2004) A subcutaneously injected UV-inactivated SARS coronavirus vaccine elicits systemic humoral immunity in mice. *Int Immunol* 16: 1423–1430. doi:10.1093/intimm/dxh143.
128. Thompson JM, Whitmore AC, Staats HF, Johnston RE (2008) Alphavirus replicon particles acting as adjuvants promote CD8+ T cell responses to co-delivered antigen. *Vaccine* 26: 4267–4275. doi:10.1016/j.vaccine.2008.05.046.
129. Thompson JM, Whitmore AC, Staats HF, Johnston R (2008) The contribution of type I interferon

- signaling to immunity induced by alphavirus replicon vaccines. *Vaccine* 26: 4998–5003. doi:10.1016/j.vaccine.2008.07.011.
130. Gruver AL, Hudson LL, Sempowski GD (2007) Immunosenescence of ageing. *J Pathol* 211: 144–156. doi:10.1002/path.2104.
 131. Rani M, Bolles M, Donaldson EF, Van Blarcom T, Baric R, et al. (2012) Increased Antibody Affinity Confers Broad In Vitro Protection against Escape Mutants of Severe Acute Respiratory Syndrome Coronavirus. *J Virol* 86: 9113–9121. doi:10.1128/JVI.00233-12.
 132. Sui J, Bolles M, Rockx B, Liddington R, Baric R, et al. (2013) Effects of Targeting Spike Protein Receptor Binding Domain on Neutralization Escape and Fitness of SARS-Coronavirus. in preparation. 39 pp.
 133. Qiu X, Audet J, Wong G, Pillet S, Bello A, et al. (2012) Successful Treatment of Ebola Virus-Infected Cynomolgus Macaques with Monoclonal Antibodies. *Science Translational Medicine* 4: 138ra81–138ra81. doi:10.1126/scitranslmed.3003876.
 134. Grandea AG, Olsen OA, Cox TC, Renshaw M, Hammond PW, et al. (2010) Human antibodies reveal a protective epitope that is highly conserved among human and nonhuman influenza A viruses. *Proc Natl Acad Sci USA* 107: 12658–12663. doi:10.1073/pnas.0911806107.
 135. Zhong L, Haynes L, Struble EB, Tamin A, Virata-Theimer ML, et al. (2009) Antibody-mediated synergy and interference in the neutralization of SARS-CoV at an epitope cluster on the spike protein. *Biochemical and Biophysical Research Communications* 390: 1056–1060. doi:10.1016/j.bbrc.2009.10.115.
 136. Meulen ter J, van den Brink EN, Poon LLM, Marissen WE, Leung CSW, et al. (2006) Human Monoclonal Antibody Combination against SARS Coronavirus: Synergy and Coverage of Escape Mutants. *PLOS medicine* 3: e237. doi:10.1371/journal.pmed.0030237.sd001.
 137. Doria-Rose NA, Louder MK, Yang Z, O'Dell S, Nason M, et al. (2012) HIV-1 Neutralization Coverage Is Improved by Combining Monoclonal Antibodies That Target Independent Epitopes. *J Virol* 86: 3393–3397. doi:10.1128/JVI.06745-11.
 138. Marasco WA, Sui J (2007) The growth and potential of human antiviral monoclonal antibody therapeutics. *Nat Biotechnol* 25: 1421–1434. doi:10.1038/nbt1363.
 139. Bradbury ARM, Sidhu S, Dübel S, McCafferty J (2011) Beyond natural antibodies: the power of in vitro display technologies. *Nat Biotechnol* 29: 245–254. doi:10.1038/nbt.1791.
 140. Wilson PC, Andrews SF (2012) Tools to therapeutically harness the human antibody response. *Nat Rev Immunol* 12: 709–719. doi:10.1038/nri3285.
 141. Diskin R, Scheid JF, Marcovecchio PM, West AP, Klein F, et al. (2011) Increasing the potency and breadth of an HIV antibody by using structure-based rational design. *Science* 334: 1289–1293. doi:10.1126/science.1213782.
 142. Cingoz O (2009) Motavizumab. *MAbs* 1: 439–442.
 143. Das SR, Hensley SE, Ince WL, Brooke CB, Subba A, et al. (2013) Defining Influenza A Virus Hemagglutinin Antigenic Drift by Sequential Monoclonal Antibody Selection. *Cell Host Microbe* 13: 314–323. doi:10.1016/j.chom.2013.02.008.
 144. Chan AC, Carter PJ (2010) Therapeutic antibodies for autoimmunity and inflammation. *Nat Rev*

- Immunol 10: 301–316. doi:10.1038/nri2761.
145. CBER (2003) Label - Palivizumab (Synagis), Medimmune, Incorporated. 7 pp.
 146. Bakker ABH, Python C, Kissling CJ, Pandya P, Marissen WE, et al. (2008) First administration to humans of a monoclonal antibody cocktail against rabies virus: Safety, tolerability, and neutralizing activity. *Vaccine* 26: 5922–5927. doi:10.1016/j.vaccine.2008.08.050.
 147. Gogtay N, Thatte U, Kshirsagar N, Leav B, Molrine D, et al. (2012) Safety and pharmacokinetics of a human monoclonal antibody to rabies virus: A randomized, dose-escalation phase 1 study in adults. *Vaccine* 30: 7315–7320. doi:10.1016/j.vaccine.2012.09.027.
 148. Kong L, Giang E, Robbins JB, Stanfield RL, Burton DR, et al. (2012) Structural basis of hepatitis C virus neutralization by broadly neutralizing antibody HCV1. *Proc Natl Acad Sci USA* 109: 9499–9504. doi:10.1073/pnas.1202924109.
 149. Flego M, Ascione A, Cianfriglia M, Vella S (2013) Clinical development of monoclonal antibody-based drugs in HIV and HCV diseases. *BMC Med* 11: 4. doi:10.1038/nbt1126.
 150. Wu H, Pfarr DS, Johnson S, Brewah YA, Woods RM, et al. (2007) Development of motavizumab, an ultra-potent antibody for the prevention of respiratory syncytial virus infection in the upper and lower respiratory tract. *J Mol Biol* 368: 652–665. doi:10.1016/j.jmb.2007.02.024.
 151. Feltes TF, Sondheimer HM, Tulloh RMR, Harris BS, Jensen KM, et al. (2011) A randomized controlled trial of motavizumab versus palivizumab for the prophylaxis of serious respiratory syncytial virus disease in children with hemodynamically significant congenital heart disease. *Pediatr Res* 70: 186–191. doi:10.1203/PDR.0b013e318220a553.
 152. Macagno A, Bernasconi NL, Vanzetta F, Dander E, Sarasini A, et al. (2009) Isolation of Human Monoclonal Antibodies That Potently Neutralize Human Cytomegalovirus Infection by Targeting Different Epitopes on the gH/gL/UL128-131A Complex. *J Virol* 84: 1005–1013. doi:10.1128/JVI.01809-09.
 153. Sui J, Hwang WC, Perez S, Wei G, Aird D, et al. (2009) Structural and functional bases for broad-spectrum neutralization of avian and human influenza A viruses. *Nat Struct Mol Biol* 16: 265–273. doi:10.1038/nsmb.1566.
 154. Du L, Jin L, Zhao G, Sun S, Li J, et al. (2013) Identification and Structural Characterization of a Broadly Neutralizing Antibody Targeting a Novel Conserved Epitope on the Influenza Virus H5N1 Hemagglutinin. *J Virol* 87: 2215–2225. doi:10.1128/JVI.02344-12.
 155. Bossart KN, Geisbert TW, Feldmann H, Zhu Z, Feldmann F, et al. (2011) A Neutralizing Human Monoclonal Antibody Protects African Green Monkeys from Hendra Virus Challenge. *Science Translational Medicine* 3: 105ra103–105ra103. doi:10.1126/scitranslmed.3002901.
 156. Cheng VCC, Lau SKP, Woo PCY, Yuen KY (2007) Severe Acute Respiratory Syndrome Coronavirus as an Agent of Emerging and Reemerging Infection. *Clinical Microbiology Reviews* 20: 660–694. doi:10.1128/CMR.00023-07.
 157. Normile D (2004) Infectious diseases. Second lab accident fuels fears about SARS. *Science* 303: 26. doi:10.1126/science.303.5654.26.
 158. Zaki AM, van Boheemen S, Bestebroer TM, Osterhaus ADME, Fouchier RAM (2012) Isolation of a novel coronavirus from a man with pneumonia in Saudi Arabia. *N Engl J Med* 367: 1814–1820. doi:10.1056/NEJMoa1211721.

159. Bolles M, Deming D, Long K, Agnihothram S, Whitmore A, et al. (2011) A Double-Inactivated Severe Acute Respiratory Syndrome Coronavirus Vaccine Provides Incomplete Protection in Mice and Induces Increased Eosinophilic Proinflammatory Pulmonary Response upon Challenge. *J Virol* 85: 12201–12215. doi:10.1128/JVI.06048-11.
160. Woo PCY, Lau SKP, Wong BHL, Tsoi H-W, Fung AMY, et al. (2005) Differential sensitivities of severe acute respiratory syndrome (SARS) coronavirus spike polypeptide enzyme-linked immunosorbent assay (ELISA) and SARS coronavirus nucleocapsid protein ELISA for serodiagnosis of SARS coronavirus pneumonia. *J Clin Microbiol* 43: 3054–3058. doi:10.1128/JCM.43.7.3054-3058.2005.
161. Xu X, Gao X (2004) Immunological responses against SARS-coronavirus infection in humans. *Cell Mol Immunol* 1: 119–122.
162. Lu L, Manopo I, Leung BP, Chng HH, Ling A-E, et al. (2004) Immunological characterization of the spike protein of the severe acute respiratory syndrome coronavirus. *J Clin Microbiol* 42: 1570–1576.
163. Cao Z, Liu L, Du L, Zhang C, Jiang S, et al. (2010) Potent and persistent antibody responses against the receptor-binding domain of SARS-CoV spike protein in recovered patients. *Viol J* 7: 299. doi:10.1186/1743-422X-7-299.
164. Traggiai E, Becker S, Subbarao K, Kolesnikova L, Uematsu Y, et al. (2004) An efficient method to make human monoclonal antibodies from memory B cells: potent neutralization of SARS coronavirus. *Nat Med* 10: 871–875. doi:10.1038/nm1080 [doi]nm1080 [pii].
165. van den Brink EN, Meulen ter J, Cox F, Jongeneelen MAC, Thijsse A, et al. (2005) Molecular and biological characterization of human monoclonal antibodies binding to the spike and nucleocapsid proteins of severe acute respiratory syndrome coronavirus. *J Virol* 79: 1635–1644. doi:10.1128/JVI.79.3.1635-1644.2005.
166. Zhang H, Wang G, Li J, Nie Y, Shi X, et al. (2004) Identification of an antigenic determinant on the S2 domain of the severe acute respiratory syndrome coronavirus spike glycoprotein capable of inducing neutralizing antibodies. *J Virol* 78: 6938–6945. doi:10.1128/JVI.78.13.6938-6945.2004.
167. He Y, Lu H, Siddiqui P, Zhou Y, Jiang S (2005) Receptor-Binding Domain of Severe Acute Respiratory Syndrome Coronavirus Spike Protein Contains Multiple Conformation-Dependent Epitopes that Induce Highly Potent Neutralizing Antibodies. *The Journal of*
168. Sui J, Li W, Murakami A, Tamin A, Matthews LJ, et al. (2004) Potent neutralization of severe acute respiratory syndrome (SARS) coronavirus by a human mAb to S1 protein that blocks receptor association. *Proc Natl Acad Sci USA* 101: 2536–2541.
169. Prabakaran P, Gan J, Feng Y, Zhu Z, Choudhry V, et al. (2006) Structure of severe acute respiratory syndrome coronavirus receptor-binding domain complexed with neutralizing antibody. *J Biol Chem* 281: 15829–15836. doi:10.1074/jbc.M600697200.
170. Sui J, Li W, Roberts A, Matthews LJ, Vogel L, et al. (2005) Evaluation of human monoclonal antibody 80R for immunoprophylaxis of severe acute respiratory syndrome by an animal study, epitope mapping, and analysis of spike variants. *J Virol* 79: 5900–5906. doi:10.1128/JVI.79.10.5900-5906.2005.
171. Hwang WC, Lin Y, Santelli E, Sui J, Jaroszewski L, et al. (2006) Structural basis of neutralization by a human anti-severe acute respiratory syndrome spike protein antibody, 80R. *J*

- Biol Chem 281: 34610–34616. doi:10.1074/jbc.M603275200.
172. Harvey BR, Georgiou G, Hayhurst A, Jeong KJ, Iverson BL, et al. (2004) Anchored periplasmic expression, a versatile technology for the isolation of high-affinity antibodies from *Escherichia coli*-expressed libraries. *Proc Natl Acad Sci USA* 101: 9193–9198. doi:10.1073/pnas.0400187101.
 173. Ahmad ZA, Yeap SK, Ali AM, Ho WY, Alitheen NBM, et al. (2012) scFv Antibody: Principles and Clinical Application. *Clinical and Developmental Immunology* 2012: 1–15. doi:10.1089/hyb.2007.0531.
 174. Maynard JA, Maassen CBM, Leppla SH, Brasky K, Patterson JL, et al. (2002) Protection against anthrax toxin by recombinant antibody fragments correlates with antigen affinity. *Nat Biotechnol* 20: 597–601. doi:10.1038/nbt0602-597.
 175. Wu H, Pfarr DS, Tang Y, An L-L, Patel NK, et al. (2005) Ultra-potent antibodies against respiratory syncytial virus: effects of binding kinetics and binding valence on viral neutralization. *J Mol Biol* 350: 126–144. doi:10.1016/j.jmb.2005.04.049.
 176. Li Y, Lipschultz CA, Mohan S, Smith-Gill SJ (2001) Mutations of an epitope hot-spot residue alter rate limiting steps of antigen-antibody protein-protein associations. *Biochemistry* 40: 2011–2022.
 177. Wu K, Peng G, Wilken M, Geraghty RJ, Li F (2012) Mechanisms of host receptor adaptation by severe acute respiratory syndrome coronavirus. *J Biol Chem* 287: 8904–8911. doi:10.1074/jbc.M111.325803.
 178. Wong S-K, Li W, Moore MJ, Choe H, Farzan M (2004) A 193-amino acid fragment of the SARS coronavirus S protein efficiently binds angiotensin-converting enzyme 2. *J Biol Chem* 279: 3197–3201. doi:10.1074/jbc.C300520200.
 179. Wang Z, Huang J-D, Wong KL, Wang P-G, Zhang H-J, et al. (2011) On the mechanisms of bananin activity against severe acute respiratory syndrome coronavirus. *FEBS J* 278: 383–389. doi:10.1111/j.1742-4658.2010.07961.x.
 180. Zhang M-Y, Shu Y, Rudolph D, Prabakaran P, Labrijn AF, et al. (2004) Improved breadth and potency of an HIV-1-neutralizing human single-chain antibody by random mutagenesis and sequential antigen panning. *J Mol Biol* 335: 209–219.
 181. Zhang M-Y, Borges AR, Ptak RG, Wang Y, Dimitrov AS, et al. (2010) Potent and broad neutralizing activity of a single chain antibody fragment against cell-free and cell-associated HIV-1. *MAbs* 2: 266–274.
 182. Scheid JF, Mouquet H, Feldhahn N, Seaman MS, Velinzon K, et al. (2009) Broad diversity of neutralizing antibodies isolated from memory B cells in HIV-infected individuals. *Nature* 458: 636–640. doi:10.1038/nature07930.
 183. Torán JL, Sánchez-Pulido L, Kremer L, del Real G, Valencia A, et al. (2001) Improvement in affinity and HIV-1 neutralization by somatic mutation in the heavy chain first complementarity-determining region of antibodies triggered by HIV-1 infection. *Eur J Immunol* 31: 128–137.
 184. Zhu Q, McAuliffe JM, Patel NK, Palmer-Hill FJ, Yang C-F, et al. (2011) Analysis of respiratory syncytial virus preclinical and clinical variants resistant to neutralization by monoclonal antibodies palivizumab and/or motavizumab. *J INFECT DIS* 203: 674–682. doi:10.1093/infdis/jiq100.

185. Ksiazek TG, Erdman D, Goldsmith CS, Zaki SR, Peret T, et al. (2003) A novel coronavirus associated with severe acute respiratory syndrome. *N Engl J Med* 348: 1953–1966. doi:10.1056/NEJMoa030781.
186. Marra MA, Jones SJM, Astell CR, Holt RA, Brooks-Wilson A, et al. (2003) The Genome sequence of the SARS-associated coronavirus. *Science* 300: 1399–1404. doi:10.1126/science.1085953.
187. Rota PA, Oberste MS, Monroe SS, Nix WA, Campagnoli R, et al. (2003) Characterization of a novel coronavirus associated with severe acute respiratory syndrome. *Science* 300: 1394–1399. doi:10.1126/science.1085952.
188. Drosten C, Gunther S, Preiser W, Werf S, Brodt H, et al. (2003) Identification of a novel coronavirus in patients with severe acute respiratory syndrome. *N Engl J Med* 348: 1967–1976.
189. Liang G, Chen Q, Xu J, Liu Y, Lim W, et al. (2004) Laboratory diagnosis of four recent sporadic cases of community-acquired SARS, Guangdong Province, China. *Emerging Infect Dis* 10: 1774–1781. doi:10.3201/eid1010.040445.
190. Hon C, Lam T, Shi Z, Drummond A, Yip C, et al. (2008) Evidence of the recombinant origin of a bat severe acute respiratory syndrome (SARS)-like coronavirus and its implications on the direct ancestor of SARS coronavirus. *J Virol* 82: 1819–1826.
191. Du L, He Y, Zhou Y, Liu S, Zheng B-J, et al. (2009) The spike protein of SARS-CoV--a target for vaccine and therapeutic development. *Nat Rev Microbiol* 7: 226–236. doi:10.1038/nrmicro2090.
192. Lai S-C, Chong PC-S, Yeh C-T, Liu LS-J, Jan J-T, et al. (2005) Characterization of neutralizing monoclonal antibodies recognizing a 15-residues epitope on the spike protein HR2 region of severe acute respiratory syndrome coronavirus (SARS-CoV). *J Biomed Sci* 12: 711–727. doi:10.1007/s11373-005-9004-3.
193. Wang S, Chou T-HW, Sakhatskyy PV, Huang S, Lawrence JM, et al. (2005) Identification of two neutralizing regions on the severe acute respiratory syndrome coronavirus spike glycoprotein produced from the mammalian expression system. *J Virol* 79: 1906–1910. doi:10.1128/JVI.79.3.1906-1910.2005.
194. Coughlin MM, Babcook J, Prabhakar BS (2009) Human monoclonal antibodies to SARS-coronavirus inhibit infection by different mechanisms. *Virology* 394: 39–46. doi:10.1016/j.virol.2009.07.028.
195. Coughlin M, Lou G, Martinez O, Masterman SK, Olsen OA, et al. (2007) Generation and characterization of human monoclonal neutralizing antibodies with distinct binding and sequence features against SARS coronavirus using XenoMouse. *Virology* 361: 93–102. doi:10.1016/j.virol.2006.09.029.
196. Berry JD, Hay K, Rini JM, Yu M, Wang L, et al. (2010) Neutralizing epitopes of the SARS-CoV S-protein cluster independent of repertoire, antigen structure or mAb technology. *MAbs* 2: 53–66.
197. Zakhartchouk AN, Sharon C, Satkunarajah M, Auperin T, Viswanathan S, et al. (2007) Immunogenicity of a receptor-binding domain of SARS coronavirus spike protein in mice: implications for a subunit vaccine. *Vaccine* 25: 136–143. doi:10.1016/j.vaccine.2006.06.084.
198. He Y, Zhu Q, Liu S, Zhou Y, Yang B, et al. (2005) Identification of a critical neutralization determinant of severe acute respiratory syndrome (SARS)-associated coronavirus: importance for

- designing SARS vaccines. *Virology* 334: 74–82. doi:10.1016/j.virol.2005.01.034.
199. Li W, Moore M, Vasilieva N, Sui J, Wong S, et al. (2003) Angiotensin-converting enzyme 2 is a functional receptor for the SARS coronavirus. *Nature* 426: 450–454. doi:10.1038/nature02145.
 200. Frieman M, Yount B, Agnihothram S, Page C, Donaldson E, et al. (2012) Molecular determinants of severe acute respiratory syndrome coronavirus pathogenesis and virulence in young and aged mouse models of human disease. *J Virol* 86: 884–897. doi:10.1128/JVI.05957-11.
 201. Li W, Greenough TC, Moore MJ, Vasilieva N, Somasundaran M, et al. (2004) Efficient replication of severe acute respiratory syndrome coronavirus in mouse cells is limited by murine angiotensin-converting enzyme 2. *J Virol* 78: 11429–11433. doi:10.1128/JVI.78.20.11429-11433.2004.
 202. Lai MM, Cavanagh D (1997) The molecular biology of coronaviruses. *Adv Virus Res* 48: 1–100.
 203. O'Donnell CD, Vogel L, Wright A, Das SR, Wrammert J, et al. (2012) Antibody Pressure by a Human Monoclonal Antibody Targeting the 2009 Pandemic H1N1 Virus Hemagglutinin Drives the Emergence of a Virus with Increased Virulence in Mice. *MBio* 3: e00120–12–e00120–12. doi:10.1128/mBio.00120-12.
 204. Perlman S, Netland J (2009) Coronaviruses post-SARS: update on replication and pathogenesis. *Nat Rev Microbiol* 7: 439–450. doi:10.1038/nrmicro2147.
 205. Bolles M, Donaldson E, Baric R (2011) SARS-CoV and emergent coronaviruses: viral determinants of interspecies transmission. *Current Opinion in Virology* 1: 624–634. doi:10.1016/j.coviro.2011.10.012.
 206. Cheng Y, Wong R, Soo YOY, Wong WS, Lee CK, et al. (2005) Use of convalescent plasma therapy in SARS patients in Hong Kong. *Eur J Clin Microbiol Infect Dis* 24: 44–46. doi:10.1007/s10096-004-1271-9.
 207. Tseng C-T, Sbrana E, Iwata-Yoshikawa N, Newman PC, Garron T, et al. (2012) Immunization with SARS Coronavirus Vaccines Leads to Pulmonary Immunopathology on Challenge with the SARS Virus. *PLoS ONE* 7: e35421. doi:10.1371/journal.pone.0035421.t002.
 208. Logtenberg T (2007) Antibody cocktails: next-generation biopharmaceuticals with improved potency. *Trends in Biotechnology* 25: 390–394. doi:10.1016/j.tibtech.2007.07.005.
 209. Prabakaran P, Zhu Z, Xiao X, Biragyn A, Dimitrov AS, et al. (2009) Potent human monoclonal antibodies against SARS CoV, Nipah and Hendra viruses. *Expert Opin Biol Ther* 9: 355–368..
 210. Coughlin MM, Prabhakar BS (2011) Neutralizing human monoclonal antibodies to severe acute respiratory syndrome coronavirus: target, mechanism of action, and therapeutic potential. *Rev Med Virol* 22: 2–17. doi:10.1002/rmv.706.
 211. Palivizumab, a Humanized Respiratory Syncytial Virus Monoclonal Antibody, Reduces Hospitalization From Respiratory Syncytial Virus Infection in High-Risk Infants. (1998) Palivizumab, a Humanized Respiratory Syncytial Virus Monoclonal Antibody, Reduces Hospitalization From Respiratory Syncytial Virus Infection in High-Risk Infants. *Pediatrics* 102: 531–537.
 212. Carbonell-Estrany X, Simoes EAF, Dagan R, Hall CB, Harris B, et al. (2010) Motavizumab for Prophylaxis of Respiratory Syncytial Virus in High-Risk Children: A Noninferiority Trial. *Pediatrics* 125: e35–e51. doi:10.1542/peds.2008-1036.

213. Russell ES, Ojeda S, Fouda GG, Meshnick SR, Montefiori D, et al. (2013) Short Communication: HIV Type 1 Subtype C Variants Transmitted Through the Bottleneck of Breastfeeding Are Sensitive to New Generation Broadly Neutralizing Antibodies Directed Against Quaternary and CD4-Binding Site Epitopes. *AIDS Research and Human Retroviruses* 29: 511–515. doi:10.1089/aid.2012.0197.
214. Chung RT, Gordon FD, Curry MP, Schiano TD, Emre S, et al. (2013) Human Monoclonal Antibody MBL-HCV1 Delays HCV Viral Rebound Following Liver Transplantation: A Randomized Controlled Study. *American Journal of Transplantation*. doi:10.1111/ajt.12083.
215. Bakker ABH, Marissen WE, Kramer RA, Rice AB, Weldon WC, et al. (2005) Novel human monoclonal antibody combination effectively neutralizing natural rabies virus variants and individual in vitro escape mutants. *J Virol* 79: 9062–9068. doi:10.1128/JVI.79.14.9062-9068.2005.
216. Smith CA, Kortemme T (2008) Backrub-Like Backbone Simulation Recapitulates Natural Protein Conformational Variability and Improves Mutant Side-Chain Prediction. *Journal of Molecular Biology* 380: 742–756. doi:10.1016/j.jmb.2008.05.023.
217. Schrödinger, LLC (2010) The PyMOL Molecular Graphics System.
218. Van Durme J, Delgado J, Stricher F, Serrano L, Schymkowitz J, et al. (2011) A graphical interface for the FoldX forcefield. *Bioinformatics* 27: 1711–1712. doi:10.1093/bioinformatics/btr254.
219. Krieger E, Koraimann G, Vriend G (2002) Increasing the precision of comparative models with YASARA NOVA—a self-parameterizing force field. *Proteins* 47: 393–402. doi:10.1002/prot.10104.
220. Chakraborti S, Prabakaran P, Xiao X, Dimitrov D (2005) The SARS coronavirus S glycoprotein receptor binding domain: fine mapping and functional characterization. *Virology* 337: 73–82.
221. Nelson AL, Dhimolea E, Reichert JM (2010) Development trends for human monoclonal antibody therapeutics: 1–8. doi:10.1038/nrd3229.
222. Zhu Q, Patel NK, McAuliffe JM, Zhu W, Wachter L, et al. (2012) Natural Polymorphisms and Resistance-Associated Mutations in the Fusion Protein of Respiratory Syncytial Virus (RSV): Effects on RSV Susceptibility to Palivizumab. *J INFECT DIS* 205: 635–638. doi:10.1093/infdis/jir790.
223. Chen W, Madden VJ, Bagnell CR, Baric RS (1997) Host-derived intracellular immunization against mouse hepatitis virus infection. *Virology* 228: 318–332. doi:10.1006/viro.1996.8402.
224. Heald-Sargent T, Gallagher T (2012) Ready, Set, Fuse! The Coronavirus Spike Protein and Acquisition of Fusion Competence. *Viruses* 4: 557–580. doi:10.3390/v4040557.
225. Hurt AC, Leang SK, Speers DJ, Barr IG, Maurer-Stroh S (2012) Mutations I117V and I117M and oseltamivir sensitivity of pandemic (H1N1) 2009 viruses. *Emerging Infect Dis* 18: 109–112. doi:10.3201/eid1801.111079.
226. Bloom JD, Nayak JS, Baltimore D (2011) A Computational-Experimental Approach Identifies Mutations That Enhance Surface Expression of an Oseltamivir-Resistant Influenza Neuraminidase. *PLoS ONE* 6: e22201. doi:10.1371/journal.pone.0022201.
227. Smith CA, Kortemme T (2011) Predicting the Tolerated Sequences for Proteins and Protein

- Interfaces Using RosettaBackrub Flexible Backbone Design. *PLoS ONE* 6: e20451. doi:10.1371/journal.pone.0020451.t001.
228. Kindler E, Jonsdottir HR, Muth D, Hamming OJ, Hartmann R, et al. (2012) Efficient Replication of the Novel Human Betacoronavirus EMC on Primary Human Epithelium Highlights Its Zoonotic Potential. *MBio* 4: e00611–12–e00611–12. doi:10.1128/mBio.00611-12.
229. Nelms K, Keegan AD, Zamorano J, Ryan JJ, Paul WE (1999) The IL-4 receptor: signaling mechanisms and biologic functions. *Annu Rev Immunol* 17: 701–738. doi:10.1146/annurev.immunol.17.1.701.
230. Li CK-F, Wu H, Yan H, Ma S, Wang L, et al. (2008) T cell responses to whole SARS coronavirus in humans. *J Immunol* 181: 5490–5500.
231. Castle S, Uyemura K, Wong W, Modlin R, Effros R (1997) Evidence of enhanced type 2 immune response and impaired upregulation of a type 1 response in frail elderly nursing home residents. *Mech Ageing Dev* 94: 7–16.
232. Cusi MG, Martorelli B, Di Genova G, Terrosi C, Campoccia G, et al. (2010) Age related changes in T cell mediated immune response and effector memory to Respiratory Syncytial Virus (RSV) in healthy subjects. *Immunity & Ageing* 7: 14. doi:10.1186/1742-4933-7-14.
233. Panda A, Arjona A, Sapey E, Bai F, Fikrig E, et al. (2009) Human innate immunosenescence: causes and consequences for immunity in old age. *Trends in Immunology* 30: 325–333. doi:10.1016/j.it.2009.05.004.
234. Jing Y, Gravenstein S, Rao Chaganty N, Chen N, Lyerly KH, et al. (2007) Aging is associated with a rapid decline in frequency, alterations in subset composition, and enhanced Th2 response in CD1d-restricted NKT cells from human peripheral blood. *Experimental Gerontology* 42: 719–732. doi:10.1016/j.exger.2007.01.009.
235. Gralinski LE, Bankhead A III, Jeng S, Menachery VD, prill S, et al. (2013) Mechanisms of SARS-CoV Induced Acute Lung Injury. *MBio*: submitted.
236. Mueller TD, Zhang J-L, Sebald W, Duschl A (2002) Structure, binding, and antagonists in the IL-4/IL-13 receptor system. *Biochim Biophys Acta* 1592: 237–250.
237. Garrone P, Djossou O, Galizzi JP, Banchereau J (1991) A recombinant extracellular domain of the human interleukin 4 receptor inhibits the biological effects of interleukin 4 on T and B lymphocytes. *Eur J Immunol* 21: 1365–1369. doi:10.1002/eji.1830210606.
238. Henderson WR, Chi EY, Maliszewski CR (2000) Soluble IL-4 receptor inhibits airway inflammation following allergen challenge in a mouse model of asthma. *J Immunol* 164: 1086–1095.
239. Schulte T, Kurrle R, Röllinghoff M, Gessner A (1997) Molecular characterization and functional analysis of murine interleukin 4 receptor allotypes. *The Journal of experimental medicine* 186: 1419–1429.
240. Sims AC, Baric RS, Yount B, Burkett SE, Collins PL, et al. (2005) Severe acute respiratory syndrome coronavirus infection of human ciliated airway epithelia: role of ciliated cells in viral spread in the conducting airways of the lungs. *J Virol* 79: 15511–15524. doi:10.1128/JVI.79.24.15511-15524.2005.
241. Mosmann TR, Yokota T, Kastelein R, Zurawski SM, Arai N, et al. (1987) Species-specificity of

- T cell stimulating activities of IL 2 and BSF-1 (IL 4): comparison of normal and recombinant, mouse and human IL 2 and BSF-1 (IL 4). *J Immunol* 138: 1813–1816.
242. Graham RL, Becker MM, Eckerle LD, Bolles M, Denison MR, et al. (2012) A live, impaired-fidelity coronavirus vaccine protects in an aged, immunocompromised mouse model of lethal disease. *Nat Med* 18: 1820–1826. doi:10.1038/nm.2972.
243. Yang Z-Y, Werner HC, Kong W-P, Leung K, Traggiai E, et al. (2005) Evasion of antibody neutralization in emerging severe acute respiratory syndrome coronaviruses. *Proc Natl Acad Sci USA* 102: 797–801. doi:10.1073/pnas.0409065102.
244. Gierer S, Bertram S, Kaup F, Wrensch F, Heurich A, et al. (2013) The spike-protein of the emerging betacoronavirus EMC uses a novel coronavirus receptor for entry, can be activated by TMPRSS2 and is targeted by neutralizing antibodies. *J Virol*. doi:10.1128/JVI.00128-13.
245. Jiang S, Lu L, Du L, Debnath AK (2013) A predicted receptor-binding and critical neutralizing domain in S protein of the novel human coronavirus HCoV-EMC. *Journal of Infection*: 1–3. doi:10.1016/j.jinf.2012.12.003.